Numerical Analysis and Simulation of Dry Sliding Wear on Maraging Steel by using LSDYNA Software

MUBAREK MOHAMMED-HUSSIEN

A thesis Submitted to Department of Mechanical Engineering

School Of Mechanical, Chemical and Material Engineering

Office of Graduate Studies

Adama Science and Technology University

June, 2023

Adama, Ethiopia

Numerical Analysis and Simulation of Dry Sliding Wear on Maraging Steel by using LSDYNA Software

Mubarek Mohammed-Hussein Hasen

Advisor:

Dr. G.M. Sayeed Ahmed (PhD)

A Thesis Submitted to

The Department of Mechanical Engineering

School of Mechanical, Chemical and Materials Engineering

Office of Graduate Studies

Adama Science and Technology University

June, 2023

Adama, Ethiopia

1. DECLARATION

I declare that this thesis entitled "Numerical Analysis and Simulation of Dry Sliding Wear on Maraging Steel by using LSDYNA Software" is my own work and has not been submitted to any University for similar purpose. The references used in this thesis were duly recognized by proper citations.

Mubarek Muhammed-Hussein Hasen	________________	________________
Name of student	Signature	Date

2. RECOMMENDATION

I, the major advisor of this thesis, here by certify that I have closely advised the student while developing this proposal and read the draft thesis proposal entitled "Numerical Analysis and Simulation of Dry Sliding Wear on Maraging Steel by using LSDYNA Software" prepared under my guidance by Mubarek Mohammed-Hussein Hasen. Therefore, I recommend the submission of the thesis to the department for further review and evaluation.

Dr. G.M. Sayeed Ahmed		24-08-2023
Main Advisor	Signature	Date

3. APPROVAL SHEET FOR THESIS

We here by certify that the recommendation and suggestion given by the thesis review committee are appropriately incorporated into the final thesis entitled "Numerical Analysis and Simulation of Dry Sliding Wear on Maraging Steel by using LSDYNA Software" by

Mubarek Mohammed-Hussein Hasen.

Dr. G.M. Sayeed Ahmed		24-08-2023
Main Advisor	Signature	Date

We, the Undersigned, members of the Board of reviewers of the open defense by Mubarek Mohammed-Hussein Hasen, have read and evaluated the thesis entitled "wear" and assessed understanding of the candidate about the thesis. This is, therefore, to certify that the thesis is accepted and we recommend the implementation of thesis.

______________________	_________________	______________
Chairperson	Signature	Date
______________________	_________________	______________
Internal Examiner	Signature	Date
Getasew A. TADDESE (PhD)		25/08/2023
External Examiner	Signature	Date

Finally approval and acceptance of the thesis is contingent upon submission of its final copy to the Office of Postgraduate studies (OPGS) through the Department Graduate council (DGC) and School Graduate Committee (SGC).

______________________	_____________	______________
Department Head	Signature	Date
______________________	_____________	______________
School Dean	Signature	Date
______________________	_____________	______________
Office of Postgraduate Studies, Dean	Signature	Date

Contents

List of Figure

List of Table

LIST OF ABBREVIATIONS

✓ 3DP	3D printed/3D printing
✓ 3DPMS	3D printed maraging Steel
✓ Adj MS	Adjusted Mean of Squares
✓ Adj SS	Adjusted Sums of Squares
✓ DF	Degrees of Freedom
✓ DMLS	Direct Metal Laser Sintering
✓ FTIR	Fourier Transform Infrared Spectroscopy
✓ MWR	Mean Wear Rate
✓ RSM	Response Surface Method
✓ R-Sq	R-Squared.
✓ SEM	Scanning Electron Microscopy
✓ SLM	Selective Laser Melting
✓ WR	Wear rate
✓ RSR	Response surface Regression
✓ GFR	General factorial Regression

ABSTRACT

The wear resistance is an important aspect that influences the functionality of the components. The wear tests in dry condition were performed on Maraging steel on pin/disc standard wear testing machine. Wear is one of the most important phenomena, apart from fatigues and corrosion, which causes replacement of parts in industrial production. This often results in increase of losses by deprivation of the surface of opposing parts. This research work aims to compare the wear rate of experimental value with conventional on Maraging steel. In this study, the dry sliding Tribological performances of maraging steel and Tribological properties of the wear were investigated by wear test as per standard. The wear characteristics were performed at constant sliding distance and load 10N, 15N and 20N. The PIN on Disc wear test is used as per as standard; the dry sliding wear characteristics test of wear rate, the Standard dimensions of the Wear specimen is D=6mm and L=12mm. conduct experiment at AASTU wear testing machine to evaluate wear characteristics. The researcher studied the wear of Maraging steel by considering L9-orthugonal array of wear parameters such as (time, sliding distance, wear load and speed). The researcher has compared the wear characteristics of Maraging Steel. Optimized the wear process parameters and study their effect on wear. The optimum results were validated. The simulations of maraging steel experiment results by LSDYNA software have been discussed.

Keywords*: Wear, Maraging steel, Wear characteristics, SEM, LS-DYNA, PIN on DISC*

CHAPTER ONE

1. INTRODUCTION

1.1. Background Study

The name Maraging is derived from the strengthening phenomenon caused by the formation of a rotten phase during hardening of steel. Martensitic steels are used where geometric complexity and mechanical properties are at their peak, such as in the tool industry and the aerospace industry. Martensitic steel is used in the manufacture of critical components in structures, aerospace, tools, fasteners, and the automotive industry. They have excellent strength because their mechanical properties are derived from the main alloying elements, namely: Ni, Co, Mo, Ti, Al. Some of them are responsible for the formation of precipitates, e.g. Ti, Ni, Al, Mo, while others influence the deposition process, e.g. Co. Martensitic steel has minimal or no porosity. The composition of Maraging steel contains 18% nickel with added titanium, aluminum and cobalt. It has excellent response to heat treatment, mechanical properties and machinability.

The production of filler metals involves melting the molten metal layer by layer. It is also popular as 3D metal printing, which is said to be the latest metal fabrication for precision manufacturing, rapid reproduction and advanced applications designed to produce complex products. Direct metal laser sintering (DMLS) is one of the established additive manufacturing (AM) processes for three-dimensional (3D) printing of functional prototypes. The three-dimensional computer-aided design (3D CAD) data of the sample is necessary for the construction process to be converted into layer data by the collection processor available in the 3D printer (3DP). 3DP software that controls positioning and slicing, such as Magics RP software and 3D Slicer integrated with the .STL (stereo lithography) editor, showed that the effect of fill and pattern density are two visible controlled variables. Direct metal laser sintering (DMLS) is useful for dimensional accuracy. Investigated custom 3D metal printing of Co Cr Mo using selective laser melting (SLM). SLM is a 3DP technology used to produce special alloys of titanium, aluminum, nickel and iron. Products made with SLM are dense, with a good surface finish and higher tensile strength than any current technology. These mechanical properties can only be achieved with a better density of parts, which is possible with SLM type 3DP technology, where all parameters affect the alloy; Laser power and scanning speed can be controlled. Some studies reported that the micro hardness of 3D printed martensitic steel (3DPMS) was higher than that produced by conventional methods. For martensitic steel, standard machined levels were obtained when produced by the SLM method.

High alloy steel fabric 18% Ni300 maraging steel microstructure has high hardness and high chromium compound carbides. It provides excellent wear resistance due to the sliding interaction with the auxiliary metals and grid materials. It offers a leading combination of abrasion resistance and degradation resistance, and is used in the supply of therapeutic decorations, businesses and auto parts.

Table 1: Chemical Composition of DMLS Maraging Steel

Material (Maraging steel)	Fe	Ni	Cobalt	Mo	Ti	Al	Cr, Cu	c	Mn, Si
Composition (Wt. %)	68.39	17.1	8.83	4.95	0.71	0.06	≤0.5	≤0.03	≤0.1

Analysis of variance and design of test methods were used to optimize the input parameters based on part hardness, ultimate tensile strength and density (relative) according to the required capacity. Since martensitic steel has a wide range of industrial applications, additional heat treatment is required to achieve the desired level of machining when produced by another manufacturing process. Short-term aging of Maraging steel showed better yield strength, higher toughness and finer microstructure with uniformly distributed precipitates.

1.2. Properties and Application

Maraging steel is used in aircraft, with applications including landing gear, helicopter undercarriages, slat tracks and rocket motor cases – applications which require high strength-to-weight material. Maraging steel offers an unusual combination of high tensile strength and high fracture toughness. The high alloy steel Maraging steel is alloyed with high Nickel, Cobalt, Carbon, Manganese, Aluminum, Titanium and Silicon. The common properties have great wear resistance, firmness, mechanical constrain, tall warm resistance and oxidization resistance it is utilized in different applications like gas turbines, motor cam, cylinder rings, motor channel esteem, shafts, warm exchangers in petrochemical industry, impeller, jolts, screws, bushings, nut sand spouts.


Shaft aircraft landing


Bolt and Nut Blade Impeller

Figure 1: High Alloy Maraging Steel Material Applications

1.3. TRIBOLOGY

Tribology, the scientific name given to the study of the mechanisms of interaction of surfaces in relative motion, is indeed one of the fundamental concepts of engineering, especially engineering. The term tribology is derived from the Greek word trib, meaning friction, and encompasses the entire science and technology of the relative motion of interacting surfaces. The main areas of analysis and application are friction, wear and lubrication. The term itself was introduced only in 1964. There are images of tribology in action from ancient Egypt, where early workers used tribology to facilitate the sliding of large figures with oil. The field is inevitably highly interdisciplinary and utilizes expertise from mechanical engineering, materials science and technology, chemistry and chemical engineering, and more. Tribology is especially important in today's world, because a lot of energy is lost due to the friction of mechanical parts. To use less energy, we need to reduce the amount of wasted vital energy. A significant amount of energy is lost due to friction in sliding joints. Therefore, for a more environmentally friendly and sustainable world, it is very important to find different ways to minimize friction and wear using new tribological technologies.

1.3.1. Importance of Tribology

Over the years, the governments of the foremost industrialized countries have developed in depth method to scale back energy waste. In 1966, the Jost Report showed that the misrecognition of tribology in Great Britain caused an enormous waste of material and energy. Similarly, in 1977, a US government economic report suggested that $16.25 billion could have been saved through the proper use of tribological science. Similar studies have been carried out in other foreign countries; For example, W. Bartz made a study related to Germany between 1979 and 1983, while in 1990 P. Jost described the possible savings in GDP to determine calculated values of 1.3 to 1.6%. It should be noted that although the study by W. Bartz only deals with lubricated contacts, it classifies the possible savings as: (I) primary savings resulting from reduced mechanical friction; (ii) secondary savings resulting from reduced replacement of machine parts due to reduced wear and tear; and (iii) third-order savings when substitute material is used to make new parts, which increases the energy content of the materials. Currently, the integration of tribology reflects a revolutionary aspect of life cycle assessment, with environmental and economic results as the main motive. In this case, the main role of tribology is not only to reduce friction in a machine, but also to extend the machine's service life.

1.3.2. Basic principles of tribology

Years of research of tribology justifies the statement that the friction and wear properties of a given material are not its internal characteristics, but depend on many factors related to the specific application. Quantitative values of friction and wear in the form of coefficient of friction and wear, which are mentioned in many engineering textbooks, depend on the following main groups of parameters

i. The structure of the system, i.e. its components and their relevant properties;
ii. The operating variables, i.e. load (stress), kinematics, temperature and time;
iii. Mutual interaction of the system's components.

1.4. WEAR

There are several precise definitions for wear. However, for engineering purposes the following definitions contains the essential elements.

- Wear is damage to a surface caused by relative motion in relation to another substance. One key point is that wear is damage and is not limited to the loss of material from the surface. But material loss is certainly one way that differences can experience wear.
- Another way included in this definition is to move material without mass loss. An example of this could be a change in part geometry or dimensions as a result of plastic deformation (e.g., repeated hammering).
- There is a third condition which is surface damage that does not cause mass loss or dimensional change. An example of this third state can be a network of cracks on the surface. This can be important in applications where maintaining optical transparency is a primary design goal. Lenses and aircraft windows are examples where this is an appropriate definition of wear.

Wear may be depicted as the fabric expulsion or surface hurt that guarantees from the virtual movement between reaching strong surfaces. Wear happens at the same time as contact since they are the result of the same tribological contact process.

1.4.1. Wear Mechanism

It is their mechanisms tend to divide wear in engineering practice into four broad general categories, namely: adhesive, surface fatigue, friction, and chemical wear. Wear is usually associated with the loss of material from contracting bodies during relative motion. It is governed by material properties, environmental and operational conditions, and the geometry of the contact parts. As an additional factor affecting the wear of certain materials, especially certain organic polymers, the relative motion kinematics in the contact zone must also be mentioned. Two groups of consumption mechanisms can be distinguished; the first includes those governed by the mechanical behavior of the materials, and the second includes those that determine the chemical nature of the materials. Wear can be abrasive and adhesive wear. Wear means that plowing through hard particles or rough surfaces does not affect the wear of the adhesive. Adhesive wear is caused by adhesive forces between atoms in close contact. When sliding, these contacts in the original interface do not break.

Abrasive wear

Abrasive wear occurs when a hard, uneven surface slides across a softer surface. The two rough wear methods are known as two-body and three-body grinding wear. Abrasive wear is a very common and at the same time very serious wear. It occurs when two interacting surfaces are in direct physical contact and one of them is significantly harder than the other. Under the influence of a normal load, impurities on the harder surface penetrate the softer surface, causing plastic deformations. Abrasive wear can occur anywhere on the surface if hard particles are present. When the stone or hard particles push the fabric away from the back surface, the result is frictional wear between the two pieces. The result is three wear on the body if the particles are not retained and can ripple and slide along the surface. Hard abrasive particles (eg droplets of the PVD film) can cause three abrasive wears during good cooling.

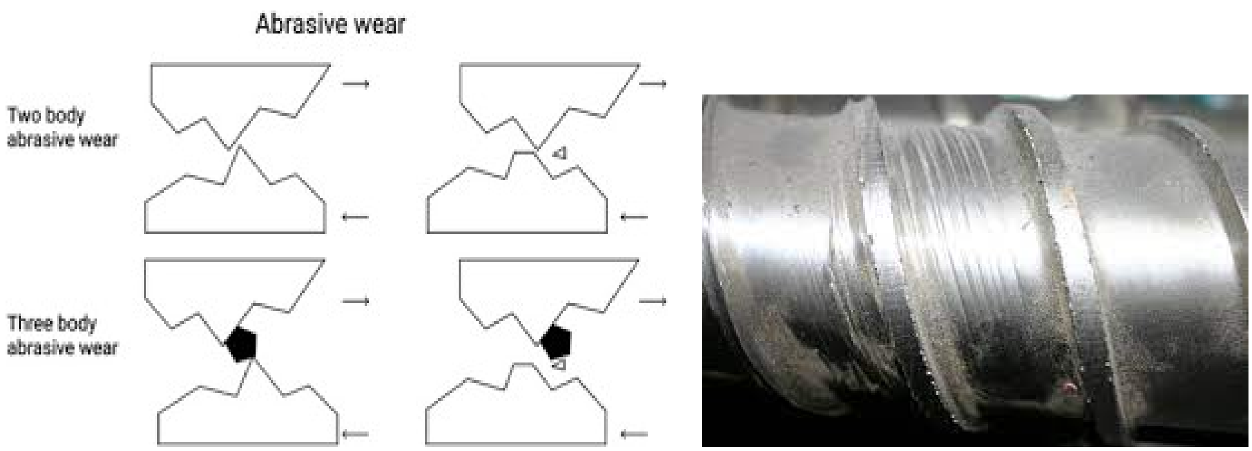

(Source: www.sciencedirect.com)

Figure 2: Abrasive Wear

The amount of material removed in this process can be estimated from the expression:

$$V_{abr} = \frac{\tan\theta}{H} WL \qquad \text{Eq.[1]}$$

Where H=hardness of the soften material

L=sliding distance

Adhesive Wear

Adhesive wear is a phenomenon that occurs when two metals rub against each other sufficient force causes the material to be removed from the less wear-resistant ones to the surface. Adhesive wear is the result of the transference of fabric from one surface to another, regularly taking place in ineffectively lubricated sliding applications. As we see further into adhesive wear, it will ended up clear that there are a few elective names regularly related with this type of wear.

This wear depends on physical and chemical factors such as material properties, the presence of corrosive atmospheres or chemicals and dynamics such as speed and load. This phenomenon is being investigated corrosion by mechanical action instead of chemical reaction. Several well-defined steps leading to adhesive wear particles can be identified: i) by the deformation of the impurities in contact; (ii) removal of surface films; (iii) forming an adhesive joint; iv) joint failure and material migration; (v) transferred change pieces; vi) Removal of displaced pieces and causing loose wear particles.

The volume of material removed by the adhesive wear process can be estimated by the expression proposed by Archard

$$V_a = K \frac{W}{H} L \qquad \text{Eq. [2]}$$

Where K= wear coefficient

L= sliding distance

H= hardness of the softer material in contact.

The adhesive wear is influenced by the following parameters characterizing the bodies in contact:

i. electronic structure;
ii. crystal structure;
iii. crystal orientation;
iv. Cohesive strength; For example, hexagonal metals, in general, are more resistant to adhesive wear than either body- centered cubic or face-centered cubic metals.

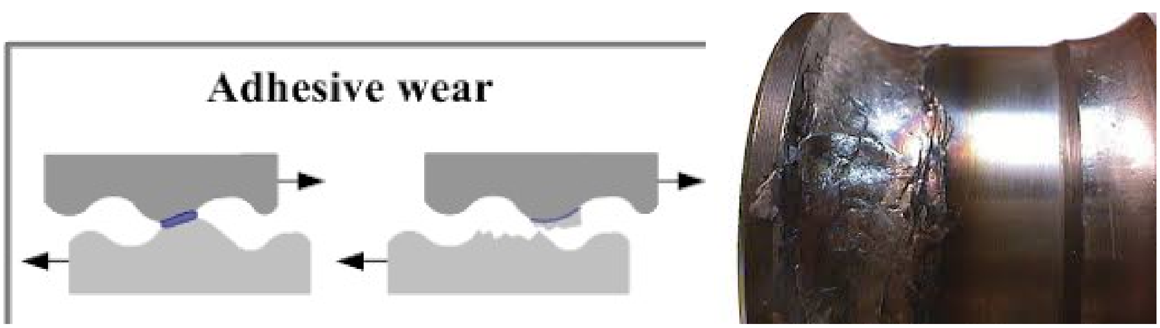

(Source: www.substech.com)

Figure 3: Adhesive Wear

1.4.2. Wear Resistance

Wear resistance is a term frequently utilized to characterize the anti-wear properties of a fabric. Be that as it may, the efficient significance of wear resistance is dubious, and there's no particular unit to describe wear resistance. In any case, the reverse of mass loss or volume loss is sometimes utilized as the (relative) wear resistance (Nohava, J et al. 2015). Wear resistance has always been the most important criteria in steels, several researchers also used polished, silicon-coated and cold sprayed 3D printed (3DP) material to enhance the wear resistance in respective materials. Several researchers conducted the wear tests on conventional metals and made a comparative study on alloys, reinforced with different metallic constituents and revealed that the wear resistance was increased considerably. Aged maraging steel when considered for 'wear during fatigue' had similar wear resistance as case hardened steel and 'thermally refined steel,' widening the application range of the former in the manufacturing of gears. Different types of wear studies were conducted in the past, especially the lubricated sliding contact type and dry sliding-type being the most prominent. Wet sliding wear test being common in aluminum alloys, with different reinforcements. Dry sliding wear test is feasible for steels. Much of the research focused on attaining optimum values of sliding speed and contact pressure to improve the wear resistance in stainless steel. Laser cladding of maraging steel and stainless steel did not have any effect on their wear resistance and rolling contact fatigue properties. Nickel-based titanium alloys have super elastic properties, making them applicable in a wide range of industries. This alloy was 3DP and with surface modifications, had the least porosity and good surface finish. Proved that melt spreading behavior also had a great impact on the wear resistance in the case of 3DP aluminum alloy An orthogonal array of L4 was developed using the Taguchi technique and process parameters were analyzed using the ANOVA technique. Sintering speed was set to a minimum to have better bonding between the materials. DMLS was employed to augment the tribological performance of different alloys of iron, nickel, and chromium. As maraging steel is termed as Fe–Ni alloy, so its wear resistance can be lowered when prepared by DMLS, compared with Fe–Ni–Cr alloy manufactured by the same method. During DMLS, the contact of metal powder with the laser beam creates molten droplets. Elongated pools of the melt are formed as a result of moving beam, observed as minor castings. The size and shape of pools of melt may be adjusted by controlling laser processing parameters.

The wear is a process in which material gets removed from either or both sliding members under the influence of prime factors namely speed, load, and distance of sliding. Many researchers conducted experiments with these parameters on commercially available metals and alloys. It emerges that some researchers have tried to improve the wear properties of maraging steel manufactured conventionally, by some surface treatment operations, but still desired results needed further improvisation. Wear rate (WR) is favored over wear coefficient as wear indicator.

1.5. PIN ON DISC WEAR TESTER

A pin is loaded against a level turning plate specimen such that a circular weary way is assigned by the machine. Figure 4 appears the schematic line chart of the pin-on disc testing machine. It can be utilized for assessment wear and friction properties of materials under pure sliding conditions. Disc or pin can serve as a specimen, whereas the other as counterparts. A helpful way is to utilize ball of commercially available materials such as bearing steel, tungsten carbide or alumina (Al2O3) as counter face, so that the title of ball on disc is utilized.

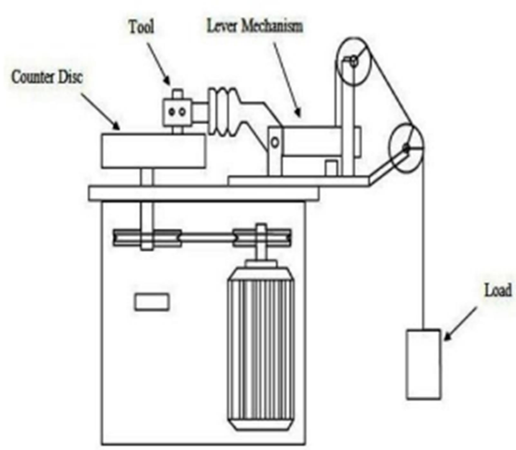

Figure 4: Schematic line diagram of PIN ON DISC Wear test machine

1.6. PROBLEM STATEMENT

The development of 3DPMS is quite common and so are the studies on its mechanical and thermal properties. But limited research has been done on the wear performance of this material. The present work aims to determine the wear performance on the maraging steel and to develop a model to predict its wear rate (WR). The experimental results will be equated with projected values and interactions among the wear test parameters are studied to obtain the conditions for minimum and most severe wear.

1.7. OBJECTIVES

1.7.1. General Objective

The main objective of this work is to Study the Numerical Analysis of Wear and Compare the wear characteristics of Maraging Steel with DMLS based Maraging steel the stress induced in the Pin Material.

1.7.2. Specific Objective

The specific objectives of this work for wear test of maraging steel:

- ✓ The wear effects on Maraging steel of different process parameters have been studied.
- ✓ By using the wear process parameters comparative study have been done for the stress induced in the Pin Material.
- ✓ To Evaluate Wear Volume and Wear Coefficient by Pin on Disc Experiment.
- ✓ To characterize surface of the samples in Micrographs by using Scanning Electron Microscope (SEM).
- ✓ To Optimize the Parameters by using Taguchi and Response Surface Method.
- ✓ A comparative Study has been done by using LSDYNA software to determine the stresses induced in the Pin Material by considering the Optimum parameters such as (Sliding Distance, time of running, Wear Load and Pin Velocity).

1.8. Scope of Study

- ✓ Prepare the ASMG-99 standard specimen for conventional Maraging steel for Pin on disk experiment
- ✓ Standard dimensions of the Wear specimen is D=6mm and L=12mm
- ✓ Conducted experiment on wear testing machine to evaluate wear characteristics.
- ✓ Study the wear of maraging steel by considering L9-orthugonal array of wear parameters such as sliding distance, wear load and speed.
- ✓ Compare the wear characteristics of both conventional and DMLS based Maraging Steel.

- ✓ Validate the optimum result with experiment and simulating the experimental results by LSDYNA software.

1.9. MOTIVATION

Nowadays, the integration of tribology represents a modern perspective in a life cycle assessment whose main objectives are the environment and financial results. In this case, the main roles of tribology are not only reduces friction in the machine, but also extends it lifetime of machines.

Tribology is especially vital in today's world because ample amount of energy is lost due to friction in mechanical parts. To use little energy, we need to reduce the amount of vital energy that is wasted. Significant energy is very much lost due to friction in sliding interfaces. Therefore, finding different ways to minimize friction and wear with the help of new technologies in tribology is very important to a greener and more sustainable world.

CHAPTER TWO

2. Literature Review

A review of available literature is to provide background information on the issues to be considered in this thesis. The review is focused on the various aspects of the Wear resistance for maraging steel by direct metal laser sintering with a special reference. This chapter contains review of existing research reports. There have been numerous studies regarding wear resistance of maraging steel and much advancement has been achieved in this area. Some of these studies are presented in the following section.

2.1. Maraging steel Research work carried out by different Authors.

Kennedy et al: Conducted a study on contact temperatures and their effects wear during pin-on-disc tribotesting are some of the most useful analytical and numerical methods that can be used to predict surface temperature climbs in dry or partially lubricated pin-on-disc tribotests. Development relatively simple, accurate and easy to use expressions that can be used for divination contact temperatures in pin-on-disk sliding contacts ceramic (zirconia) wear, metal (stainless steel) and polymer (polyethylene) are performed in pin-on-disk tests out

M. Pardal (2007): The magnetic properties and hardness of a Ni–Co–Mo–Ti maraging steel 300 grade were measured as function of aging temperature. The aging at 560 C for 1 h allows high mechanical resistance and good magnetic properties (Br/Bs,Hc,ms) in the maraging steel 300. The material chosen for the research is a 20 mm · 10 mm · 2.5 mm sheet samples of maraging 300 steel, whose composition is given in Table 1. Specimens were solution treated at 900 C ± 10 C for 40 min, followed by cold rolling with true deformations 0.85 and 1.61. Some samples were solution treated and aged, and others were aged without solution treatment after deformation. Precipitation hardening curves of the maraging 300 steel aged at 440, 480, 510 and 560 C.

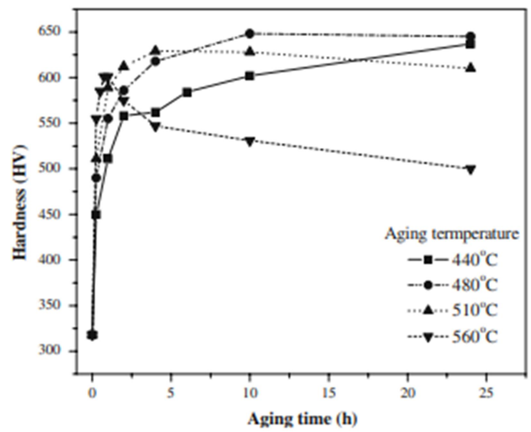

Figure 5: Hardness Vs aging time at 440, 480, 510 and 560 C

The aging at 560 C for 1 h allows high mechanical resistance and good magnetic properties ($B_r/B_s, H_c, m_s$) in the maraging steel 300.

Bortoleto et al. presented an experimental and numerical analysis of dry contact pin on disk test This work presents a computational study based on linear Archard's wear law and finite element modeling (FEM) to analyze the un lubricated sliding wear is observed in typical pin plate tests. Such was modeling developed using finite element software ABAQUSS with 3-Ddeformable geometries of contact surfaces and behavior of elastic-plastic materials. The Archard wear model was implemented as a FORTRAN user subroutine describes sliding wear. Waste modeling and oxide formation mechanisms were taken into account using global friction factor obtained from experimental measurements.

Xinmin et al. use pin-on-disk, they study the properties of tribology sintered compared to conventional steel gear materials and simulates the sliding part contact of gear teeth in boundary and mixed lubricated areas, cf tribological properties of two sintered box materials with those of the standard equipment material. The comparison looked at damage mechanisms, wear and tear between these materials in different configurations (i.e. standard vs standard, sintered vs sintered and sintered vs standard). In RS-PM combinations, Mo contacts appear higher wear resistance than AQ needles because their pores are larger and more numerous allows good lubrication. The pin for the Mo-RS combination were the highest wear resistance, mainly because the pores of Mo plates hold lubricant, lubricant to the contact surface and prevents adhesive wear. RS pin of Mo-RS combination and AQ pin in RS-AQ, the damage mechanism is slightly sticky attrition For PM-PM, RS-PM, AQ-RS and RS-RS contacts in combinations, the damage mechanism is more severe abrasion-type adhesive wear coefficient of friction. In PM and RS combinations, both PM contacts have a smaller.

G. Casalino: Selective Laser Melting (SLM) is an Additive Manufacturing process (AM) that built parts from powder using a layer-by-layer deposition technique. Maraging steels are also age-harden able in the 400–650 1C temperature range. The aging below 450 1C produces ordered and coherent phases in a martensitic matrix. The experiments showed that parts with a relative density as high as 99% can be built and that ρr% increases with the energy density. Parts with the relative density higher than 99% had a very low porosity that presented closed and regular shaped pores. The pores diameters were smaller than 30 μm. High level of the relative density improved the tensile properties and the fracture behavior in terms of a higher ductility.

Verma et al, Brake pad disc system: wear mechanisms and wear development fragments Tribological phenomena occurring in braking systems are interesting even in aspects other than the braking function. One important thing, that is In recent years, the importance of the environment has grown the effect of wear residues during braking. In this context, the present moment research focuses on the tribological behavior of a commercial friction pad material dry sliding against the cast iron plate. Pin-on-disk tests were performed in the room temperature under light wear conditions according to load and speed. The effect of some components of the pad material, especially copper the dynamics of the formation of the tribological layer and wear debris are presented. The results were obtained in this way, although we refer to a much simpler system that slows down systems, can still provide interesting references, for example by consideration development of new brake pad materials and brake control systems.

EA Jägle (2014): Materials produced by selective laser melting (SLM) experience a thermal history that is markedly different from that encountered by conventionally produced materials. The material was obtained in powder form from LPW Technology Ltd. (Runcorn, Cheshire, UK) and was processed using a Concept Laser M3 SLM machine (Lichtenfels, Germany) using a layer thickness of 30 lm, a laser scan speed of 150 mm/s, and a scan spacing of 112 lm. The microstructure of the maraging steel after the additive manufacturing process is shown in Fig. 1(a) as a light-optical micrograph and in Fig. 1(b) as a scanning electron micrograph.

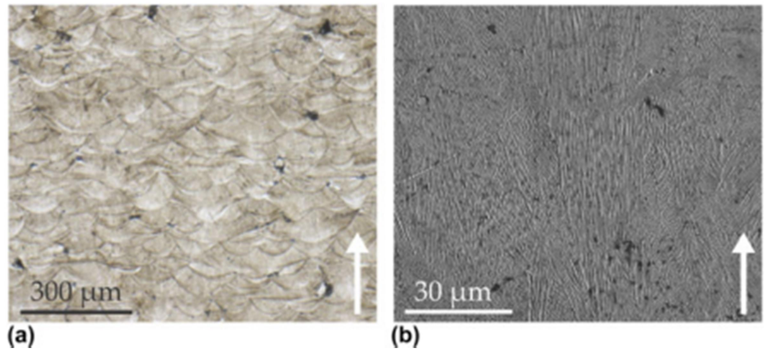

Figure 6: LM and SEM micrographs of an etched cross section of the material

The researcher investigated the microstructure of Co-bearing maraging steel (Fe–18Ni–9Co–3.4Mo–1.2Ti) produced by SLM in the as-produced and in the peak-aged state by electron microscopy and APT.

Yucong Wang et al. Describes in his study a fast and repeatable wear test using genuine piston rings and engine sections of cylinder diameters with custom contacts for tribological determination characteristics of the sliding contact between the piston edge and the cylinder bore counter surface Saturn 1.9L L-4 engine parts used for wear simulation tests. Two reciprocal bench test machines were used in the evaluation tribological behavior of coated piston/bore materials. Simulate movement pistons against the cylinder bores while the engine was running, test pieces were cut pistons and cylinder liners so that the piston edge matches the cylinder on the wall The cylinder bore was in place during the wear and friction tests. The following test conditions were used to simulate normal wear and tear: duration - 20h; temperature - 125◦C; stroke- 6.77 mm; frequency - 10 Hz; load - 120 N; to experiment lubricant - SAE 5W-30 and quantity - 8 ml (for wear test only). Collection of data 21 the system monitored the coefficient of friction, the contact potential (or elect contactor resistance) and changes in test parameters such as temperature.

Guicciardi et al. (2002): performed ten pin-on-disk sliding wear tests for each test conditions were performed with commercial tungsten carbide (WC) pins into silicon carbide (SiC) discs to determine wear and friction data variance The tests were repeated at two sliding speeds (v), 0.1 and 1.0 m/s. and two applied loads (P), 5 and 50 N. The wear data showed degradation between 28-47 and 32-56% for plate and pin. to disk, dispersion decreased as both sliding speed and load increased; for pin, no clear connection found. Friction values range between 5– With 15% less dispersion under heavy loads, regardless of slippage speed from a statistical point of view, it was found that in all experimental about 20% of wear and friction values can be considered under approved conditions deviations

P. Prabhu Elemental analysis usually ignores wear and surface changes due to wear. However, attrition can be significant all structures exposed to repetitive loading and can be critical for certain tribological applications including compaction potential prediction surfaces This article proposes a procedure to reduce the effect of attrition calculate and include in the general analysis of the structure. that of Archard the equation is used to calculate the wear used for conversion elastic deformation of the element in a clear way. Extensions of the theory are also suggested and example using wear control clear creep together

XQ Wang, 2016: Samples of laser powder bed processed AlSi10Mg have been examined using scanning electron microscopy (SEM), transmission electron microscopy (TEM), and scanning TEM so that the complex microstructures of as-fabricated samples could be characterized. The powder used and the details of the powder bed technique used to produce samples have been described earlier and will not be repeated. The observations reported in the researcher's paper cover two areas, which will be discussed in turn; firstly, the microstructure of as fabricated samples and secondly, the role of the Si particles within cells and of Al-Si boundaries in limiting dislocation path length. Micro diffraction in TEM at a spatial resolution of 10's of nms is essential if the microstructures of as-fabricated SLM samples are to be characterized. The heterogeneous microstructure, varying between columnar and equiaxed would be expected to lead to local differences in strength if the distribution of the Si particles and the Al-Si eutectic is different in different regions, which presents a challenge to this technology if critical components are to be produced.

Imam Syafa et al. conducted an experiment in which two surfaces were joined, the deformation occurs in the uneven plane. Distribution of local pressure and the deformations of the contact surfaces are important from the point of view of wear. The paper describes a wear model to predict the wear of rough sliding contacts. The wear model is based on the general wear equation of Archard combined finite element analysis (FEA). Roughness is represented in this article uniformly distributed spherical asperities. Offered model, in FE combination Archard's law of wear has proven to be an effective tool for predicting wear rough surfaces.

LN Carter, (2016): Specimens of Selectively Laser Melted (SLM) CM247LC powder have been characterized using analytical scanning and transmission electron microscopy. In our recent SLM work on AlSi10Mg, it was shown that Al (with very little Si in solution) forms cells which, in this near eutectic alloy, leads to the production of a high volume fraction of the Al-Si eutectic liquid which is formed mostly at cell (and grain) boundaries, but a significant amount is trapped at the liquid solid interface leading to sub cells within the long cells, delineated by regions of Al-Si eutectic. TEM and STEM analyses of the microstructure in SLM-processed CM247LC have focused on the effects of the rapid cooling associated with SLM on the microstructure and tensile strength.

S. C. Lim: Developed a wear map model, this article provides a summary culminating in the author's personal view of the development of wear mechanism maps in the introduction to some recently proposed cards. These cards that show wear data graphically, can give a more general picture of how Relatively mobile materials behave under different sliding conditions exposed; they also provide relationships between different dominants wear mechanisms occurring under different sliding conditions 20 and expected level of attrition. Some thoughts on future directions research in this field is also presented

D Grzesiak, (2019): The article presents the influence of the type of reinforcing phase (micro and nano crystalline titanium carbide) and temperature of conducted tests, on the mechanical properties of a 316L stainless steel based metal matrix composites, made additively by the Selective Laser Melting technology. The samples were compared by testing their compression strength at temperatures in the range of 25–1100 °C. The preparation of specimens involved two materials in the form of powder: gas-sprayed 316L stainless steel (average particle diameter of 45 lm, spherical shape) and titanium carbide (particle size of 1 mm – mTiC and 50 nm – nTiC). The 316L steel was mixed in a ball mill with TiC, with a concentration of 2.5 vol% and 15 vol%. Milling procedure was described before.

R. Novak and T. Polcar, (2014): Analyzed the friction uncertainty in detail coefficient measured with a standard needle-on-disk device and the like degree of coating wear. Application of the method to two large populations is then reported substrates, one coated with titanium nitride (TiN), the other coated with hydrogen diamond-like carbon coating (DLC). Let's find out the most important ones contributes to the overall measurement uncertainty, which can help either redesign the test procedure to reduce the measurement uncertainty, or simplify it by ignoring some parameters. We show this estimate uncertainties can help distinguish the variation of a random value from the real one trends (ie the dependence of the measured values on the selected variable or set variables).

Marcisz, 2017: Ultra-high strength MS350 maraging steel achieves tensile strength at the level of 2400 MPa and yield strength of 2300 MPa at total elongation ca. Research material was manufactured in laboratory conditions. Ingots of cross section 60x150 mm and weight ca. 70 kg of MS350 maraging steel (18Ni350) were melted in vacuum furnace and cast into molds. Chemical compositions of laboratory heats are given in Table 1. The ingots were subjected to homogenization heat treatment at temperature of 1250°C during 24 hours in argon atmosphere.

Table 2: Chemical composition of examined material (MS350 maraging steel), weight%

Heat no	C	Mn	Si	P	S	Ni	Co	Mo	Ti	$Al_{tot.}$
1	0.007	0.05	0.02	0.010	<0.01	18.0	12.8	4.6	1.6	0.01
2	0.007	0.05	<0.05	0.007	<0.01	18.0	13.1	4.5	1.8	0.02
3	0.008	<0.05	<0.05	0.008	<0.01	18.1	12.8	4.2	1.8	0.02

Ageing of maraging steel in temperature range 400-550°C for short-time (from 15 to600 seconds) was conducted in a Gleeble 3800 simulator. Based on the results of mechanical properties measurements variants for examination of microstructure using transmission electron microscope Titan 80-300 were selected. Results of mechanical properties determination after short-time ageing have shown that this type of heat treatment of MS350 maraging steel enables achievement of strength at the level reached after standard ageing however at higher ductility and impact toughness. For optimum variants of short-time ageing from the combination of strength and ductility point of view the following properties were achieved: YS = 1900-2150 MPa; UTS = 2100-2250 MPa; A = 7-8% and notch impact toughness KV = 20 J/cm2 at temperature minus 40°C. Microstructure after short-time ageing is composed of martensitic matrix of high density of dislocations and dispersed precipitates of intermetallic phases of rod-like shape. Ni3Mo precipitates have been identified in the material subjected to ageing at temperature of 550°C. Length of precipitates reaches ca. several dozen nanometers and dimensions of cross section below 4 nm.

Zmitrowicz: Published the article "Uses and attrition rules: an overview" and proposed that wear is a process of gradual removal of material surfaces of contacting and sliding solids. There is damage to the contact surfaces the effects of wear and tear. They can have different patterns (friction, fatigue, plowing, surge, erosion and cavitation). The effects of abrasive wear are recognized irreversible changes in body shapes and the formation of gaps between them in contact with solids. The surface wear depth profile is a useful measure removed material. The definition of the gap between the organs of touch is considered 18 taking into account the deformations of the parts and the evolution of the wear profiles. Depth of consumption can be estimated using the wear laws. Derived from this study, constitutive the anisotropic wear equations are extensions of Archard's wear law. The equations describe the friction of materials with microstructures. Illustrative the example shows calculations of frictional mass and temperatures stack-disk test device.

Nohava, J et al- 2015: Pin-on-disk tribological tests were performed at temperatures in between room temperature and 800°C, and the results compared to a conventional AlTiN coating. The typical morphology of the wear tracks on the nitride and ox nitride samples was characterized by two features: material removal and build-up. The hollowing out was created due to erosive material removal during the wear tests while build-up was mainly due to re deposition of the wear debris originating from the displaced material from both the wear track and the alumina ball. The superior wear resistance of this oxide coating was due to the nitrogen-free, purely oxide composition and its stable alpha-alumina structure, which hindered high temperature oxidation and subsequent severe wear. EDX and SEM analyses of FIB cuts into the wear tracks showed that even if coating adhesive failure could be ruled out, the wear mechanisms especially at high temperatures are still very complex and characterization of wear resistance cannot merely be based on the wear track profile and calculation of the volume of material removed.

Sharma et al. The work focused on the disc tribometer pin, which is advanced tribometer that accurately measures friction and wear combination of metals and lubricants at selected loads, speed and conditions temperature the used model runs at very low rpm with a stable sliding speed and a fixed radius of the wear circle. Data collection includes maximum depth penetration and special wear on both aluminum and mild steel. Precisely attrition rate is calculated; wear resistance helps determine wear resistance offered by the metal under working conditions. This study is related different aspects (friction coefficient, wear model, lubrication test, result diagrams) obtained with a disk tribometer.

V Tirth, 2018: AA2218–Al2O3(TiO2) composites are synthesized by stirring 2, 5 and 7 wt% of 1:2 mixture of Al2O3:TiO2 powders in molten AA2218 alloy. T61 heat-treated composites characterized for microstructure and hardness. Dry sliding wear tests conducted on pin-on-disc set-up at available loads 4.91 N to 13.24 N, sliding speed of 1.26 m/s up to sliding distance of 3770m.

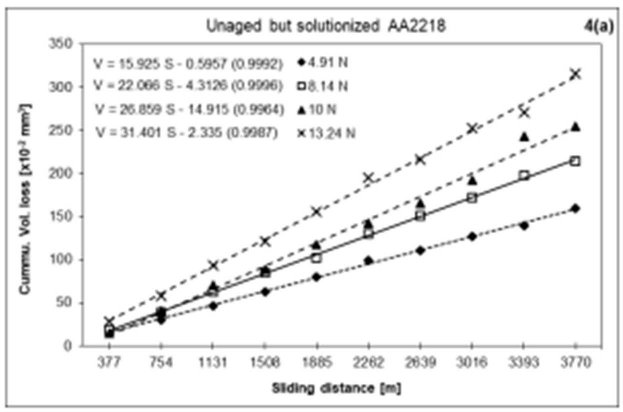

Figure 7: Cumulative volume loss Vs sliding distance at loads 4.91, 8.14,10 and 13.2N under sliding condition; un-reinforced, solutionized AA22218

In the present study, T61 aged gravity cast AA2218- Al2O3(TiO2) hybrid (in-situ + ex-situ) composites are developed by stir casting and the effect of aging and particle reinforcement on wear behavior is reported in the light of synergy between microstructure, hardness, wear rate and surface characterization of worn surfaces. Particles retained and porosity content is also measured and reported.

PriitPodra, Soren Andersson: Performed a sliding wear simulation with finite element method; wear of parts is often a critical influencing factor product life. Therefore, predicting attrition is an important part of planning. Use a simulation method using commercial finite element (FE) software ANSYS is presented in this document. The modeling and simulation procedure is with linear wear law and Euler integration model proposed and used. However, the validity and quantification of the model must be monitored convergence of solutions. Spherical pin plate lubricated steel contact was analyzed both experimentally and with FEM and Lim and Ashby wear maps used to identify the wear mechanism.

A Edacherian : Several challenges stand in the way of the production of metal matrix composites (MMCs) such as higher processing temperatures, particulate mixing, particulate–matrix interface bonding issues, and the ability to process into desired geometrical shapes. Tribological wear can be assessed either by ball-on disc type tribotesters or by using pin-on-disc tribometers. In this study, cylindrical wear pins were prepared from three different sections of the composite castings to conduct wear test under dry sliding test conditions in compliance with ASTM G-99 standards using a pin-on-disc tribometer.

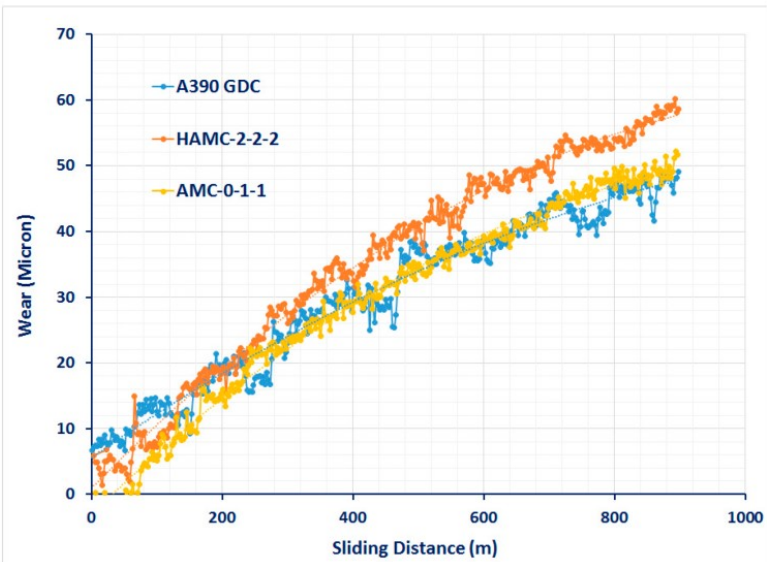

Figure 8: Wear behavior (computer generated) of a few test samples

The results obtained from computerized wear tests (wear height (μm) at various sliding distance (m)) were very sensitive to analyze and to understand the performance of each samples. Hence, to appropriately evaluate the wear property, a weight loss method was devised. The wear study proposes that predominant wear mechanisms in HAMCs are brittle fracture due to two and three body abrasion of dislodged SiC, Gr, and MoS2 particulates, and the resulting fatigue and micro-cracking of MML. The HAMCs exhibited better dry sliding wear behavior than die cast A390 matrix alloy, indicating enhanced tribological characteristics of HAMCs with soft phase constituents such as Gr and MoS2 in the presence of hard phase reinforcements like SiC.

E.M. Bortoleto et al, (2013): Analyzed T1 considering the displacement of the wear system pin in plate system and two different steels in dry contact. The analysis was done and by numerical simulation (FEM) and experimental tests. Attach to the plate tests were performed without lubrication according to ASTM G99-05, which describes the sample geometry and preparation conditions. The experiment was carried out for 3600 s, which corresponds to a distance of 360 m. Normal load varied from 5 to 140 N, with 5 repetitions for each load condition Friction coefficient values were determined by the ratio between 22 friction load and applied normal load. Mass variability was determined measurements were made on a scale with an accuracy of 1e-5 g. Creates a generic FEM model capable of more complex wear prediction geometric systems using input parameters obtained from experimental wear tests.

Y Ohue, 2007: Gears in power transmissions have been required the higher surface durability and higher wear resistance. In this study, maraging steel was used to increase the reliability of the gears from the viewpoint of the surface durability and the wear resistance. The mechanical properties of the maraging steel are superior to those of the steel. The maraging steel was surface-hardened by ion-nitriding instead of aging. The conditions of ion-nitriding are shown in Table below. The heating temperature and time are almost the same as those of aging.

Table 3: Ion-nitriding conditions

Heat treatment	Ion-nitriding
Heating time	803K x5h
Pressure	399Pa
Gas component	N_2:H_2=2:1

To provide fundamental understandings on the surface durability and the wear resistance of the maraging steel, the sliding–rolling contact fatigue tests were conducted using a two cylinder testing machine. In these tests, the fatigue strength of aged Maraging steel was compared with that of alloy steel with case-hardening. Furthermore, the surface durability of the nitrided Maraging steels with fine particle shot-peening was investigated.

Johansson et al. Works related to a method that can simulate the real behavior of the engine at the limit and mixed lubrication methods to minimize friction losses and wear. This the work focused on the development and research of test equipment methodology current and future candidate materials. Using actual production components (as opposed to simplified geometries) that include the correct surface morphology, coating thickness and material composition is the best comparison of components to real engine tests done However, this was not possible in the simplified tribometer test use the same speeds, loads and temperatures as in the engine. The So the goal was to find a parameter with which to compare the contact of the upper part piston ring vs cylinder liner in engine and tribometer.

You Wang et al: Evaluated the wear resistance of ceramics surface coatings with diamond abrasives. They used plasma spray technology layer coatings with regenerated nanostructured Al_2O_3/TiO_2 powders. The abrasive wear tests were performed using a modified grinding/polishing machine. Wear frequencies (wear rates) are calculated using the average measured value three samples as the amount of material removed per unit load and sliding distance against the diamond grinding pad.

SR Lewis, 2012: This paper presents results of testing carried out to assess the tribological and fatigue performance of various laser cladding materials to establish if they could be potentially be used to repair rail. Wear was measured by weighing the discs before and after each test. The only consistent wear rates are shown by the satellite samples which also show the lowest rail wear rate with an average of 2.55μg/cycle. This compares favorably with the 2.77 μg/cycle given by the reference sample. The Stainless and Hadfield steel samples showed the least consistency in wear rates. However, the test duration of 5000 cycles was not enough for steady state wear to be achieved in some of the samples for example Maraging steel which work hardens and therefore may give a lower wear rate with time.

The biggest discrepancy between wheel and rail wear rate is again seen with both the Stellite 6 samples. In the fatigue tests the Maraging samples both showed almost equal wear rates between the wheel and rail. During the fatigue tests the dry stage was too short for traction to reach its steady state value and therefore dry values are not comparable between wear and fatigue tests. The Table below shows that the average traction coefficient was higher for the fatigue tests. However, this average value incorporates the initial rising part of the traction curve where the traction is rising from zero to its steady state range.

Table 4: Average wet Traction coefficients

Material	Wet traction	
	Wear	Fatigue
Baseline 260 Grade	0.15	0.22
Hadfield 1 Layer	0.18	0.20
Hadfield 2 Layers	0.20	0.22
Stellite 6 1 Layer	0.19	0.21
Stellite 6 2 Layers	0.17	0.22
Maraging 1 Layer	0.20	0.20
Maraging 2 Layers	0.19	0.20
stainless 1 Layer	0.21	0.24
stainless 2 Layers	0.20	0.23

Finally, under wet conditions; Hadfield, Stellite 6, Maraging and 316 Stainless claddings show traction levels similar to the 260 Grade reference materials. Wheel wear rates were higher for all of the clad discs compared to the reference wheel wear in the wet tests. In the dry conditions all but two of the clad samples showed higher wheel wear than the reference case.

2.2. Research Gap

Wear tests were carried out by considering different process parameters, identified from the published literature on different materials such as Fe30Ni20Mn25Al25, Ni– Ti [23], Fe–Ni–Cr alloy, and iron powder. A different surface is known among the literature review modification techniques were studied. In this study, a new surface modification techniques that this hardened and tempered technology An efficient and economical way to make finely tempered martensite free of ferrite and fine dispersion of alloy carbide unchanged chemical composition. Therefore, it is assumed that the changed surface Maraging steel substrate can be useful to improve the strength, Tribological properties and adhesion of Maraging steel coatings.

CHAPTER THREE

3. MATERIALS AND METHODS

This chapter describes the materials used by the researcher for the study and methods used to have the results those indicated and discussed in the next chapter. The materials include different machines, measuring tools and methodology for the results.

3.1. MATERIALS

A model fabrication of PIN on DISC Wear Test Machine, items/materials such as Electrical motor, sheet mild steal, square pipe for supporting stand & Arm of the PIN Holder, hardened steel/high carbon steel/ bronze solid pipes for test, EN Steel Disc, L-Shaped Angular Strips, Corner Bracket, Support Plates, Steel Ruler, Rotary Torque Sensors, Accelerometer, Electrical Accessories, Electric Motor Belt, Speed Tachometer & LVDV are needed. The figures below are the image of wear test machine captured from Addis Ababa Science and Technology University (AASTU).

Figure 9: photograph image of real manufactured PIN on DISC wear test machine

3.1.1. Sample preparation

On the Pin on disc machine that the present test done the sample holder size extent must be 6mm diameter and 12mm of height to touch the Disk, therefore to take an experimental wear test the material to be tested had cut in to 9 samples. The instrument used for the measuring the sample height and diameter is a Varner caliper. The figure below shows process of resizing the samples for the PIN on DISC wear test machine.

Figure 10: Sample preparation

3.2. METHODOLOGY

3.2.1. MATHEMATICAL MODEL

Numerical analysis is the study of the algorithms used numerical approximation of mathematical analysis problems. These problems usually arise from real-world applications of algebra and geometry and count and contain variables that change continuously; this problem is ubiquitous in the natural sciences, social sciences, engineering, medicine, and business. In the problem of the wear rate analysis, it have been used Minitab to solve.

Regression Model

The projected value for WR in mm^3/m may be estimated using regression equation and analysis of variance, given by Eq. [1]

$$WR = 46 - 7.8\ Load - 0.044\ Speed + 0.453\ Load*Load + 0.000183\ Speed*Speed - 0.0020\ Load*Speed \ldots \text{(a)}$$

WR = 57 - 7.8 Load - 0.044 Speed + 0.453 Load*Load + 0.000183 Speed*Speed - 0.0020 Load*Speed… (b)

WR = 78 - 7.8 Load - 0.044 Speed + 0.453 Load*Load + 0.000183 Speed*Speed - 0.0020 Load*Speed… (c)

Where for (a), (b) and (c) time is 10, 12 and 15 min respectively.

Regression equation for wear Eq. [1]

Short Description of the Wear Testing Machine

Electric motor to drive spindle & chuck for holding the revolving disk, Rotary Torque Sensors, Speed Tachometer (Accelerometer), Electrical Accessories, a lever-arm to hold the pin, and attachments to allow the pin specimen to be forced against the revolving disk specimen with a controlled load. The pin on disk wear testing equipment presses a stationary pin or ball against the revolving disk. Measure the wear rate, wear volume, friction force, coefficient of friction (COF), and several other tribology data.

3.2.2. Technical Specifications

✓ Normal load range -	Up to 200 N
✓ Frictional force range -	Up to 200 N0
✓ Disc diameter -	Ø165 mm (Max)
✓ Disc track diameter -	10 to 140 mm
✓ Disc speed -	100 to 2000 rpm
✓ Pin Length -	9 to 12 mm
✓ Pin diameter -	Ø5.7 mm to Ø6 mm
✓ Wear measurement (LVDT) -	±2 mm
✓ Pre-set timer range -	up to 100 Hours

3.2.3. Wear Tests

Wear tests carried out by considering different process parameters, identified from the published literature on different materials such as Fe30Ni20Mn25Al25, Ni– Ti, Fe–Ni–Cr alloy, and iron powder. After the tests, these parameters will be optimized to obtain minimum wear. 3DP specimens will be tested for wear using Pin/Disk test rig in sliding condition (dry) in conformance with ASTM G99. The results obtained experimentally will be optimized and validated with regression analysis. ANOVA and interaction plots are going to be used to determine the wear behavior of 3DPMS. The wear pin specimen was held against the rotating disc made from EN-31 steel with a track diameter of 20 cm. The specimen pin becomes forced over the rotating counter face (disc) by a normal load system. The wear tests for the specimens were will be conducted under different normal loads, sliding distance, and sliding velocity. The pin surface and the counter face then become cleaned with acetone intermittently.

The WR was determined as volume loss per unit distance of sliding. The cleaned specimens were weighted using Toledo balance (accuracy±0.1 mg). The procedural steps for making wear test of specimens developed by the DMLS process in this is. The first step is to develop a 3D model with the help of LS-DYNA software. WR in dry sliding conditions, W in mm^3/m, may be expressed by rearranging the Archard's equation given in Eq. (1)

Where: v_w is wear volume (mm^3), and s_d is distance of sliding (m).

$$\boldsymbol{w = \frac{v_w}{s_d}}$$

The WR of the sliding pin will be estimated by volume loss divided by distance of sliding. Weight loss of specimen is going to be determined by measuring the weight of the flathead pins after and before the tests. The curve fitting, optimization, and experiment design procedures are going to be done using Minitab software.

- ❖ Simple calculations have been done such as:

✓ ***Determination of wear rate (WR) for all 9 samples***

(Wear rate, WR) (mm^3/mm) = Wear volume (mm^3) / Sliding distance (mm)

$$\boldsymbol{w = \frac{v_w}{s_d}} \qquad \text{Eq 2: Wear rate}$$

✓ ***Determination of wear coefficient***

Wear coefficient = volume lost (mm^3) * surface Hardness (N/mm^2)/ Force(N) * total rotating distance(mm)

$$\boldsymbol{k = \frac{w*H}{F*St}} \qquad \text{Eq 3: Wear coefficient}$$

- ✓ ***Determination of wear volume (volume lost)***

(Wear volume, *w*) (m^3) = weight loss (kg) /density (kg/m^3)

$$\boldsymbol{w} = \frac{\boldsymbol{m_{loss}}}{\rho} \quad \text{Eq 4: Wear volume}$$

- ✓ ***Determination of specific wear rate***

Specific wear rate (mm^2/N) = wear volume / load * sliding distance

$$WR_{specific} = {}^{\boldsymbol{w}}/_{\boldsymbol{F} * \boldsymbol{s}} \quad \text{Eq 5: Specific wear rate}$$

- ✓ ***Determination of Weight loss***

$$\text{Weight loss} = \boldsymbol{m_b} - \boldsymbol{m_a} \quad \text{Eq 6: Weight loss}$$

Where: m_b= weight of a sample before wear, m_a= weight of the sample after wear

The average value of the weight loss percentage as a function of test time will be calculated using the equation below. From weight loss of the specimens (Δm) it is possible to evaluate a dimensionless parameter known as w, "wear rate" define by Archard's equation:

$$W = \frac{\Delta m}{\rho.v.t.A} \quad \text{Eq 7: Archard's equation of wear rate}$$

Where: ρ = average density of material, t = test time (s) and A = apparent contact area (mm^2).

3.2.4. Test Specimens and its Preparation

I. **Materials:-** This test method may be applied to a variety of materials. The only requirement is that specimens having the specified dimensions can be prepared and that they will withstand the stresses imposed during the test without failure or excessive flexure. The materials being teste shall be described by dimensions, surface finish, material type, form, composition, microstructure, processing treatments, and indentation hardness (if appropriate).

II. **Test Specimens**:- The typical pin specimen is cylindrical or spherical in shape. Typical cylindrical or spherical pin specimen diameters range from 2 to 10 mm. The typical disk specimen diameters range from 30 to 100 mm and have a thickness in the range of 2 to 10 mm.

III. **Surface Finish**:- A ground surface roughness of 0.8 µm (32 µin.) arithmetic average or less is usually recommended. Care must be taken in surface preparation to avoid subsurface damage that alters the material significantly. Special surface preparation may be appropriate for some test programs. State the type of surface and surface preparation in the report.

IV. **Test Parameters for wear tester machine**

- ✓ **Load**:-Values of the force in Newton at the wearing contact.
- ✓ **Speed**:-The relative sliding speed between the contacting surfaces in metres per second.
- ✓ **Time**:- How long does the Pin rotates on the Disc in second, Minute and hour.
- ✓ **Distance**:-The accumulated sliding distance in meters.
- ✓ **Temperature**:-One or both specimens at locations close to the wearing contact.
- ✓ **Atmosphere**:-The atmosphere (laboratory air, relative humidity, argon, lubricant, etc.) surrounding the wearing contact.

The wear measurements will be reported as the volume loss in cubic millimeters for the pin and disk, separately.

Using the following equations for calculating volume losses when the pin has initially a spherical end shape of radius R and the disk is initially flat, under the conditions that only one of the two members wears significantly:

$$pin\ volumr\ loss, mm^3 = \frac{\pi(wear\ scar\ diameter, mm)^4}{64(pin\ radius, mm)}$$

$$disk\ volume\ loss, mm^3 = \pi\frac{(wear\ track\ radius, mm)(track\ width, mm)^3}{6(sphere\ radius, mm)}$$

Procedure for the Wear Test:

1. Clean the surface of disc and the specimen (brass, aluminium)
2. Weigh the specimen accurately by using electronic weighing machine (W1)
3. Fix the specimen (pin) on the horizontal arm and measure the track radius by a scale. The specimen should be in contact with disc.
4. Switch on the motor and note the speed of the (rpm) on the indicator.
5. Load the specimen and note the force.
6. Run the motor for a specified time interval (say 15min). Switch off the motor.
7. Clean the specimen and weigh the same Note down the final weight (W2).
8. Calculate the total sliding distance for the specified running time.
9. Repeat the experiment for different rpm, load and material.
10. Wear rate is calculated by using the equation

3.2.5. Simulation Method

LS-DYNA is a finite element program used for e.g simulations of a real engineering problem. The software uses three different ones stages which are pre-processing, solving and post-processing to solve the problems. There are ten modules in this software. The preprocessing step includes geometry creation and FEM model preparation, element type definition, Material properties and interactions. In the solution phase, LS-DYNA software creates mesh, which describes the behavior of each node and element, computes unknown values of output field variables such as total tension, tension-strain induced, friction behavior, pressure distribution, wear rate, contact pressure, and so on. In the post-processing phase, it is rendering. At this point the results can be analyzed and plotted.

LS-DYNA is software used for both modeling and analysis mechanical components and assemblies (pre-processing) and visualization of the end the result of finite element analysis. It is a general purpose finite element analyzer use an indirect integration system. It runs as a background process and works actual numerical calculations. After the simulation is finished, the results can be monitored in the post-processing phase. LS-DYNA is also used to view, plot and process data.

Assumptions

A general assumption that helps to simplify and reduce the simulation process of contact mechanic on LS-DYNA software. The guessing begins model the wear analysis with software using the disc model instead point of contact between contact line and pantograph.

The assumptions used to simulate attrition in this thesis are as follows LS-DYNA software analysis.

- ✓ The assembly contact between the pin and the disk is a friction contact option of LS-DYNA without any clearance.
- ✓ The analysis performed is non-linear.
- ✓ Analysis of modeled elements is considered as rigidly flexible contact where one element of the model is taken as fixed and the other as rigid and vice versa.
- ✓ Model validation helps support and transfer the load to the analyzed model
- ✓ The contact behavior of the modeled elements is considered asymmetric

- ✓ The Contact formulation used in Augmented Langrage.
- ✓ The stiffness value used is 0.1.
- ✓ The analysis is performed by assuming the deflection of the modeled elements is small and neglected.

Method of Wear simulation

To carry out the wear simulation, a contact analysis is performed using LS-DYNA software the following main steps:

- ➢ Select if contact analysis is in LS-DYNA parametric design Language (APDL) or Workbench in this paper carries simulation done in LS-DYNA Workbench
- ➢ Create model geometry and mesh
- ➢ Identify the contact surfaces and materials used for each part of the model
- ➢ Define solution options
- ➢ Use boundary conditions and normal force and rotational speed disk pin is for disk simulation
- ➢ Solve the contact problem.

Geometric Modeling

Two solid models are to be created in this module, which are pin and disc.

The assembled model of pin and disc setup will as follows.

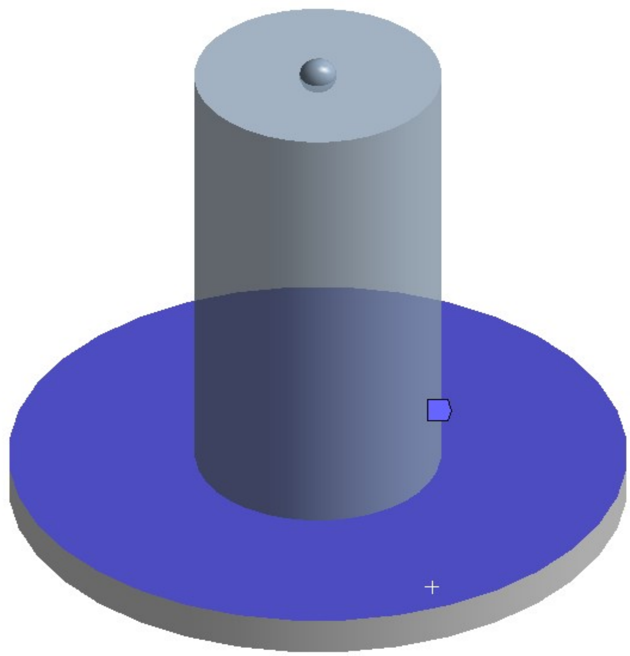

Figure 11: Geometrical Modeling

Dimension of Pin

- Diameter: 6 mm
- Height: 12 mm

Dimension of Disc

- Diameter: 18 mm
- Thickness: 2 mm

Properties of PIN and Disc materials:

Table 5: Properties of PIN and DISC Materials

Properties of material	Material properties of the PIN	Material properties of the Disc
Young's Modulus	200Gpa	200GPa
Poisson's Ratio	0.3	0.3

Shear Modulus	76Gpa	76GPa
Bulk Modulus	166GPa	166GPa
Density	7850Kg/mm^3	7850Kg/mm^3
Expansion Effect	1.2x10^{-6}m/mK	1.2x10^{-6}m/mK

Connections

Pin and disc assembly have two main connector types. The Interfaces are defined as the interface surfaces of different types of assembly. There are different connections that can be configured to stimulate desired movement. In particular, we have two necessary connections define different contacts and common characteristics for them.

Contacts:

Contacts are mainly three types:

- ✓ Frictional
- ✓ Frictionless
- ✓ Bonded
- ✓ Rough

We use a frictional setting in our simulation. It generally means that keep COF below 0.3 for a faster and easier approach. In our contacts we used three different assumptions in our simulations:

- The Disc is rigid and the pin is flexible
- The pin is rigid and the Disc is flexible
- Both the Pin and Disc are flexible.

The Disc is rigid and the pin is flexible

Contact Type: We kept the board rigid and the surface flexible because we want to calculate the deformation of the pin itself. We chose friction contacts with very low COF and asymmetric behavior. Our findings the method is common for targeting on a per-node basis. We turned off the trim contact. These are all configuration parameters necessary for rapid approach.

Since LS-DYNA does not have a wear mechanism simulation module, it is present for this, it is necessary to develop external program code. The program can be added to implement the wear mechanism in LS-DYNA and later only. This command must be run to connect definition between pin and disc.

The programming language can be changed for LS-DYNA compatibility module used, even FORTRON, PYTHON, C++ and others LS-DYNA simply accepts programming languages. Code script PYTHON language is created here to simulate this problem manuscript. The same program can be modeled in other programming languages.

Mesh

Meshing is the creation of a polygon or polyhedral mesh that approximates geometric area. The term "network" is often used alternately. Typical uses are to image to a computer screen or for physical simulation such as finite element analysis. Three dimensional Meshes created for finite element analysis must consist of tetrahedral, pyramids, prisms or hexahedra. Those used for limited volume the method can consist of arbitrary polyhedral. They are used for limited separation methods should generally consist of piecewise structured arrays 48 hexahedra are known as multi block meshes. Moreover, the network is a discretization of a one-, two- or three-dimensional domain.

Structured Meshes

A structured network is characterized by regular connectivity that can be expressed as a two- or three-dimensional matrix. This limits the selection of elements quadrilaterals in 2D or hexahedra in 3D. The example network above is structured mesh because we could store the mesh as a 40 x 12 array. Regularity thanks to connections, we can save space from neighboring relationships defined in the storage arrangement. A further classification can be made whether the network is adaptive or not.

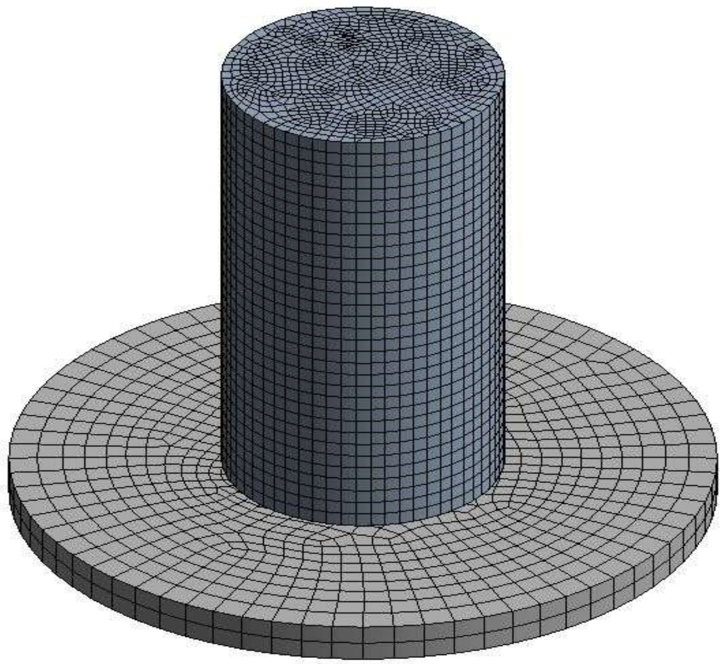

Figure 12: Mesh View

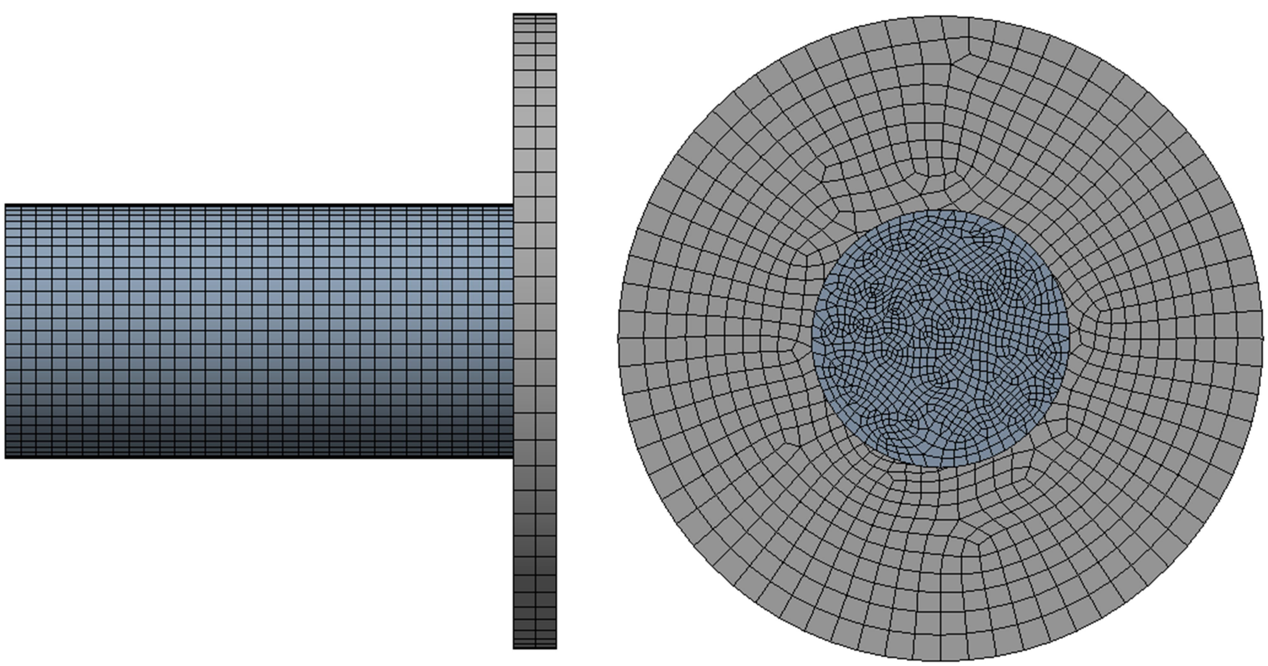

Figure 13: Side and top view Mesh

The mesh, often called adaptive mash refinement (AMR), refers to modifying an existing network to control flow characteristics. In general, these changes are aimed at improving stream resolution functions without excessive computing power. We are talking internally briefly about some concepts important in web adaptation.

Mesh adaptation strategies can generally be classified into one of three general types: r-refinement, h-refinement or p- refinement. There are also their combinations possible, for example hp-refinement and hr-refinement. Let's get these guys together detail below.

r-Refinement

Refinement is the modification of the mesh resolution without changing the number network nodes or cells or network connection. Update at the resolution is done by moving the grid points into the resulting work areas to a greater accumulation of points in these regions. Moving nodes can to lead differently. A common technique is to treat the network as if it were elastic solid and solve the shape-changing system equations (some forced) the original network. However, care must be taken to avoid overdoing it the grid will be distorted.

h- Refinement

h-refinement is the modification resolution of a mesh by changing the mesh connectivity Depending on the technology used; this may not make a difference in the total number of grid cells or points. The easiest strategy for this Refinement type divides cells into subgroups, while more complex operations can add or remove nodes (or cells) to change the general topology of the network**.**

p- Refinement

A very popular finite element modeling (FEM) modeling tool instead in finite Volume modeling (FVM), achieves better resolution by adding order of precision of the polynomial for each element (or cell). The pin and plate are taken as a dependent subassembly, so splicing must be done separately for both parts. And we element type of loading space select an element type with a hexagonal shape for both the pin and the Disc.

- ✓ Pin- Element shape- Hexagonal
  Geometric order- Linear

Number of elements-786

- ✓ Plate- Element Shape- Hexagonal

  Geometric order- Linear

  Number of elements-1454

Load and Boundary Condition

Boundary condition

The boundary condition is achieved to obtain data that is accurate and compatible with real conditions. Here the rounded outer surfaces of the pin are stopped from moving in the X and Z directions, so the value as zero. However, a freely given Y direction change allows the pin to move only in the Y direction. Then, the circular outer surfaces of the hollow disk are simultaneously released in the X and Z directions; the displacement in the Y direction is stopped by changing the value to zero to allow the movement of the hollow disk in the X and Z direction. We now analyze the wear of the shearing effect of the needle plate.

For simulation purpose a load 10N, 15N and 20N, and on force is applied on top surface of pin holder. Force 10N is taken as the lowest possible tension load condition. The above three load conditions are applied on pin and the analysis continues.

Rotational Velocity

The rotational speed is applied in the disc model; the tribometer disc rotates with a specified rotation speed provided by the electric motor installed in it. The rotational speed used in the model is the value that the Tribometer uses.

CHAPTER FOUR

4. RESULT AND DISCUSSION

4.1. EXPERIMENTAL SET UP

4.1.1. Design of Experiments for Wear Tests

The statistical response surface method (RSM) is a versatile method for experiment design using high quality orthogonal arrays that gives optimum control of process parameters during experiments with the least variance.

An integrated method is going to be used; to determine the performance, efficiency and high quality of design, which is economical in cost. An orthogonal array in RSM is then used to determine multiple interactions and the effect of all the parameters by reduced iterations. The main aim is to minimize the objective function by using the optimum values of these designed parameters. This is done by optimizing the parameters, by using RSM. The RSM includes the following procedural steps; identifying the aim and response of experiment, assessment of influential parameters and their measurement, identifying main factors that affect the response of experiments and possible interactions, selecting appropriate orthogonal array, deciding their levels, and assigning the factors at these levels in the design. Experiments were conducted for wear tests as per the results of orthogonal array and validation of the values with the experimental results. Regression analysis is employed to determine the association amid the dependent variable (WR) and the independent variables (speed, load, distance of sliding). Furthermore, ANOVA analysis is employed to verify their optimum values.

4.1.2. PIN on DISC wear test Result

Experimental result obtained from the Pin on Disc machine by using process parameters Load, Speed and Time each of them by different three conditions as illustrated in the table below. The experimental result obtained is by a graph as wear rate versus time, sliding velocity versus time Cof versus time and friction force versus time for all 9 samples. The wear (microns) versus time graph of smallest and largest wear of the samples is shown in the figure bellows.

Table 6: Wear test Conditions

Wear parameters	Value
Sliding speed, RPM	150, 375, 700
Sliding distance, mm	40,
Wear load, N	10, 15, 20
Temperature, °C	20
Material of the PIN	Maraging steel
Material of the disc	EN-31, bearing steel
Surface finish	0.8 µm Ra

The first test done for sample (1) as result in the figure below shows on the beginning the wear of the sample were even less than 0 in microns but on about 30 second time running for the experiment it starts to wear rapidly. Then as the smaller about 3.5 min the wear in microns were almost zero even if there is a fluctuation on the wear but it was increasing up to the final time 10 min as shown in the figure 14 .

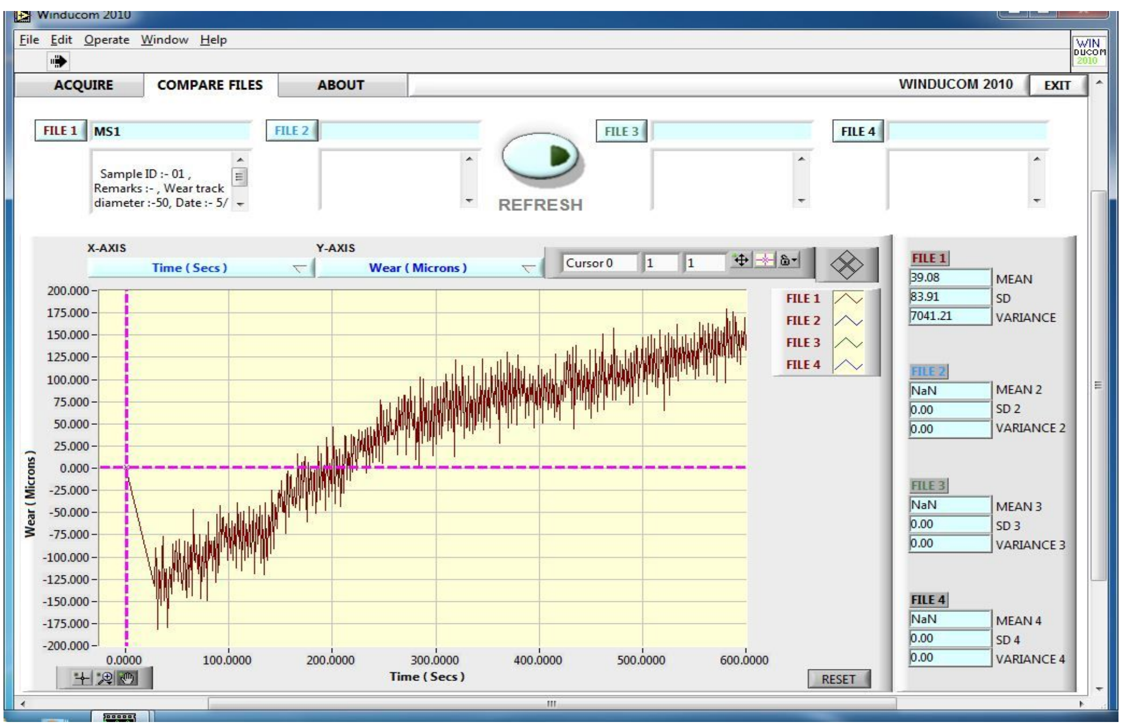

Figure 14: Wear versus time graph obtained from PIN on DISC test for sample 1

The first test done for sample (9) as result in the figure below shows even on the beginning the wear of the sample were about 100-150 in microns. Then up to about 5 min of the time running the wear were increase in a linear form without any up and downs as shown in figure 15. Then after 5 min it increases rapidly but within the up and down shown by graphical representation. By graph of wear in microns to time in second graph as shown below figure 15.

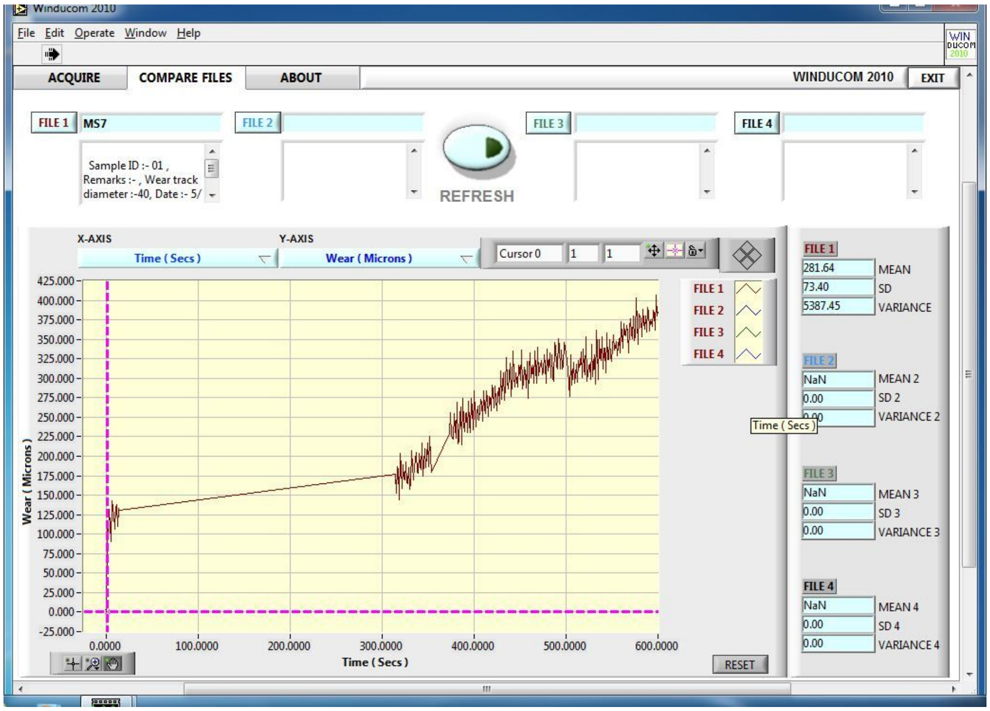

Figure 15: Wear versus time graph obtained from PIN on DISC test for sample 9

4.1.3. Scanning Electron Microscope Examination.

Material preparations for SEM were done in order to characterize the surface of the sample the samples should properly prepare for the micrographs. The maraging steel which machined for the wear test has been machined again for the SEM characterization. As shown in figure below the all samples height was reduced to 6mm from 12mm. figure 16 shows samples after being machined for the wear some are machined for SEM and the left to be machined.

Figure 16: Sample preparing for SEM

The SEM micrographs of Maraging steel after the wear tests at a magnification 0f 300x and 400x are shown in Figure 17 (a) at 50 μm and in Figure below at 100μm. The surface appears intact and sound. Layers are visible due to the signatures of additive, Maraging steel manufacturing process.

Worn surface of a sample after wear tests with optimal test parameters; load, 15 N, running time 15 min and speed 375 rpm is shown in Fig. 18 (a) at 400x magnification. Good wear marks are marked inside the circle, and worn groove laminations are marked with blue arrows. The SEM micrograph shows traces of the transfer layer with a huge piece of metal in the center that may have been released when the transfer layer broke. Wear can be seen in the form of a scratched surface that appears pale. A closer look shows faint signs of wear. There are no pores and cracks on the macro scale. The SEM image in Figure 18 (a) is a typical sign of wear-resistant material. Wear marks on the surface indicate abrasive wear. Fig. 18(b) shows the severe wear of the test parameters; load 20 N, working time 12 min and speed 700 rpm. The surface appears to be in a layer pattern, which is created by sintering the metal with different process parameters. Excessive wear marks are observed on the worn surface, marked inside the circle. There is no sign of deep furrows to indicate the absence of serious splitting or plowing. This layer has a positive effect on wear resistance. Surface changes of the maraging steel sample due to friction, delamination and material wear can be observed during wear tests. The direction of wear marks is indicated by a wide arrow.

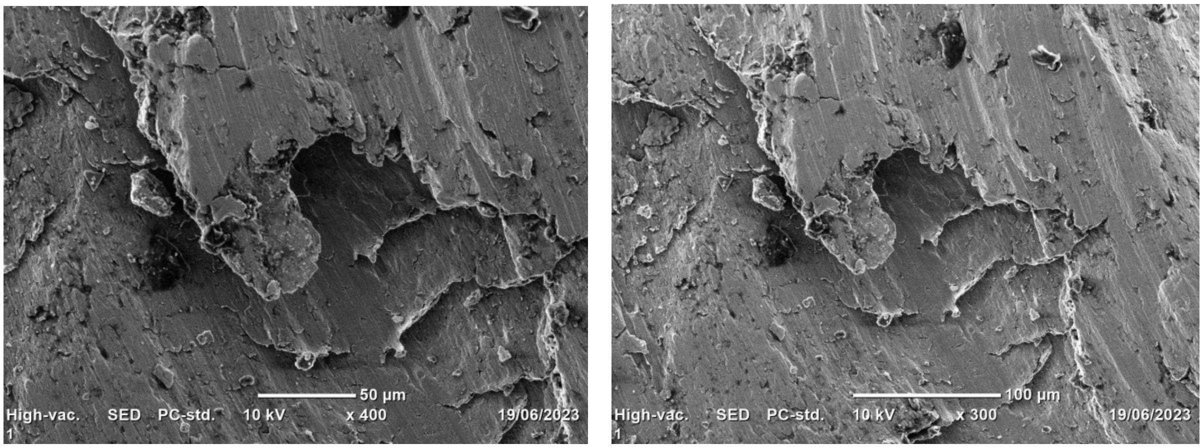

(a) (b)

Figure 17: SEM Micro graph of sample 1 at (a):50µm and (b): 100µm

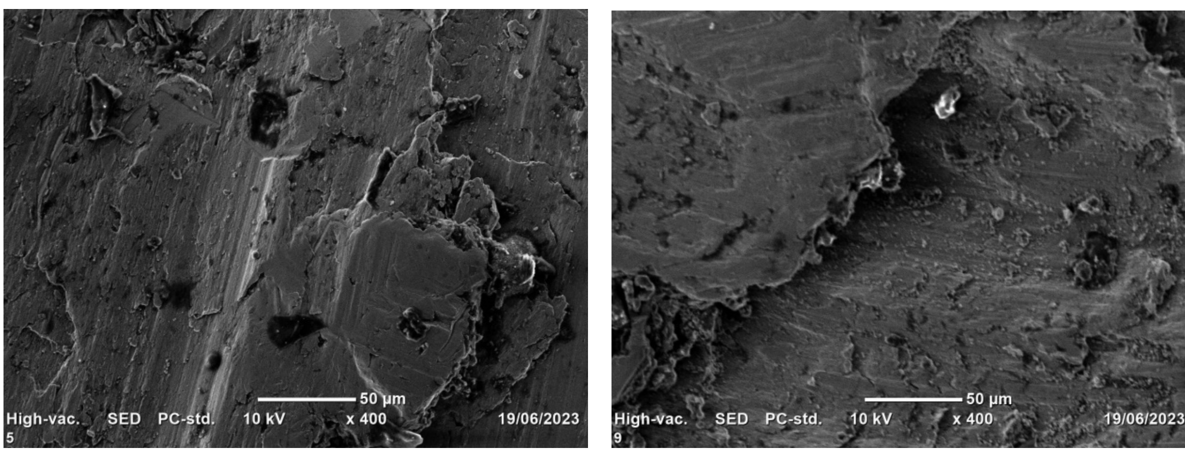

4

(a) (b)

Figure 18: SEM Micrograph at 50 µm (a) at optimum test condition (b) at maximum wear rate

4.2. Optimization Analysis

An optimization refers a procedure which is executed iteratively by comparing various solutions till an optimum or a satisfactory solution is found.

4.2.1. Optimization by Minitab software

In this study minimization optimization using the Minitab software on TAGUCHI, ANOVA, Response Surface method and General factorial has done.

Taguchi Analysis: wear rate versus Load, Speed, Time

Smaller is better

Table 7: Response table for Signal to Noise Ratios

Level	Load	Speed	Time
1	-28.53	-27.71	-29.53
2	-33.49	-33.94	-33.22
3	-38.66	-39.03	-37.93
Delta	10.13	11.31	8.40
Rank	2	1	3

Table 8: Response table for means

Level	Load	Speed	Time
1	41.14	45.26	47.32
2	54.52	50.41	57.61
3	90.54	90.53	81.28
Delta	49.39	45.28	33.96
Rank	1	2	3

The following below graph figure 18 is the main effect plot graph on Taguchi Analysis indicates that (a) mean of means is directly proportional to the parameters or mean of means increased with the increasing of the all parameters (Load, Speed and Time). But from the figure 19 (a) it can be decided as load is more significant. (b) Mean of SN ratio is inversely proportional to the parameters or SN ratio of means declined with the increasing of the all parameters. As shown in the figure 19 (b) below it can be considered as speed is more significant.

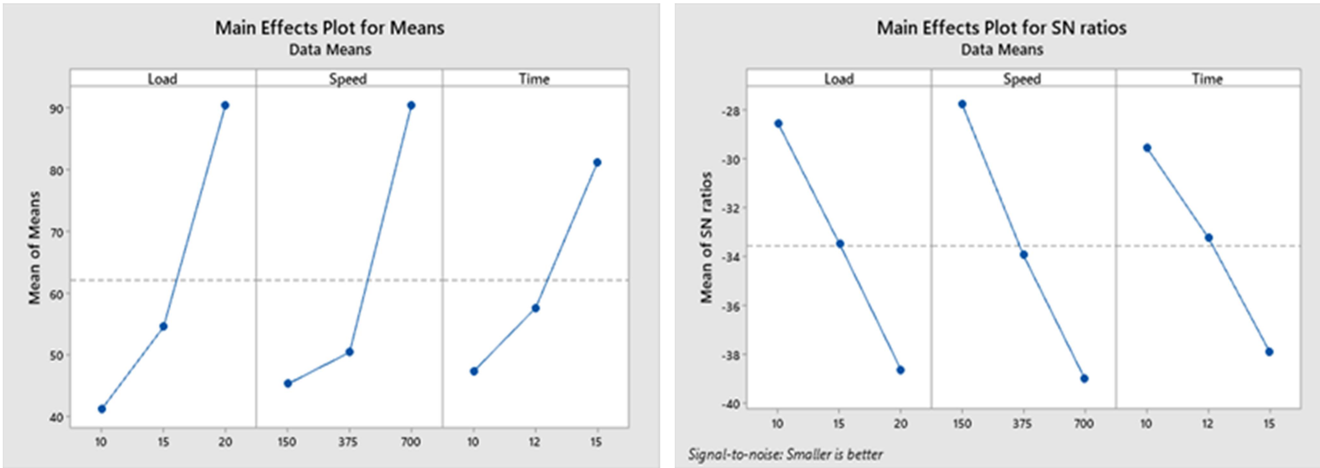

(a) (b)

Figure 19: Main effect plot for (a) mean of means versus load, speed and time; (b) mean of SN ratio versus load, speed and time

Response Surface Regression: wear rate versus Load, Speed, Time

The following terms cannot be estimated and were removed:

Load*Time, Speed*Time

Coded Coefficients

Table 9: Coded coefficients obtained from RSR

Term	Coef	SE Coef	T-Value	P-Value	VIF
Constant	46.5	25.5	1.82	0.319	
Load	24.5	13.7	1.79	0.324	1.01
Speed	22.6	13.6	1.66	0.345	1.01
Time					
10	-14.0	17.0	-0.83	0.560	1.55
12	-3.4	18.2	-0.19	0.883	1.79
Load*Load	11.3	23.6	0.48	0.715	1.00
Speed*Speed	13.8	24.5	0.56	0.673	1.01
Load*Speed	-2.7	23.4	-0.11	0.927	2.01

Table 10: Model summary obtained from RSR

S	R-sq	R-sq(adj)	R-sq(pred)
33.3432	89.46%	15.67%	0.00%

Regression Equation in Uncoded Units

The projected value for WR in mm^3/m may be estimated using regression equation and analysis of variance, given by the equation below. The Equation below considers all parameters regardless of their significance and p-values, which include load, time and sliding speed. In regression analysis, working time is highlighted as an extremely important variable based on its p-value and R-Sq value, but in experimental studies, workload also seems to be an important parameter. As the load increases, the combination of tribolic layer formation and debris accumulation at the interface and debris densification within that layer causes a decrease in mean WR (MWR) at initial conditions. Gradually, as this layer crumbles, the MWR increases faster than the travel time as time and speed increase. It is likely due to the initial decrease in MWR that the load's p-value is higher and the R-Sq value is lower.

Time			
10	wear rate	=	46 - 7.8 Load - 0.044 Speed + 0.453 Load*Load + 0.000183 Speed*Speed - 0.0020 Load*Speed
12	wear rate	=	57 - 7.8 Load - 0.044 Speed + 0.453 Load*Load + 0.000183 Speed*Speed - 0.0020 Load*Speed
15	wear rate	=	78 - 7.8 Load - 0.044 Speed + 0.453 Load*Load + 0.000183 Speed*Speed - 0.0020 Load*Speed

The result of ANAVO are presented in table below, where DF is the total degrees of freedom, Adj SS (adjusted sums of the squares) is the variation for different components, Adj MS (adjusted mean of squares) is the variation, F-value represents lack of fit, p-value represents the probability against null hypothesis, which affects the WR and is within the limits of the hypothesis of p-value obtained from Minitab 16.0 software, from the experimental data as per the conditions of the regression analysis.

Table 11: Analysis of Variance Obtained from ANOVA

Source	DF	Adj SS	Adj MS	F-Value	P-Value
Model	7	9435.3	1347.90	1.21	0.606
Linear	4	7356.9	1839.22	1.65	0.520
Load	1	3572.1	3572.11	3.21	0.324
Speed	1	3074.8	3074.83	2.77	0.345
Time	2	907.9	453.97	0.41	0.742
Square	2	609.6	304.79	0.27	0.804
Load*Load	1	256.0	256.05	0.23	0.715
Speed*Speed	1	353.5	353.54	0.32	0.673
2-Way Interaction	1	14.6	14.62	0.01	0.927
Load*Speed	1	14.6	14.62	0.01	0.927
Error	1	1111.8	1111.77		
Total	8	10547.0			

In figure 20, a residual plot for wear rate is shown which is obtained using the regression analysis and ANOVA method. The normal probability plot gives the correlation of the experimental data with predicted data from the regression analysis. The fitted values shown are the variation of predicted values of the wear from the experimental data obtained with a confidence interval of 95%.

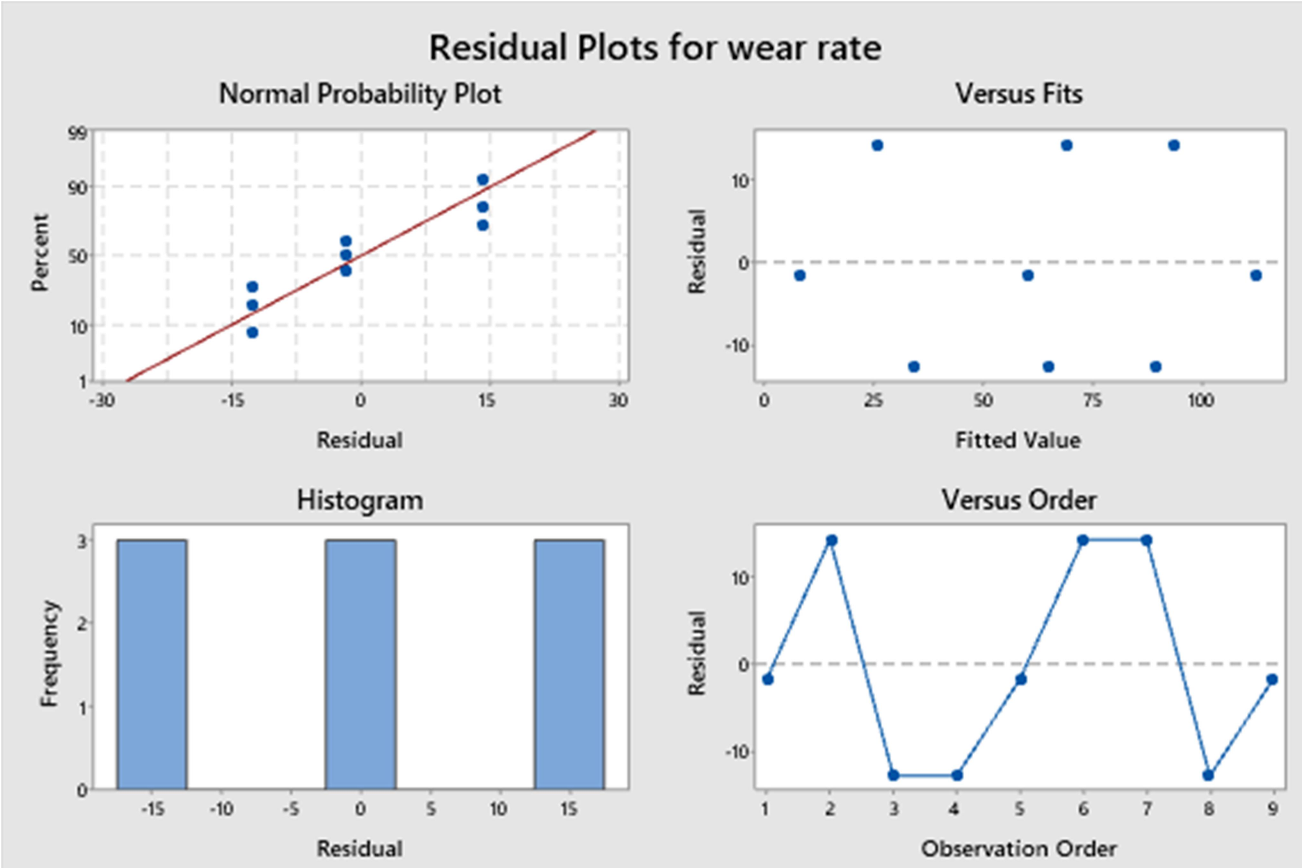

Figure 20: Residual Plot of wear rate

General Factorial Regression: wear rate versus wear volume, Load, Speed, Time

The following terms cannot be estimated and were removed:

Load*Speed, Load*Time, Speed*Time, Load*Speed*Time

Table 12: Factor Information for GFR

Factor	**Levels**	**Values**
Load	3	10, 15, 20
Speed	3	150, 375, 700
Time	3	10, 12, 15

Table 13: Analysis of variance for GFR

Source	DF	Adj SS	Adj MS	F-Value	P-Value
Model	7	10547.0	1506.72	3.01110E+11	0.000
Covariates	1	1126.4	1126.39	2.25103E+11	0.000
wear volume	1	1126.4	1126.39	2.25103E+11	0.000
Linear	6	0.0	0.00	6.88	0.284
Load	2	0.0	0.00	10.32	0.215
Speed	2	0.0	0.00	0.75	0.631
Time	2	0.0	0.00	10.60	0.212
Error	1	0.0	0.00		
Total	8	10547.0			

Table 14: Model summary for GFR

	R-sq	R-sq(adj)	R-sq(pred)
0.0000707	100.00%	100.00%	100.00%

Table 15: coefficients for GFR

Term	Coef	SE Coef	T-Value	P-Value	VIF
Constant	0.000360	0.000133	2.71	0.225	
wear volume	24.9998	0.0001	474450.31	0.000	9.36
Load					
10	-0.000085	0.000055	-1.53	0.368	3.67
15	-0.000162	0.000037	-4.38	0.143	1.64
Speed					
150	-0.000057	0.000049	-1.17	0.450	2.84

375	-0.000023	0.000041	-0.54	0.683	2.06
Time					
10	-0.000210	0.000046	-4.60	0.136	2.49
12	0.000026	0.000035	0.74	0.594	1.44

Figure 21 (a) line plot of mean graph shows that wear rate in terms of time at speed of 150 rpm increases by the increasing of the time and as the rotation time of the disc precedes 12 min at the same speed the wear rate increases highly as shown in the figure 21 (a). At the same figure wear rate at the rotational speed of 700 rpm highly increased linearly to the pick up to 12 min and goes down linearly as the time precedes 12 min Figure 21 (b) indicates the graph of mean of load versus time in terms of speed as shown below.

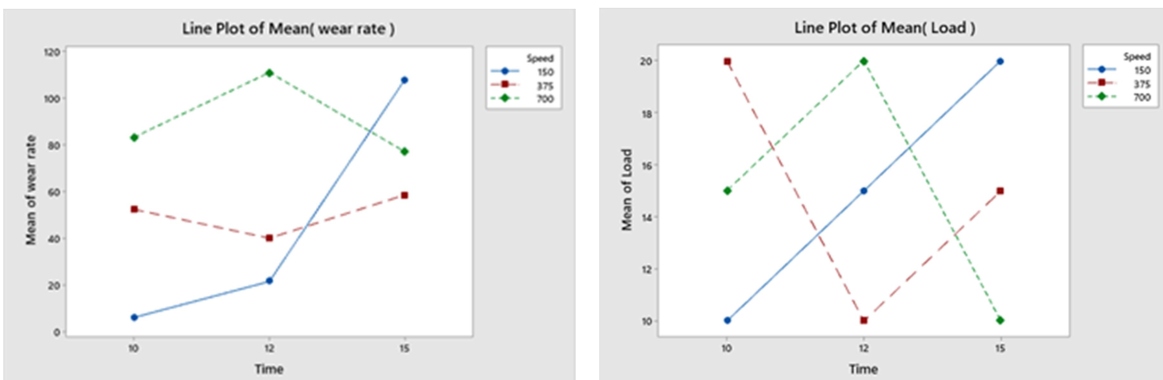

(a) (b)

Figure 21: Line plot of mean (a) mean of wear rate versus time, (b) mean of load versus time

The fitted curve plots of WR with the time of running, normal load, and speed are given in figure 22 (a)-(c) correspondingly. The R-squared values represent the ratio of the response variable deviation in percent. The R-Squares values are 35.0%, for WR-speed curve fit, which indicates that the regression model explicates range of the response data, close to the mean value. For wear rate-normal load curve fit, the R-Sq is 37.1%, which is reasonably close to the mean, while for wear rate-speed curve fit; the R-Sq value is the least (20.6%) indicating that the running time has the least signification on WR.

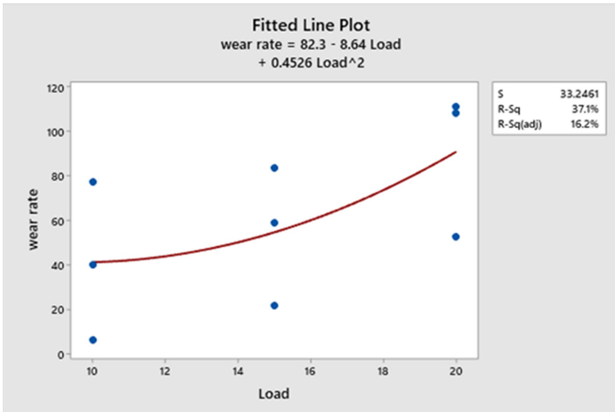

(a)

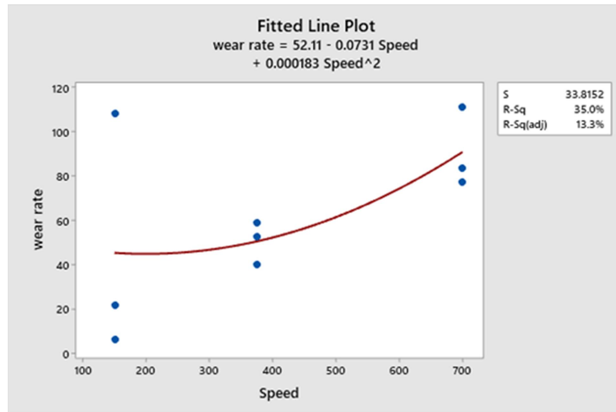

(b)

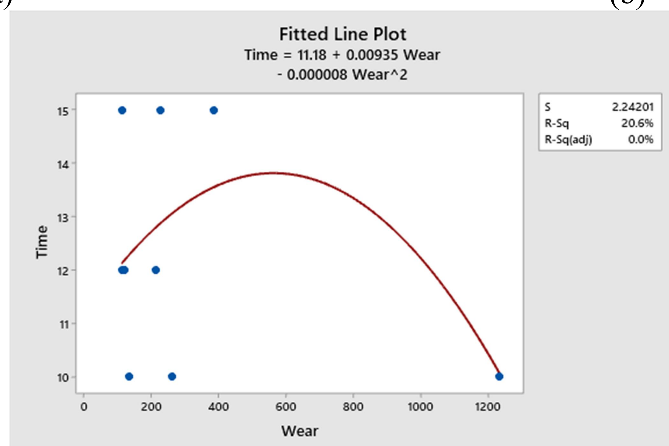

(c)

Figure 22: Fitted curve plots of wear rate with; (a) load, (b) speed and (c) time

The interaction plots of WR under the influence of various variables are shown in Figure below. Larger the alteration in slope amid the lines in a plot, greater is the degree of interaction. Best performance of the material is predicted at low load and low speed, in synergy with the contour plots in Figure 23. The projected WR is less at a mean time of running. Even at mean load, the WR tends to drop. High initial WR is apparent due to the excessive wear in the running-in period after which, the asperities start collapsing and the transfer layer develops. Load appears to be a primary factor, determining the WR.

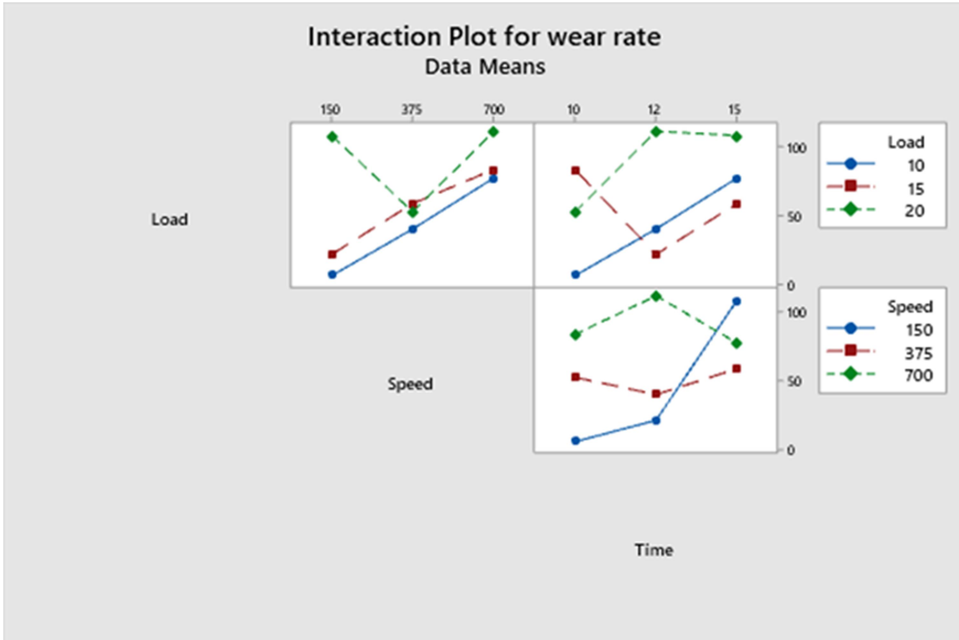

Figure 23: Interaction plot of wear rate

A surface plot is a three-dimensional graph that is useful for determining response values under various operating conditions. The response surface curve is a curve profile because it contains the significant factors in the quadratic regression model. The surface plots or curves shown in Figure 24 (a)-(c) provide the WR response values based on the regression analysis with two continuous variables.

The contour plots of WR are drawn and the different colors of the curve indicate the optimal values of the minimum parameters used. The different influencing factors and their variability are presented most differently in WR. Figures 24 (a)-(c) show the variation of WR with speed and load, the darker the color, the higher the wear rate. It can be observed that the best wear performance occurs at low speed and low load, indicating the optimal interaction between load speed conditions. The contour plots in Figures 24 (b) and (c) graphically represent the range and can be used to identify a possible relationship between the main factors in the wear tests. The best performance (minimum WR) can be achieved with a mean load despite a mean time of running. Therefore, Figure 24 (a) and (b) have load as a controlled factor. Figure 24 (c) shows the combined result of speed and load. It was found that the best wear characteristics can be achieved at low loads and low speeds after the travel speed was increased by 500 rpm. In this condition, almost wearable material even in dry sliding conditions.

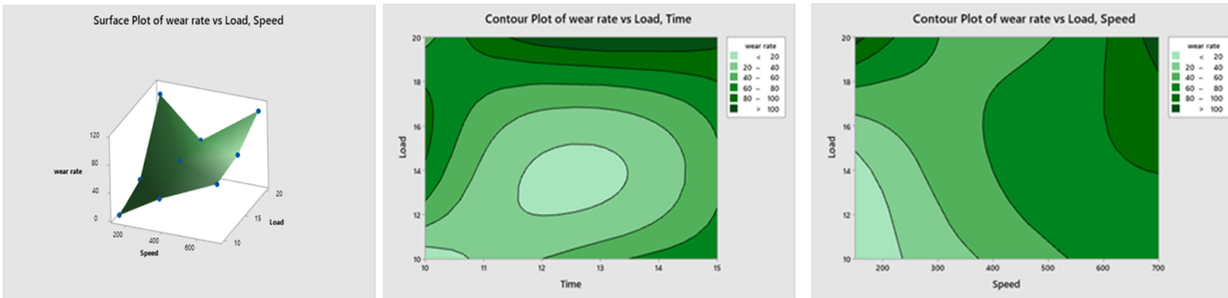

(a) (b) (c)

Figure 24: (a) Surface plot of wear rate with speed and load; (b) contour plot for load and time; (c) contour plot for load and speed

4.2.2. Calculated Result

Wear rate, specific wear rate, wear coefficient and wear volume is calculated by using the formula's on Eq. (1)-(4) and resulted as follows:

Table 16: Calculated result of wear rate

Sample No:	Load (N)	Speed (rpm)	Time of running (min)	Weight before test (g)	Weight after test (g)	Wear coefficient $K*10^{-3}$	Specific wear rate (mm^2/N) $*10^{-3}$	Wear volume (mm^3)	Wear rate (mm^3/mm) $*10^{-3}$
1	10	150	10	2.521	2.519	0.0189	0.615	0.246	6.15
2	10	375	12	2.577	2.564	0.0412	4.012	1.6049	40.1225
3	10	700	15	2.500	2.475	0.0339	7.716	3.0864	77.16
4	15	150	12	2.553	2.546	0.0369	1.44	0.864	21.6
5	15	375	15	2.446	2.427	0.0321	3.9095	2.3457	58.6425
6	15	700	10	2.497	2.470	0.0366	5.5555	3.3333	83.3325
7	20	150	15	2.577	2.542	0.1108	5.40125	4.321	108.025
8	20	375	10	2.412	2.395	0.0323	2.6235	2.0988	52.47
9	20	700	12	2.553	2.497	0.0305	5.5555	4.4444	111.11

The following below graph is the wear rate, specific wear rate, wear coefficient and wear volume graph in terms of the parameters (Load, Speed and Time).

Wear rate in terms of load versus speed

The figure below indicates that as the parameters load and speed increased the color changed from blue to red, which indicates wear rate increases by increasing both parameters load and speed. Even wear rate is also increases by increasing one of the parameters. Therefore both parameters are directly proportional to the wear rate but the best performance for the material is having minimum wear rate. So it can be summarized as the higher the parameters load and speed the higher the wear as shown in the figure 25.

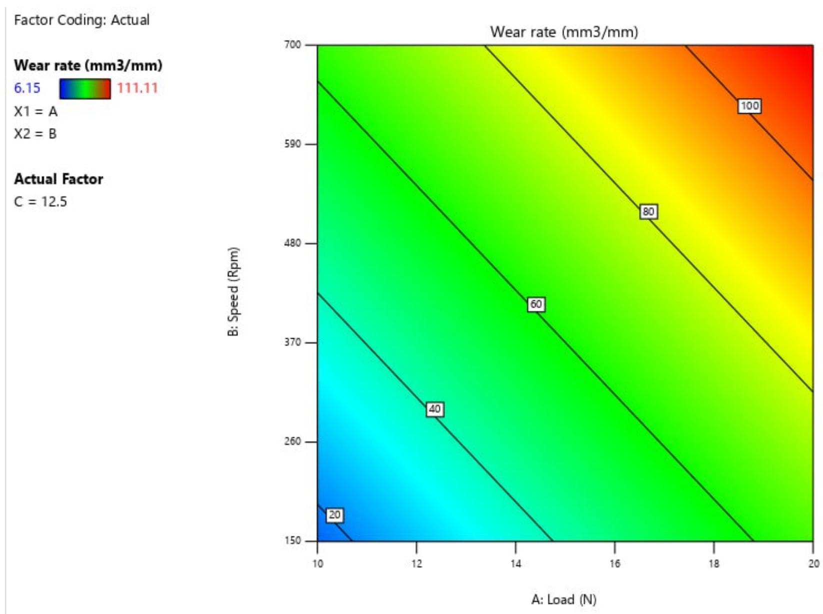

Figure 25: wear rate in terms of load versus speed graph

Specific wear rate in terms of load versus speed

The figure below indicates that as the parameter load increased the color is not changed it indicates that load have no effect on specific wear load but the color changed in to yellow by increasing the value of speed this shows that specific wear rate have directly increases by increasing in to the speed. As shown in the figure 26.

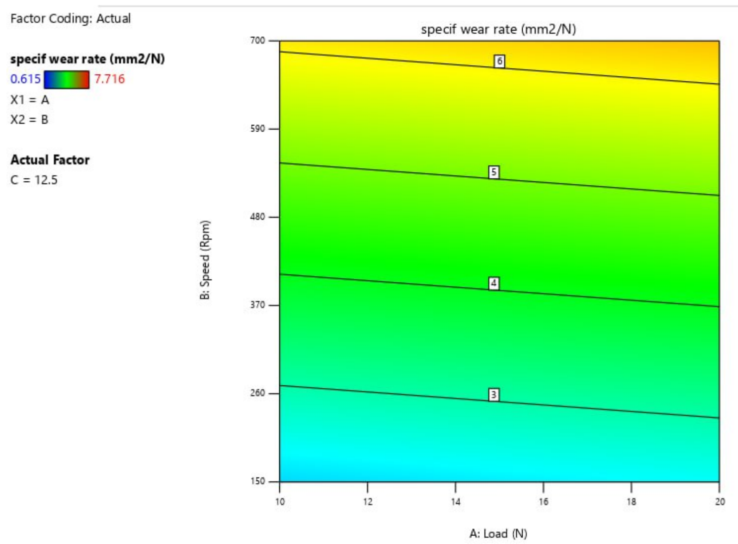

Figure 26: Specific wear rate in terms of load versus speed graph

Wear Volume in terms of load versus speed

The figure below indicates that as the parameters load and speed increased the color changed from blue to red, which indicates wear rate increases by increasing both parameters load and speed. Even wear rate is also increases by increasing one of the parameters. Therefore both parameters are directly proportional to the wear rate but the best performance for the material is having minimum wear rate. So it can be summarized as the higher the parameters the higher the wear as shown in the figure 27.

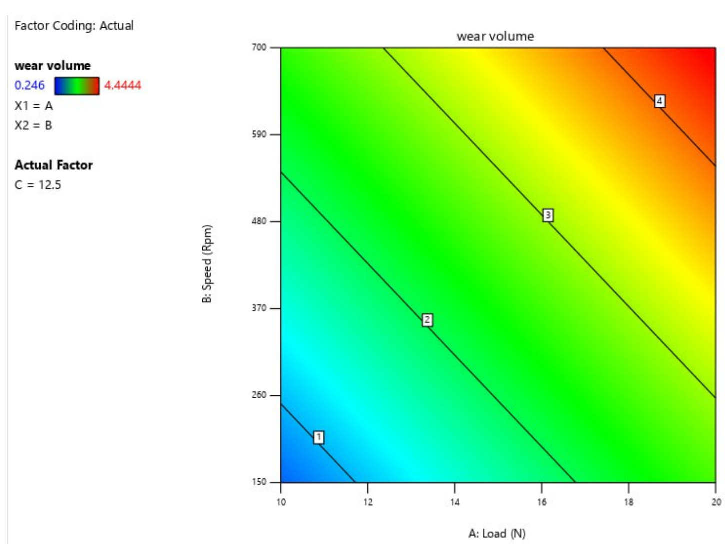

Figure 27: wear volume in terms of load versus speed graph

Wear Coefficient in terms of load versus speed

The figure below indicates that as the parameters load and speed increased the color changed from blue to green, which indicates wear coefficient increases by increasing both parameters load and speed. But on the top of the graph at the right side its color back to the first color blue, which indicates as both parameters increase the wear coefficient decreases. Therefore it is concluded as wear coefficient increases by increasing one of the two parameters but not both at the same time as shown in the figure 28.

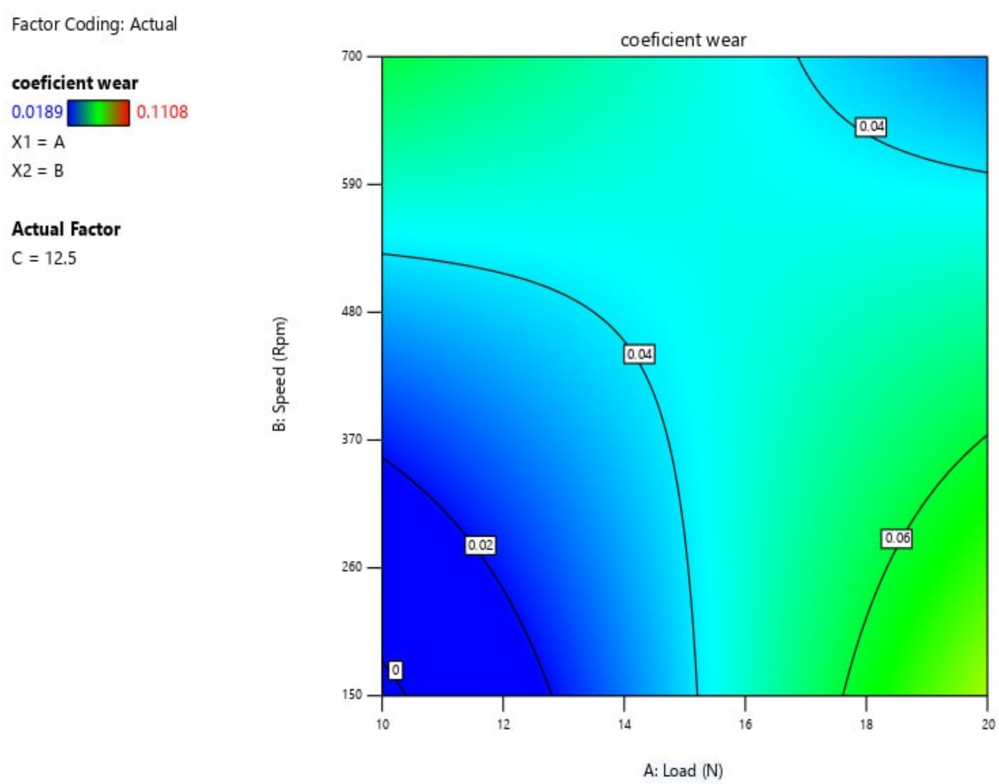

Figure 28: wear coefficient in terms of load versus speed graph

4.3. Simulation Result obtained from LS-DYNA

The wear model and analysis is performed using the finite element method LS-DYNA software; for designed to achieve maximum equivalent stress, total stress, and deformation. On this model the location and depth highly stressed zone also determined with implication of red color area. The simulation for the stress and deformation is done. Boundary conditions, contact behavior of the system and application of different loads cases also in this part of the FEM analysis. The final stage of the FEM analysis gates maximum equivalent voltage and maximum equivalent voltage locations.

Equivalent Stress result

The corresponding stress results obtained by circular simulations are shown in the following figures. The corresponding stress results according to the parameters; load, speed and time is obtained in the below figures.

For minimum load 10 N

The figure 29 (A) on 150 rpm speed indicates that the small red region shows the equivalent stress is highest 3.0965e6pa, whereas the dark blue color indicates the points where the equivalent stress is minimum about 1.02e6pa. Figure 29 (B) on 375 rpm speed indicates that the red regions shows the equivalent stress is highest 4.3789e6pa, whereas the dark blue color indicates the points where the equivalent stress is minimum about 1.066e6pa. Figure 29 (C) on 700 rpm speed indicates that the dense red region shows the equivalent stress is highest 7.698e6pa, whereas the small dark blue color on the tip of the circle indicates the points where the equivalent stress is minimum about 2.7732e6pa.

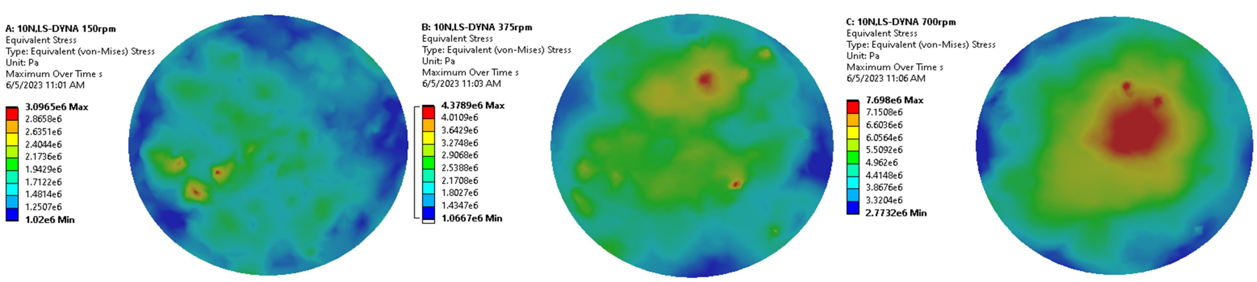

Figure 29: Simulation representation of equivalent stress for 10N

The graph below figure 30 shows that the equivalent stress fluctuates by the increasing of time of rotation running shows by simulation representation on figure 29.

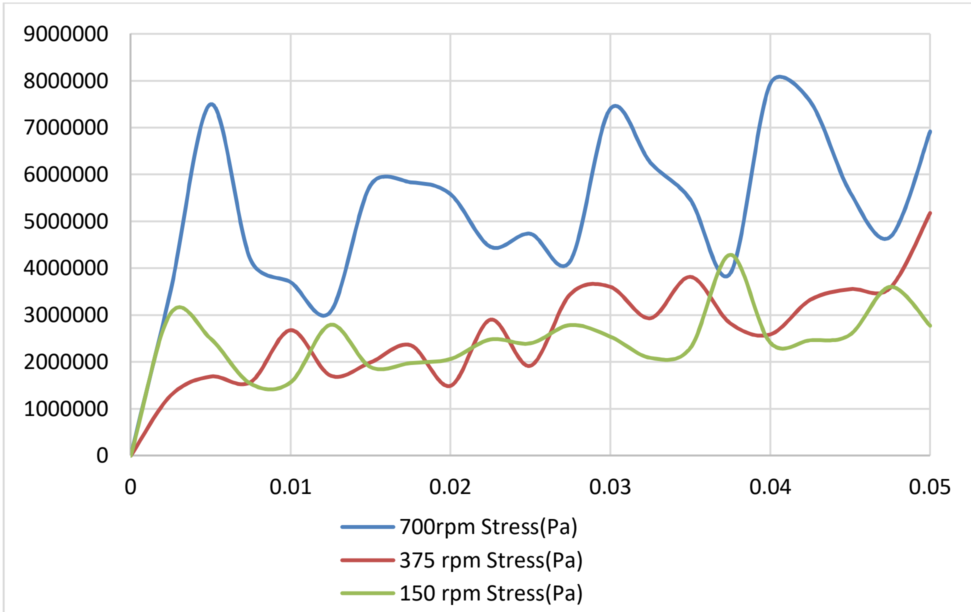

Figure 30: Graphical representation of equivalent stress for 10N

For maximum load 20 N

The figure 31 (G) on 150 rpm speed indicates that the small red region shows the equivalent stress is highest 4.286e6pa, whereas the dark blue color indicates the points where the equivalent stress is minimum about 1.2908e6pa. Figure 31 (H) on 375 rpm speed indicates that the red regions shows the equivalent stress is highest 5.1764e6pa, whereas the dark blue color indicates the points where the equivalent stress is minimum about 1.2436e6pa. Figure 31 (I) on 700 rpm speed indicates that the red region shows the equivalent stress is highest 7.926e6pa, as the figure shows that the equivalent stress is more about the average of 6.7711e6pa(the yellow color), whereas the small dark blue color on the tip of the circle indicates the points where the equivalent stress is minimum about 2.7732e6pa.

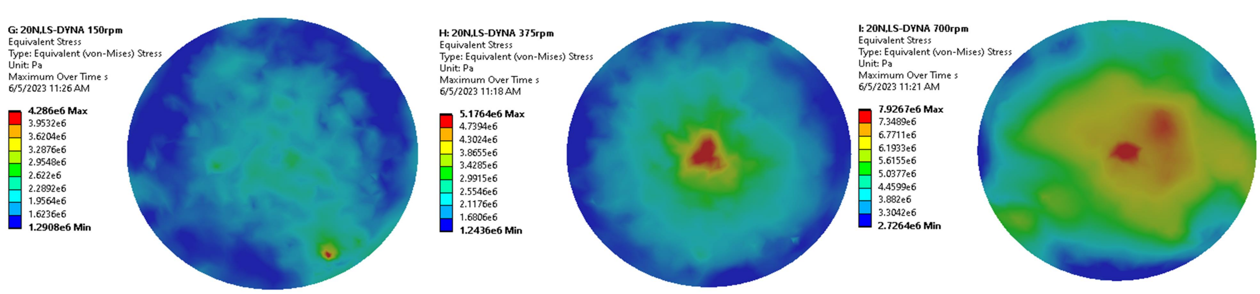

Figure 31: Simulation representation of equivalent stress for 20N

The graph below figure 32 shows that the equivalent stress fluctuates by the increasing of time of rotation running shows by simulation representation on figure 31.

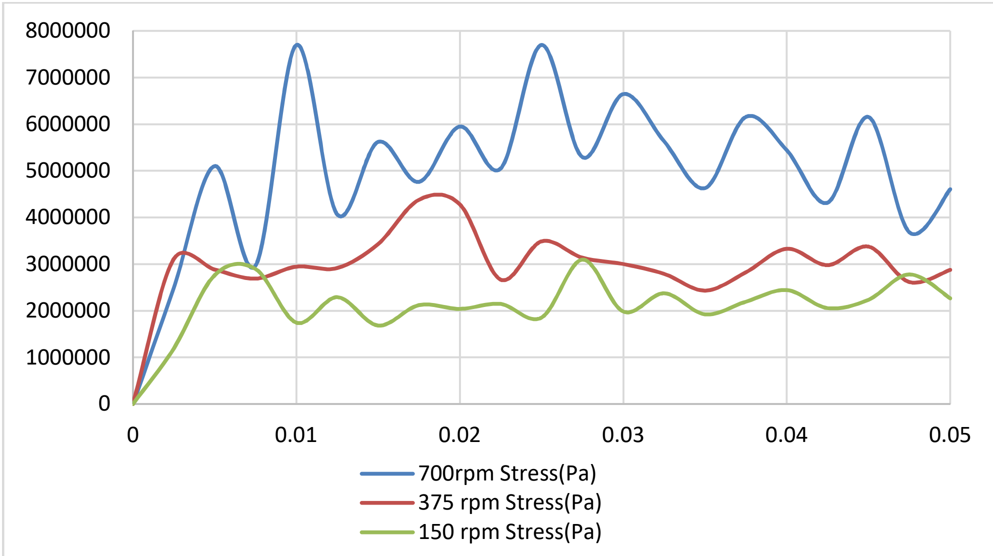

Figure 32: Graphical representation of equivalent stress for 20N

Total Deformation Result

The corresponding deformation results obtained by circular simulations are shown in the following figures.

For minimum Load 10N

As shown on figure 33 (A) the total deformation applying 10N load by 150 rpm is higher on the tip by the red color which is maximum deformation (2.2697mm) and minimizing to the center showed by the blue color is the minimum deformation (1.2638mm). Figure 33 (B), also defined as the same as figure 33 (A) but by 375 rpm maximum red color is 5.0884mm and minimum or blue color is 0.24768mm. Whereas figure 33 (C) on the 700 rpm maximum or red color is 6.1207mm and minimum or blue color is 0.30469mm.

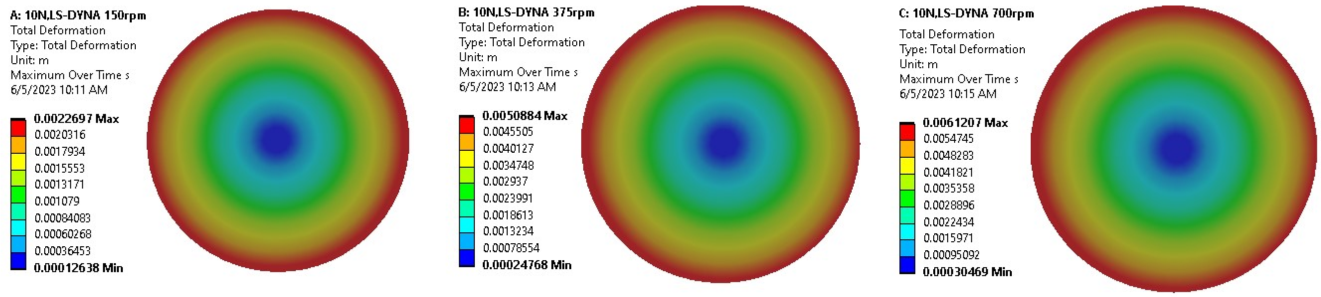

Figure 33: Simulation representation of total deformation for 10N

The graph below figure 34 shows that total deformation graph on 10N for rotational speed of 150 rpm and 375 rpm increases linearly as increasing in time, whereas for rotational speed 700 rpm increases as the time increases but decreases after some time as shown in the figure below.

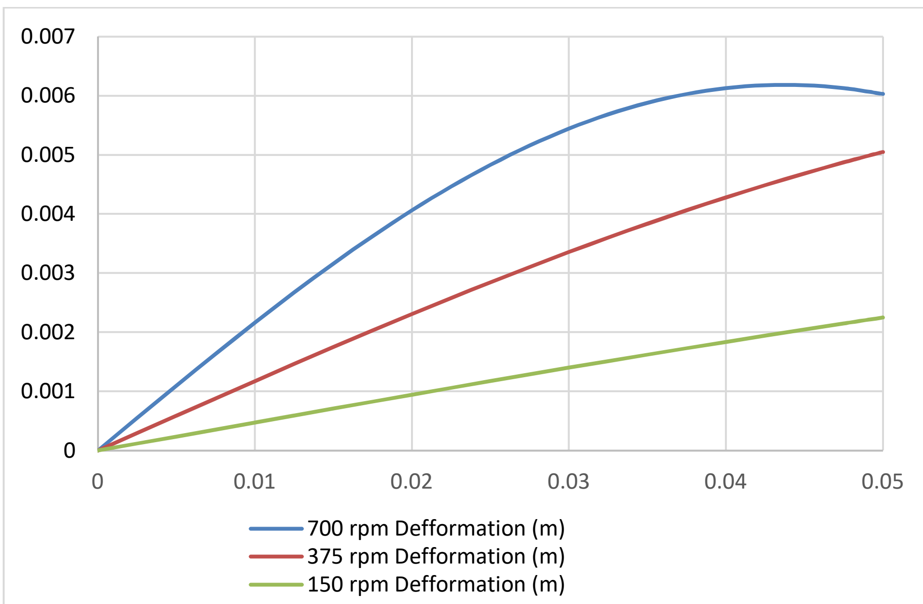

Figure 34: Graphical representation of total deformation for 10N

For maximum Load 20N

As shown on figure 35 (G) the total deformation applying 20N load by 150 rpm is higher on the tip by the red color which is maximum deformation (2.2495mm) and minimizing to the center showed by the blue color is the minimum deformation (0.18577mm). Figure 35 (H), also defined as the same as figure 35 (G) but by 375 rpm maximum red color is 5.0489mm and minimum or blue color is 0.37544mm. Whereas figure 35 (I) on the 700 rpm maximum or red color is 6.1777mm and minimum or blue color is 0.40366mm.

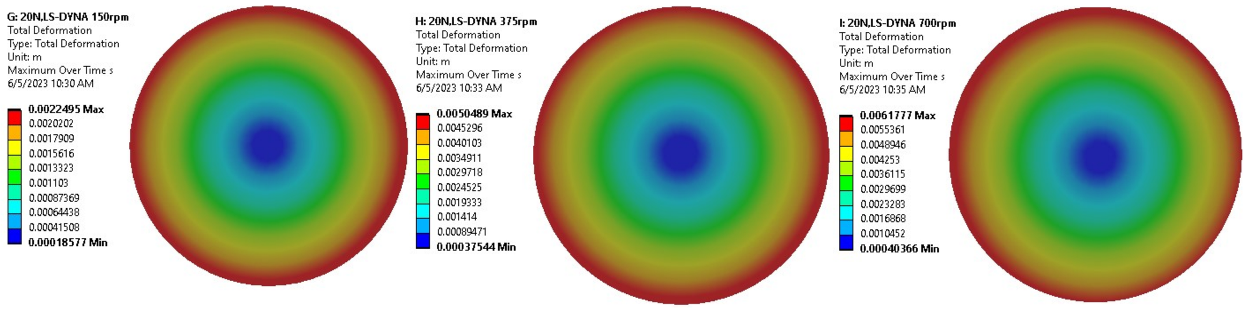

Figure 35: Simulation representation of total deformation for 20N

The graph below figure 36 shows that total deformation graph on 20N for rotational speed of 150 rpm and 375 rpm increases linearly as increasing in time, whereas for rotational speed 700 rpm increases as the time increases but decreases after some time as shown in the figure below.

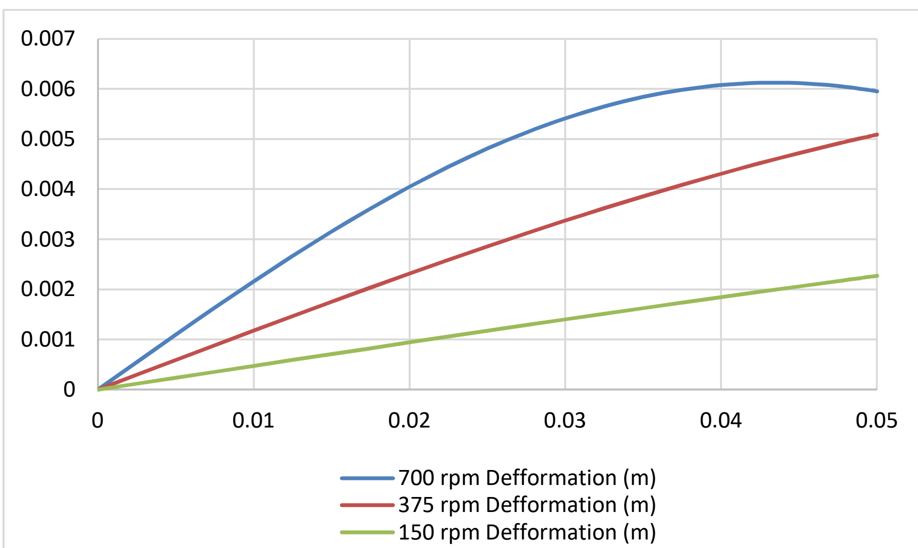

Figure 36: Graph representation of total deformation for 20N

4.4. COMPARISON

The hardness and density of 3DPMS are given in table below. The average HV_{10} value is 694 and the density is 8.2 g/cm^3. A comparison is made with the properties of wrought 18Ni1900 Maraging steel (solution annealed at 820°C followed by aging at 480°C for 3 h) made by conventional process, taken from the literature. The hardness of conventional Maraging steel varies from 531-645 HV due to the variation in the presence of elements such as Ni, Mo. Ti and Co, within the composition range and their precipitates.

Table 17: Hardness and density of Maraging steel

Material	RC	Density g/cm3
Maraging steel	Min 50 Max 57	8.1*
Source: Obtained from nickel development institute, INCO data books.		

Wear rate = -131.7 + 4.94 Load + 0.0852 Speed + 6.88 Time Eq. (7)

The value of WR predicted from the regression analysis, using Eq. (7) is 0.1093mm^3/mm and that determined experimentally is 0.1111mm^3/mm. Hence, the predicted value is in close proximity with the experimental value. The optimized parameters to obtain minimum wear for Maraging steel is given in the below Table.

Table 18: Experiment validation with optimized parameters

Optimized wear test parameters		
Load, N	Time running, min	Sped, R.P.M
20	12	700
Wear rate, mm^3/m		
Regression equation value	Experimental value	
0.1093	0.1111	

5. CONCLUSION AND RECOMMENDATION

5.1. CONCLUSION

This study shows the wear characteristics of the Maraging steel using pin on disc apparatus. In addition, the study has also investigated the wear characteristics of Maraging steel under dry sliding at room temperature using Pin on Disc apparatus. The important findings are drawn based on the results found from the experimental and parametric studies.

- ✓ Experiments were conducted for wear tests as per the results of orthogonal array and validation of the values with the experimental results. Which is compared for the optimized wear test parameters the regression analysis is 0.1093 and experimental value 0.1111 Furthermore, ANOVA analysis is employed to verify their optimum values.
- ✓ The SEM micrographs of Maraging steel after aging after the wear tests at a magnification 0f 300x and 400x are shown at 50 µm and at 100µm. The surface appears intact and sound Layers are visible by figure which indicates there is a surface crack during the sample preparation and during the wear test experiment.
- ✓ In this study minimization optimization using the Minitab software on TAGUCHI, ANOVA, Response Surface method and General factorial has done. On response for signal to ratio ranking speed is significant and on response for mean load is more significant.
- ✓ Points absorbed from the optimization described as the minimum wear rate is $6.15x10^{-3}$ mm^3/mm by the parameters load 10N, speed 150 rpm and time 10 min whereas the point was shows the more damage or more wear rate is $111.11x10^{-3}$ mm^3/mm on the parameter values load 20N, speed 700 rpm and time 12 min and it has be validated with the LS-DYNA results.
- ✓ The interaction plots of WR under the influence of various variables load, speed and time are shown in Figure described that on the load to speed interaction the wear performance is less on the minimum load (10N) for the three speed variables relatively and on the load to time interaction in the minimum time (10 min) the wear performance is less on the minimum load (10N), but for time 12 and 15 min the wear performance is best on load 15N.

- ✓ Contour plot can be observed that the best wear performance occurs at low speed (below 150 rpm) and low load (below 10N), indicating the optimal interaction between load speed conditions.
- ✓ The wear model and analysis is performed using the finite element method LS-DYNA software; for designed to achieve maximum equivalent stress, total stress, and deformation simulation have been done.

5.2. RECOMMENDATION

By adopting the analysis made in this thesis, this research can be extended with increased number of Experiments and different types of wheel materials with increased levels for obtaining comparatively better results.

- This research can be extended to study more about types of Wear rate and mechanisms for load applied and types of stress on cylindrical machining
- This research can be extended for increased number experiments for better analysis and conducting SEM characterization in order to get different surface damage comparison.

5.3. Scope for future research

This study shows the wear characteristics of the Maraging steel using dry sliding pin on disc apparatus. Following are the scope for future research in this area:

- ✓ Measurement of the adhesive strength of Maraging steel coating with unhardened and hardened & tempered steel substrate.
- ✓ Study of the wear characteristics of Maraging steel coated on hardened and tempered with solid lubricant (MoS2) using Pin on disc test method.
- ✓ Study of erosion and corrosion behavior of Maraging steel coating on unhardened/ hardened & tempered steel substrate.
- ✓ Study of nano lubricating coating of Maraging steel coating on an unhardened / hardened & tempered steel substrate.
- ✓ Evaluation of wear graph of Maraging steel coating on an unhardened / hardened & tempered steel substrate.

References

(Casalino, G., Campanelli, and Ludovico, A.D.,2015. Experimental investigation and statistical optimisation of the selective laser melting process of a maraging steel. Optics & Laser Technology, 65, pp.151–158., pp. DOI 10.1007/s10853-006-1317-8)

(pp. 2007. Influence of temperature and aging time on hardness and magnetic properties of the maraging steel grade 300. Journal of Materials Science, 42(7), pp.2276–2281)

(pp. Fernandez-Vicente, Miguel, et al. "Effect of infill parameters on tensile mechanical behavior in desktop 3D printing." 3D printing and additive manufacturing 3.3 (2016): 183-192.)

(https://www.sciencedirect.com/science/article/pii/S2214860422006819, p. https://doi.org/10.1016/j.optlastec.2014.07.021)

(Jägle, Eric A., et al. "Precipitation and austenite reversion behavior of a maraging steel produced by selective laser melting." Journal of Materials Research 29.17 (2014): 2072-2079.)

(Li, Sheng, et al. "The development of TiNi-based negative Poisson's ratio structure using selective laser melting." Acta Materialia 105 (2016): 75-83.)

(Zhao, Xiaoli, et al. "Comparison of the microstructures and mechanical properties of Ti–6Al–4V fabricated by selective laser melting and electron beam melting." Materials & Design 95 (2016): 21-31.)

(Wu, Jing, et al. "Microstructure and strength of selectively laser melted AlSi10Mg." Acta Materialia 117 (2016): 311-320.)

(Wang, Xiqian, et al. "Microstructure and yield strength of SLM-fabricated CM247LC Ni-Superalloy." Acta Materialia 128 (2017): 87-95.)

(Qiu C, Adkins NJ, Attallah MM. Selective laser melting of Invar 36: Microstructure and properties. Acta Materialia. 2016 Jan 15;103:382-95.)

(Grzesiak, Dariusz, et al. "Selective laser melting of TiC reinforced stainless steel nanocomposites: mechanical behaviour at elevated temperatures." Materials Letters 256 (2019): 126633.)

(Marcisz, J., Adamczyk, M., & Garbarz, B. (2017). Optimisation of mechanical properties of 18% Ni350 grade maraging steel using novel heat treatment.)

(Tirth, V., Algahtani, A. and Mahmoud, E.R., 2018. Tribological characterization of stir casting. Materials Express, 8(6), pp.475-488.https://doi.org/10.1166/mex.2018.1464)

(Tirth, Vineet. "Dry sliding wear behavior of 2218 Al-Alloy-Al2O3 (TiO2) hybrid composites. https://doi.org/10.1115/1.4037697)

(Edacherian, A., Algahtani, A., & Tirth, V. (2018). Investigations of the tribological performance of A390 alloy 11(12), 2524.Materials 2018, 11(12), 2524; https://doi.org/10.3390/ma11122524)

(Ohue Y. Sliding–rolling contact fatigue and wear of maraging steel and fine particle shot-peening. Wear. 2007 Sep 10; https://doi.org/10.1016/j.wear.2007.01.055)

(Pettersson U, Jacobson S. Influence of surface texture on boundary lubricated sliding contacts.; https://doi.org/10.1016/S0301-679X(03)00104-X)

(Lewis, S.R., Lewis, R. and Fletcher, D.I., 2012. Assessment of laser cladding as an option for repair of rails. growth, 5, p.6.)

(Wear resistance of maraging steel developed by direct metal laser sintering.Materials Express 10.7 (2020): 1079-1090.; https://doi.org/10.1166/mex.2020.1715)

(Jiri Nohava, Pascal Dessarzin, Pavla Karvankova, Marcus Morstein, Characterization of tribological behavior and wear mechanisms of designed for applications at High temperatures, Tribology International, http://dx.doi.org/10.1016/j.triboint.2014.08.016)

(Cox, T.B., Low, J.R. An investigation of the plastic fracture of AISI 4340 and 18 Nickel-200 grade maraging steels. Metall Trans 5, 1457–1470 (1974). https://doi.org/10.1007/BF02646633)

(Vaz Penna, R., Bartlett, L.N. & Constance, T. Understanding the Role of Inclusions on the Dynamic Fracture Toughness of High Strength Lightweight FeMnAl Steels. Inter Metalcast 13, 286–299 (2019). https://doi.org/10.1007/s40962-018-0273-9)

(Van Swam, L.F., Pelloux, R.M. & Grant, N.J. Fatigue behavior of maraging steel 300. Metall Trans A 6, 45–54 (1975). https://doi.org/10.1007/BF02673669)

(Ana Larissa Melo Feitosa Universidade de São Paulo, Escola Politécnica, http://orcid.org/0000-0002-4276-838X)

(Kennedy, F. E., Lu, Y., & Baker, I. (2015). Contact temperatures and their influence on wear during pin-on-disk tribotesting. Tribology International, 82, 534–542. doi:10.1016/j.triboint.2013.10.022)

(Bortoleto, E. M., Rovani, A. C., Seriacopi, V., Profito, F. J., Zachariadis, D. C., Machado, I. F., … Souza, R. M. (2013). Experimental and numerical analysis of dry contact in the pin on disc test. Wear, 301(1-2), 19–26. doi:10.1016/j.wear.2012.12.005)

(Chandra Verma, P., Menapace, L., Bonfanti, A., Ciudin, R., Gialanella, S., & Straffelini, G. (2015). Braking pad-disc system: Wear mechanisms and formation of wear fragments. Wear, 322-323, 251–258. doi:10.1016/j.wear.2014.11.019)

(https://www.scopus.com/scopus/inward/record.url?partnerID=10&rel=3.0.0&view=basic&eid=2-s2.0-84896971833&md5=910a3340d7b1189fd2b6459f257665ad)

(Novak, Rudolf, and Tomas Polcar. "Tribological analysis of thin films by pin-on-disc: Evaluation of friction and wear measurement uncertainty." Tribology International 74 (2014). https://doi.org/10.1016/j.triboint.2014.02.011)

(Sivkov, A.A., Gerasimov, D.Y. A Study of the Electroerosive Wear of Surfaces of Accelerating Channels of a Coaxial Magnetoplasma Accelerator. Russ. Electr. Engin. 89, 340–342 (2018). https://doi.org/10.3103/S1068371218050085)

(Guicciardi, S., Melandri, C., Lucchini, F., & De Portu, G. (2002). On data dispersion in pin-on-disk wear tests. Wear, 252(11-12), 1001-1006. https://doi.org/10.1016/S0043-1648(02)00066-2)

(Basavarajappa, S., Chandramohan, G., Mukund, K. et al. Dry sliding wear behavior of Al 2219/SiCp-Gr hybrid metal matrix composites. J. of Materi Eng and Perform 15, 668–674 (2006). https://doi.org/10.1361/105994906X150803)

(Niclas Strömberg, Lars Johansson, Anders Klarbring, Derivation and analysis of a generalized standard model for contact, friction and wear, (https://www.sciencedirect.com/science/article/pii/0020768395001409) https://doi.org/10.1016/0020-7683(95)00140-9.)

(Xinmin Li, Mario Sosa, Ulf Olofsson,A pin-on-disc study of the tribology characteristics of sintered versus standard steel gear materials, https://doi.org/10.1016/j.wear.2015.01.032.))

(Michael G. Hamblin & Gwidon W. Stachowiak (1996) Description of Abrasive Particle Shape and Its Relation to Two-Body Abrasive Wear, Tribology Transactions, 39:4, 803-810, DOI: 10.1080/10402009608983598)

(ZMITROWICZ, Alfred. Wear patterns and laws of wear – a review. Journal of Theoretical and Applied Mechanics, [S.l.], v. 44, n. 2, p. 219-253, Jan. 2006. ISSN 1429-2955. <http://www.ptmts.org.pl/jtam/index.php/jtam/article/view/v44n2p219>)

(Cockeram, B. V., & Wilson, W. L. (2001). The hardness, adhesion and wear resistance of coatings developed for cobalt-base alloys. Surface and Coatings Technology, 139(2-3), 161-182. https://doi.org/10.1016/S0257-8972(00)01153-1)

(Gee, M. G., A. Gant, and B. Roebuck. "Wear mechanisms in abrasion and erosion of WC/Co and related hardmetals." Wear 263, no. 1-6 (2007): 137-148. https://doi.org/10.1016/j.wear.2006.12.046)

(Hintermann, H. E. "Adhesion, friction and wear of thin hard coatings." Wear 100, no. 1-3 (1984): 381-397. https://doi.org/10.1016/0043-1648(84)90023-1)

(Jahangiri, M., M. Hashempour, H. Razavizadeh, and H. R. Rezaie. "Application and conceptual explanation of an energy-based approach for the modelling and prediction of sliding wear." wear 274 (2012): 168-174. https://doi.org/10.1016/j.wear.2011.08.025)

(Chen, G., Schott, D.L. and Lodewijks, G. (2017), "Sensitivity analysis of DEM prediction for sliding wear by single iron ore particle", Engineering Computations, Vol. 34 No. 6, pp. 2031-2053. https://doi.org/10.1108/EC-07-2016-0265)

(Hirth, A., A. Haufe, and L. Olovsson. "Airbag simulation with LS-DYNA past-present-future." presentation in 6 (2007).)

(Abedini, M., Zhang, C. Performance Assessment of Concrete and Steel Material Models in LS-DYNA for Enhanced Numerical Simulation, A State of the Art Review. Arch Computat Methods Eng 28, 2921–2942 (2021). https://doi.org/10.1007/s11831-020-09483-5.)

(Ferreira, Daniel FS, João S. Vieira, S. P. Rodrigues, Filipe J. Oliveira,"Dry sliding wear and mechanical behaviour of selective laser melting processed 18Ni300 and H13 steels for moulds." Wear 488 (2022): https://doi.org/10.1016/j.wear.2021.204179)

(Jeong-Jung Oak, Heesoo Lee, Wookjin Lee, Yong Ho Park,(Effect of heat treatment, building direction, and sliding velocity on wear behavior of selectively laser-melted maraging 18Ni-300 steel against bearing) https://doi.org/10.1016/j.wear.2021.203962.)

APENDEX

Time versus wear graphs of pin on disc Wear test result obtained from all the 9 samples of experiment.

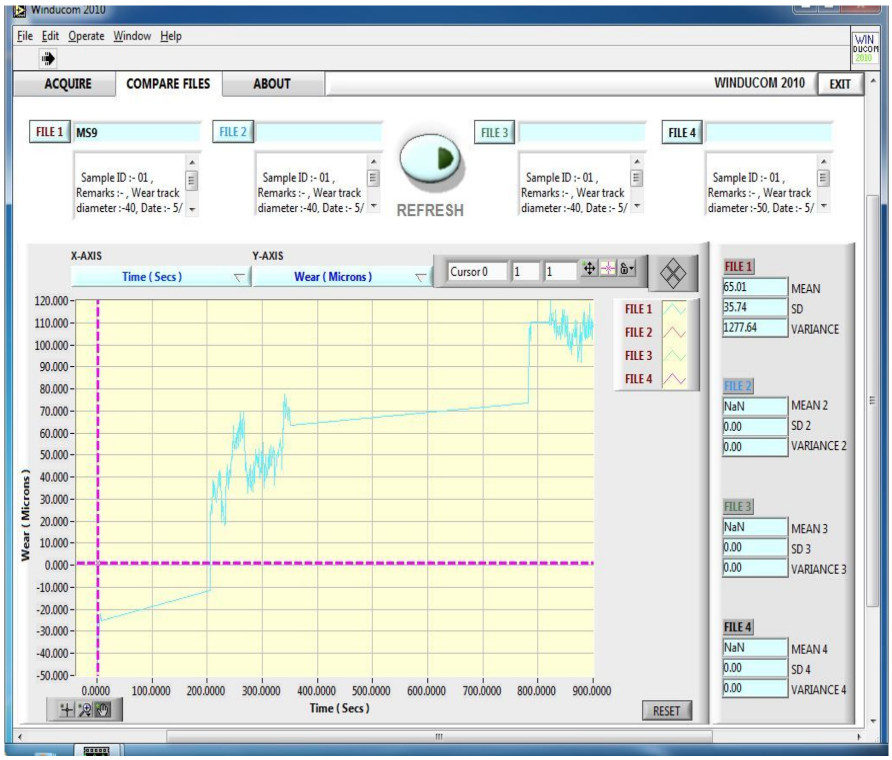

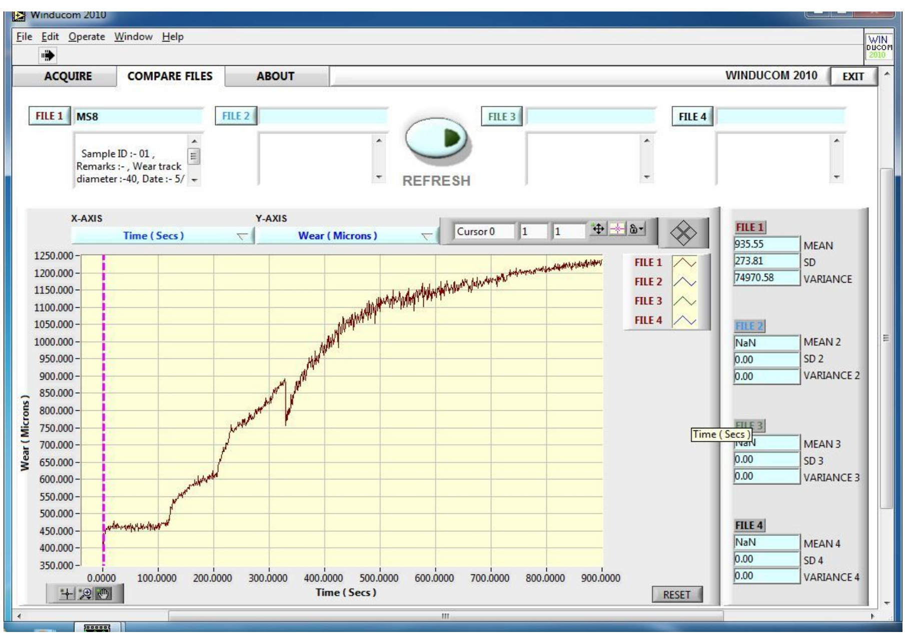

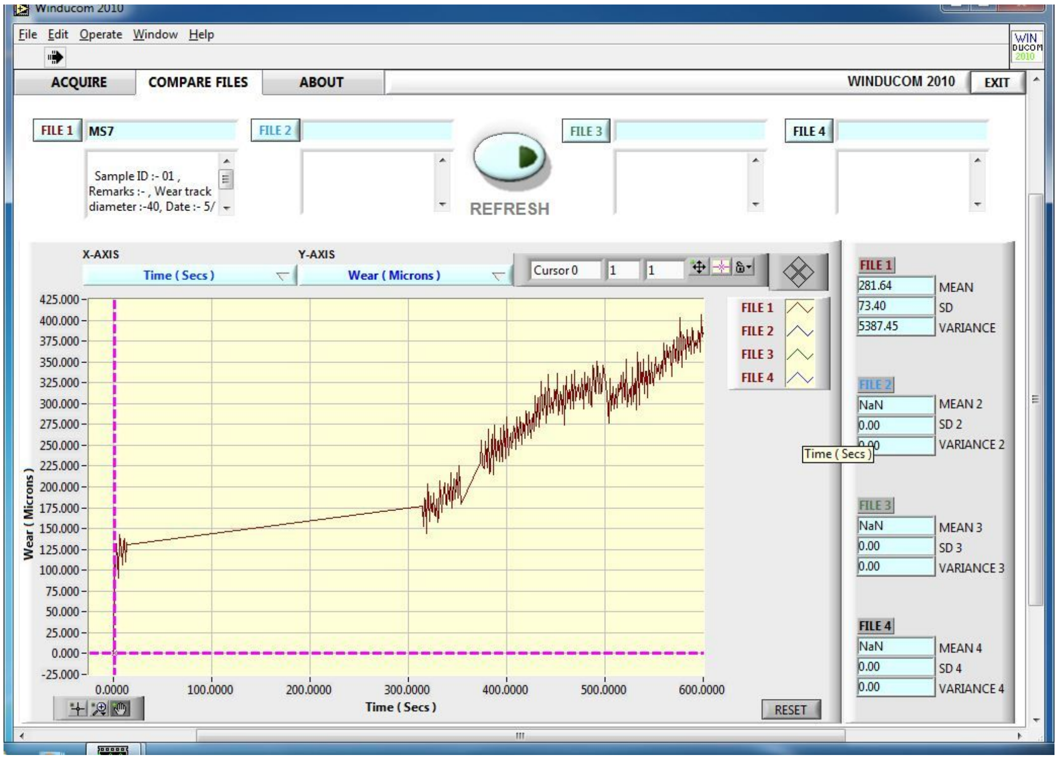
Winducom 2010
File Edit Operate Window Help
ACQUIRE
COMPARE FILES
ABOUT
WINDUCOM 2010
EXIT
FILE 1 MS7
FILE 2
FILE 3
FILE 4
Sample ID :- 01 , Remarks :- , Wear track diameter :-40, Date :- 5/
REFRESH
X-AXIS
Time (Secs)
Y-AXIS
Wear (Microns)
Cursor 0
Wear (Microns)
Time (Secs)
RESET
FILE 1 281.64 MEAN 73.40 SD 5387.45 VARIANCE
FILE 2 NaN MEAN 2 0.00 SD 2 0.00 VARIANCE 2
FILE 3 NaN MEAN 3 0.00 SD 3 0.00 VARIANCE 3
FILE 4 NaN MEAN 4 0.00 SD 4 0.00 VARIANCE 4

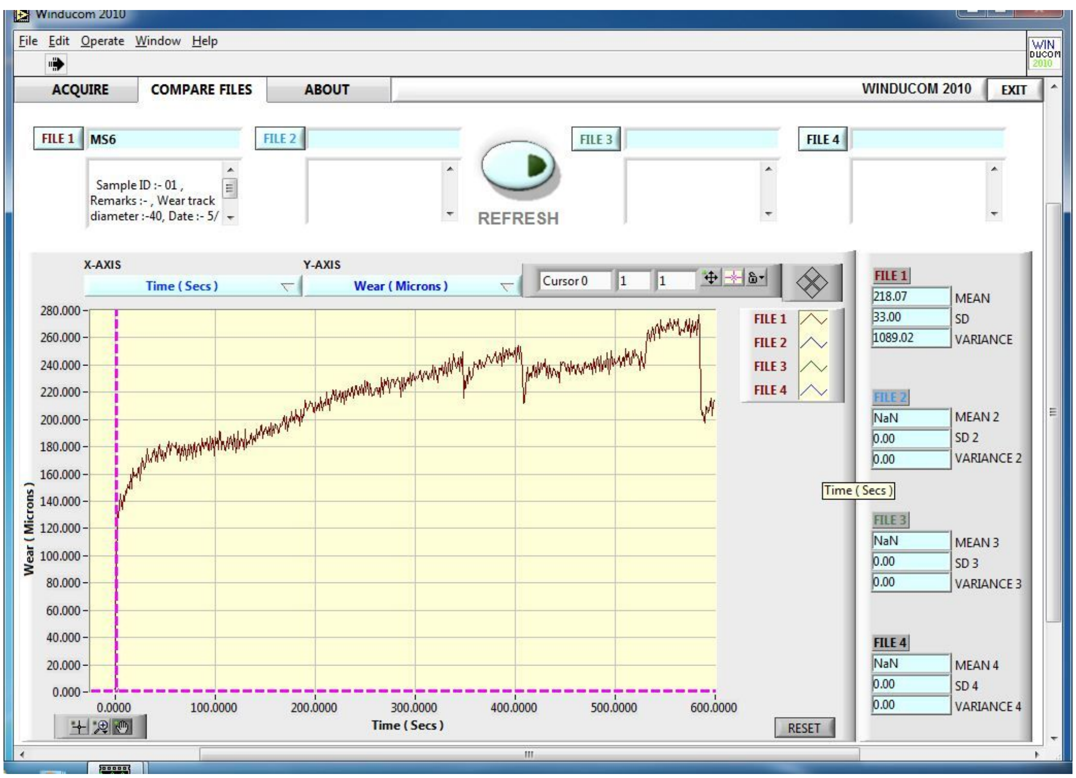
Winducom 2010
File Edit Operate Window Help
ACQUIRE
COMPARE FILES
ABOUT
WINDUCOM 2010
EXIT
FILE 1 MS6
FILE 2
FILE 3
FILE 4
Sample ID :- 01 , Remarks :- , Wear track diameter :-40, Date :- 5/
REFRESH
X-AXIS
Time (Secs)
Y-AXIS
Wear (Microns)
Cursor 0
Wear (Microns)
Time (Secs)
RESET
FILE 1 218.07 MEAN 33.00 SD 1089.02 VARIANCE
FILE 2 NaN MEAN 2 0.00 SD 2 0.00 VARIANCE 2
FILE 3 NaN MEAN 3 0.00 SD 3 0.00 VARIANCE 3
FILE 4 NaN MEAN 4 0.00 SD 4 0.00 VARIANCE 4

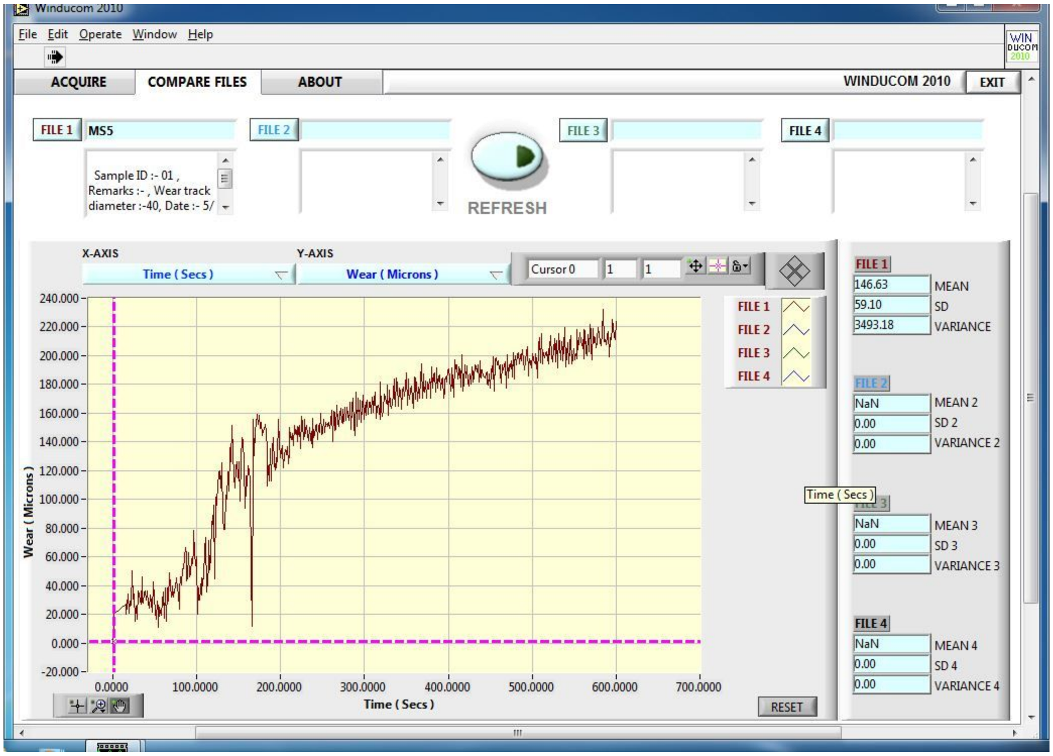
Winducom 2010
File Edit Operate Window Help
ACQUIRE
COMPARE FILES
ABOUT
WINDUCOM 2010
EXIT
FILE 1 MS5
FILE 2
FILE 3
FILE 4
Sample ID :- 01 , Remarks :- , Wear track diameter :-40, Date :- 5/
REFRESH
X-AXIS
Time (Secs)
Y-AXIS
Wear (Microns)
Cursor 0
Wear (Microns)
Time (Secs)
RESET
FILE 1
146.63 MEAN
59.10 SD
3493.18 VARIANCE
FILE 2
NaN MEAN 2
0.00 SD 2
0.00 VARIANCE 2
NaN MEAN 3
0.00 SD 3
0.00 VARIANCE 3
FILE 4
NaN MEAN 4
0.00 SD 4
0.00 VARIANCE 4

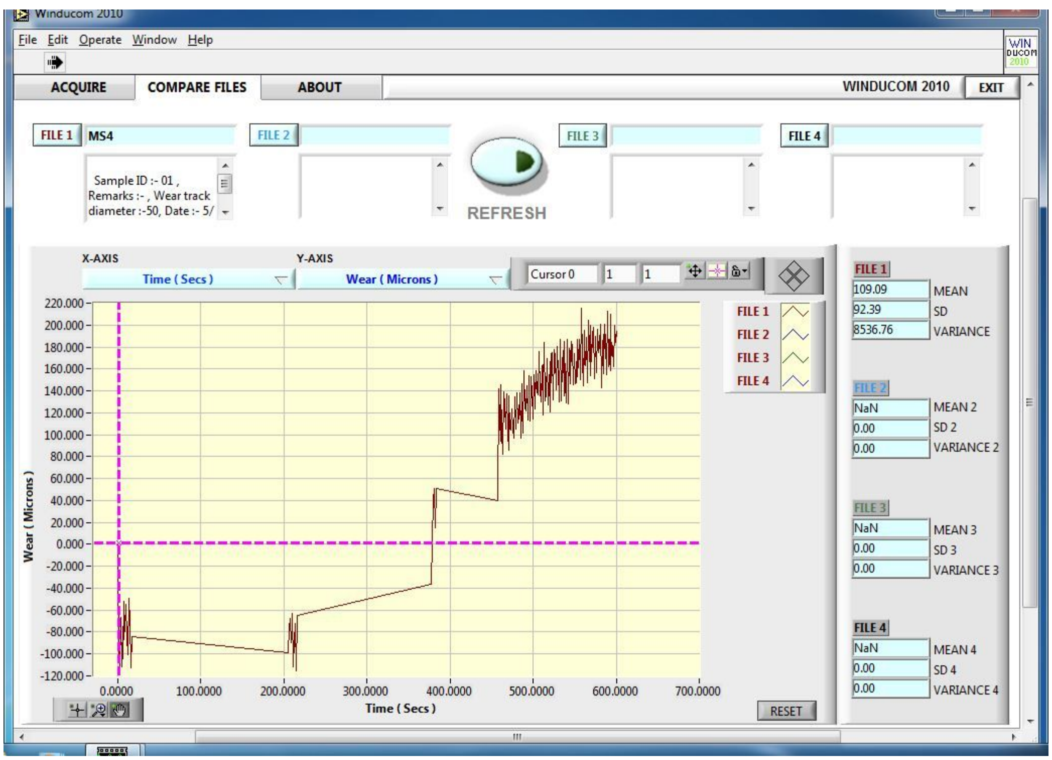
Winducom 2010
File Edit Operate Window Help
ACQUIRE
COMPARE FILES
ABOUT
WINDUCOM 2010
EXIT
FILE 1 MS4
FILE 2
FILE 3
FILE 4
Sample ID :- 01 , Remarks :- , Wear track diameter :-50, Date :- 5/
REFRESH
X-AXIS
Time (Secs)
Y-AXIS
Wear (Microns)
Cursor 0
Wear (Microns)
Time (Secs)
RESET
FILE 1
109.09 MEAN
92.39 SD
8536.76 VARIANCE
FILE 2
NaN MEAN 2
0.00 SD 2
0.00 VARIANCE 2
FILE 3
NaN MEAN 3
0.00 SD 3
0.00 VARIANCE 3
FILE 4
NaN MEAN 4
0.00 SD 4
0.00 VARIANCE 4

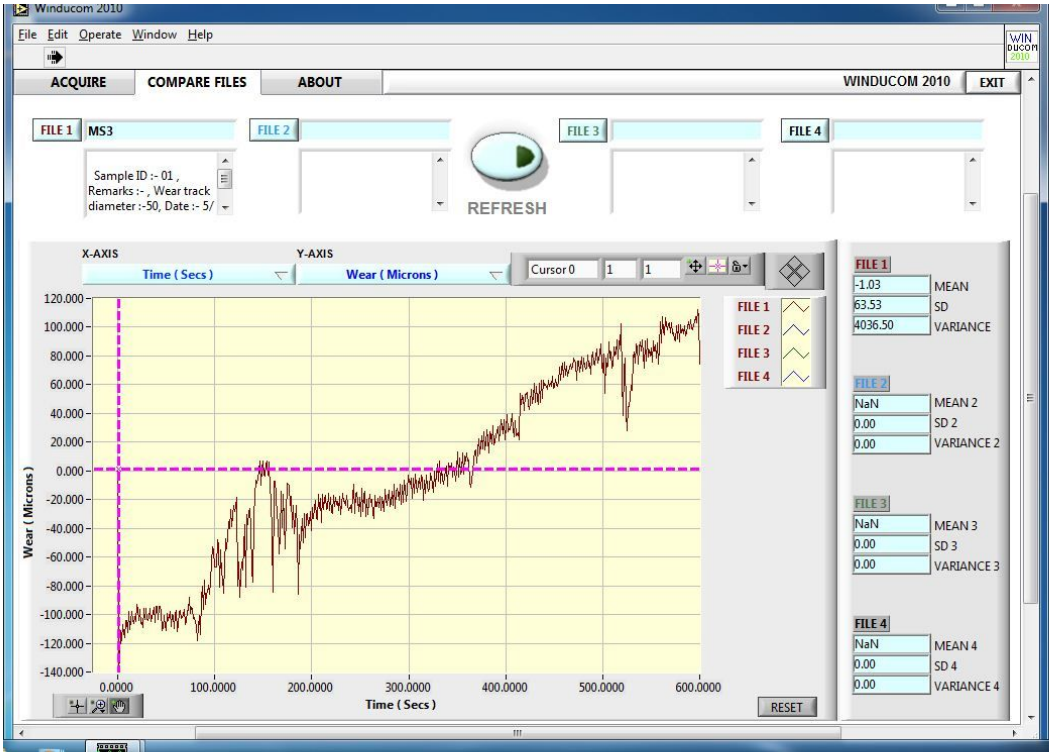
Windućom 2010
File Edit Operate Window Help
ACQUIRE
COMPARE FILES
ABOUT
WINDUCOM 2010
EXIT
FILE 1 MS3
FILE 2
FILE 3
FILE 4
Sample ID :- 01 , Remarks :- , Wear track diameter :-50, Date :- 5/
REFRESH
X-AXIS
Y-AXIS
Time (Secs)
Wear (Microns)
Cursor 0
Wear (Microns)
Time (Secs)
RESET
FILE 1
-1.03 MEAN
63.53 SD
4036.50 VARIANCE
FILE 2
NaN MEAN 2
0.00 SD 2
0.00 VARIANCE 2
FILE 3
NaN MEAN 3
0.00 SD 3
0.00 VARIANCE 3
FILE 4
NaN MEAN 4
0.00 SD 4
0.00 VARIANCE 4

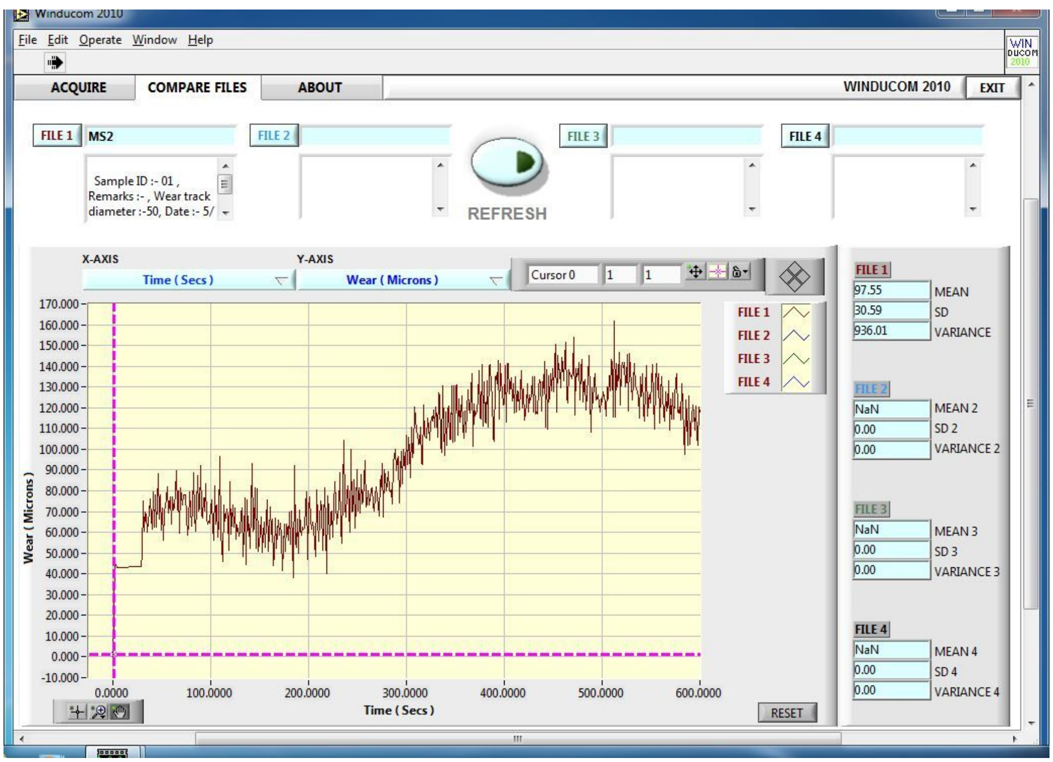
Windućom 2010
File Edit Operate Window Help
ACQUIRE
COMPARE FILES
ABOUT
WINDUCOM 2010
EXIT
FILE 1 MS2
FILE 2
FILE 3
FILE 4
Sample ID :- 01 , Remarks :- , Wear track diameter :-50, Date :- 5/
REFRESH
X-AXIS
Y-AXIS
Time (Secs)
Wear (Microns)
Cursor 0
Wear (Microns)
Time (Secs)
RESET
FILE 1
97.55 MEAN
30.59 SD
936.01 VARIANCE
FILE 2
NaN MEAN 2
0.00 SD 2
0.00 VARIANCE 2
FILE 3
NaN MEAN 3
0.00 SD 3
0.00 VARIANCE 3
FILE 4
NaN MEAN 4
0.00 SD 4
0.00 VARIANCE 4

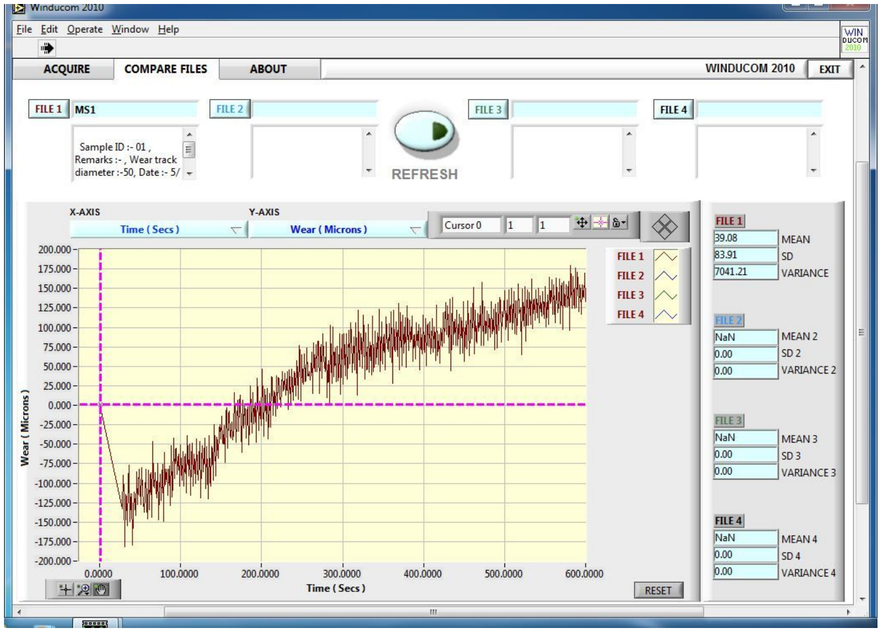

Time versus Friction force comparison graphs between the samples having the same speed of running by pin on disc Wear test result obtained from all the 9 samples of experiment.

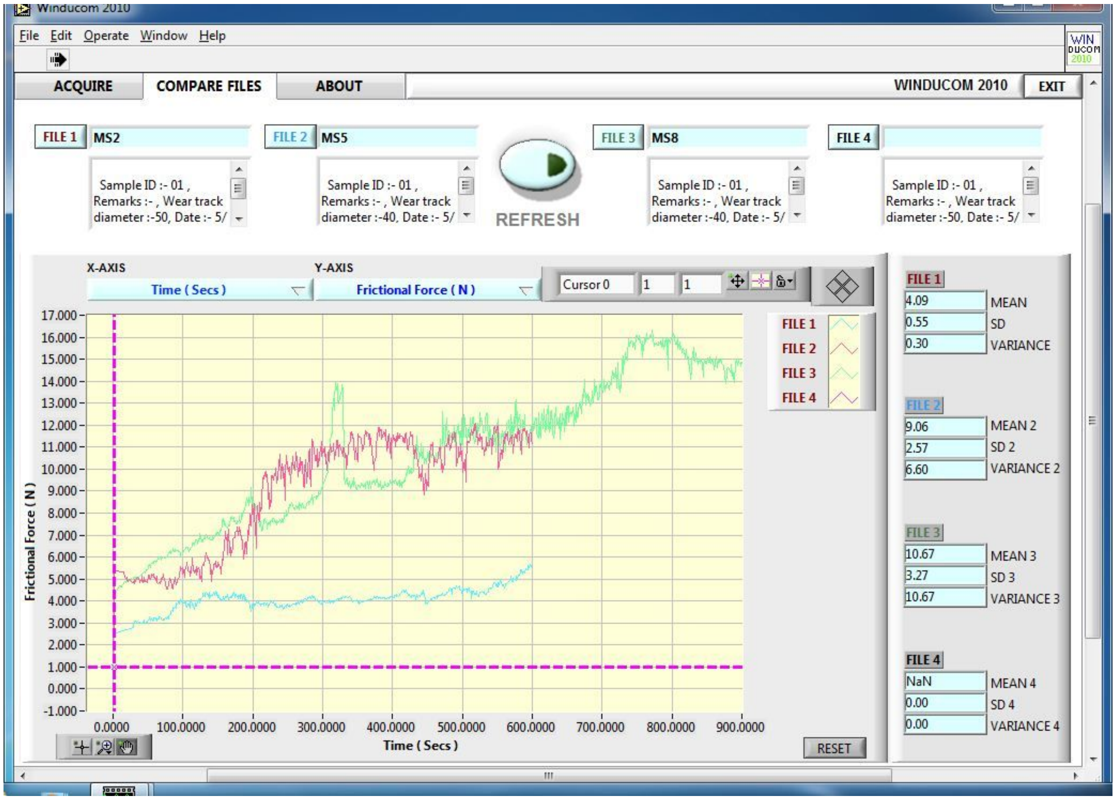
Winducom 2010
File Edit Operate Window Help
ACQUIRE
COMPARE FILES
ABOUT
WINDUCOM 2010
EXIT
FILE 1 MS2
FILE 2 MS5
FILE 3 MS8
FILE 4
Sample ID :- 01 , Remarks :- , Wear track diameter :-50, Date :- 5/
Sample ID :- 01 , Remarks :- , Wear track diameter :-40, Date :- 5/
Sample ID :- 01 , Remarks :- , Wear track diameter :-40, Date :- 5/
Sample ID :- 01 , Remarks :- , Wear track diameter :-50, Date :- 5/
REFRESH
X-AXIS
Time (Secs)
Y-AXIS
Frictional Force (N)
Cursor 0
FILE 1
4.09 MEAN
0.55 SD
0.30 VARIANCE
FILE 2
9.06 MEAN 2
2.57 SD 2
6.60 VARIANCE 2
FILE 3
10.67 MEAN 3
3.27 SD 3
10.67 VARIANCE 3
FILE 4
NaN MEAN 4
0.00 SD 4
0.00 VARIANCE 4
Frictional Force (N)
Time (Secs)
RESET

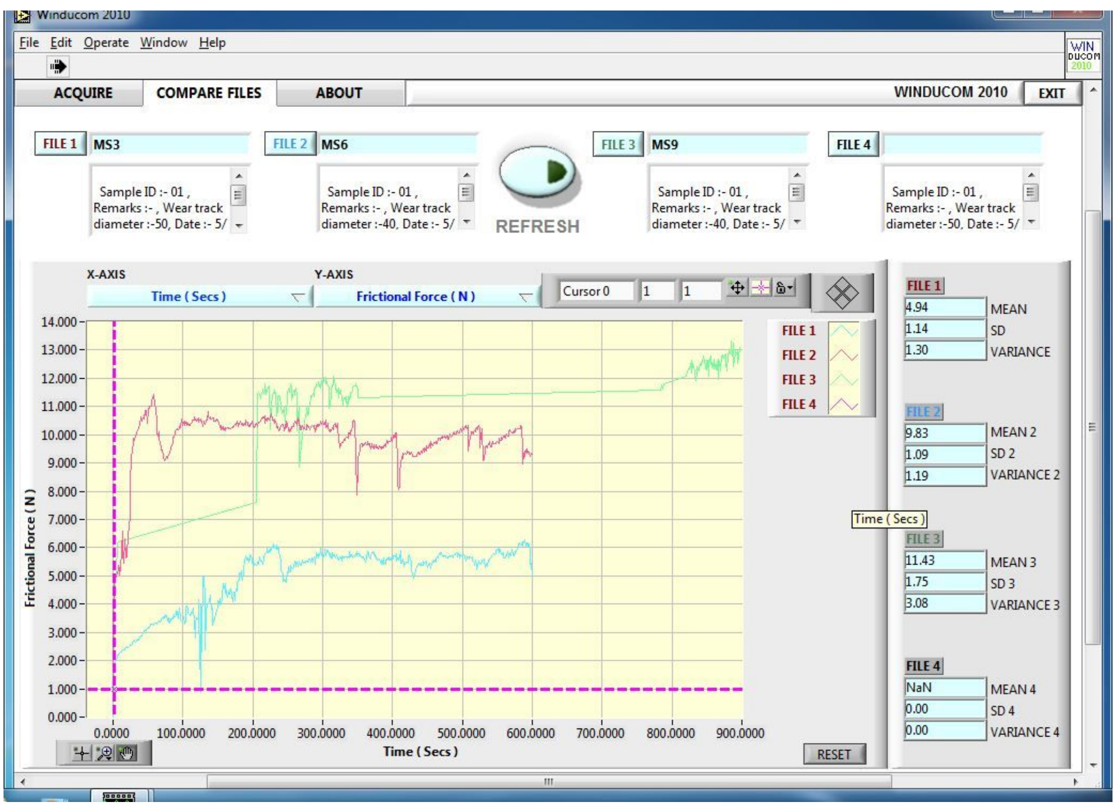
Winducom 2010
File Edit Operate Window Help
ACQUIRE
COMPARE FILES
ABOUT
WINDUCOM 2010
EXIT
FILE 1 MS3
FILE 2 MS6
FILE 3 MS9
FILE 4
Sample ID :- 01 , Remarks :- , Wear track diameter :-50, Date :- 5/
Sample ID :- 01 , Remarks :- , Wear track diameter :-40, Date :- 5/
Sample ID :- 01 , Remarks :- , Wear track diameter :-40, Date :- 5/
Sample ID :- 01 , Remarks :- , Wear track diameter :-50, Date :- 5/
REFRESH
X-AXIS
Time (Secs)
Y-AXIS
Frictional Force (N)
Cursor 0
FILE 1
4.94 MEAN
1.14 SD
1.30 VARIANCE
FILE 2
9.83 MEAN 2
1.09 SD 2
1.19 VARIANCE 2
FILE 3
11.43 MEAN 3
1.75 SD 3
3.08 VARIANCE 3
FILE 4
NaN MEAN 4
0.00 SD 4
0.00 VARIANCE 4
Frictional Force (N)
Time (Secs)
RESET

SEM material photo

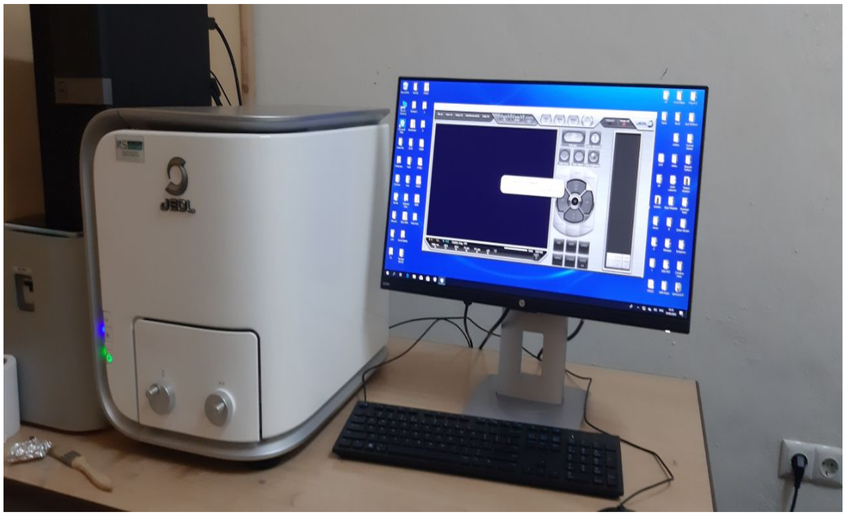	$CM_**FORMAT JEOL/EO** $CM_VERSION 0.2 $CM_COMMENT _ $CM_DATE 2023-06-19 $CM_TIME 10:25:43

SEM Images for all 9 samples at 50 µm and 100 µm for each

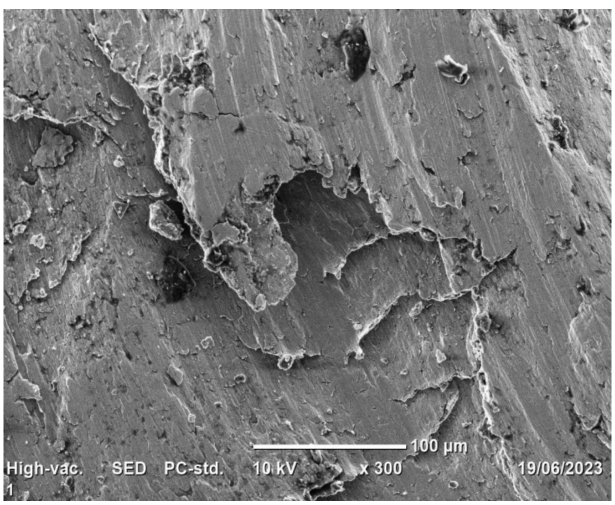

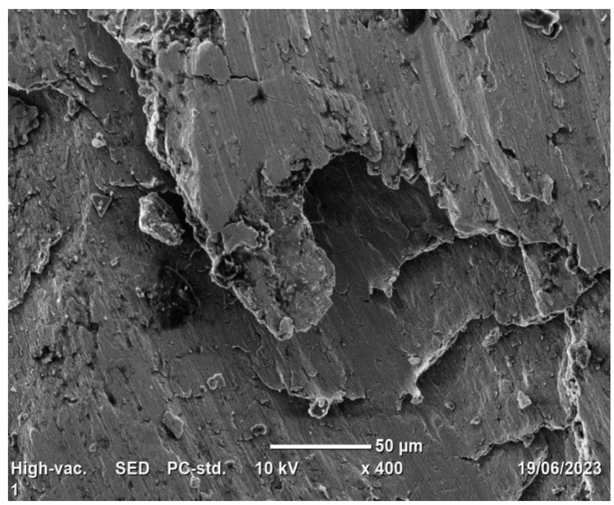

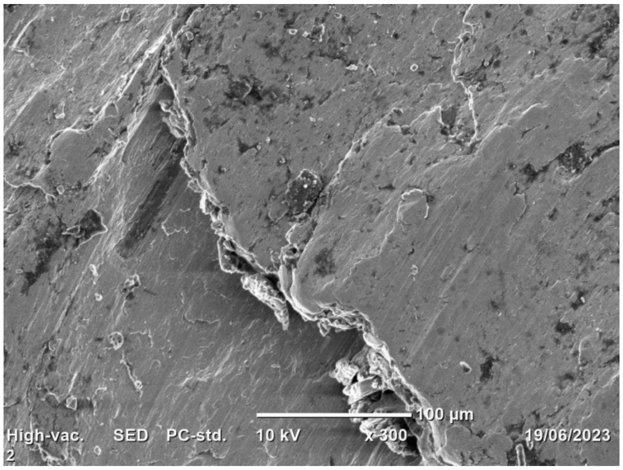
100 µm
High-vac. SED PC-std. 10 kV x 300 19/06/2023
2

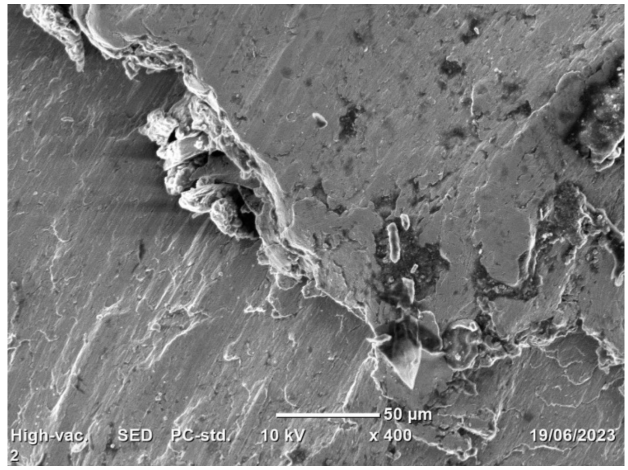
50 µm
High-vac. SED PC-std. 10 kV x 400 19/06/2023
2

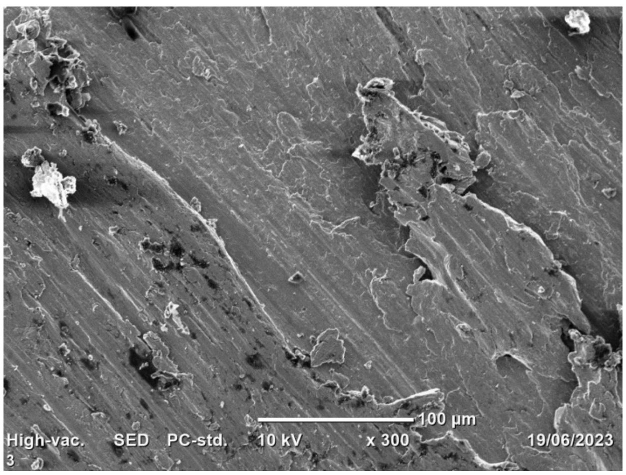
100 µm
High-vac. SED PC-std. 10 kV x 300 19/06/2023
3

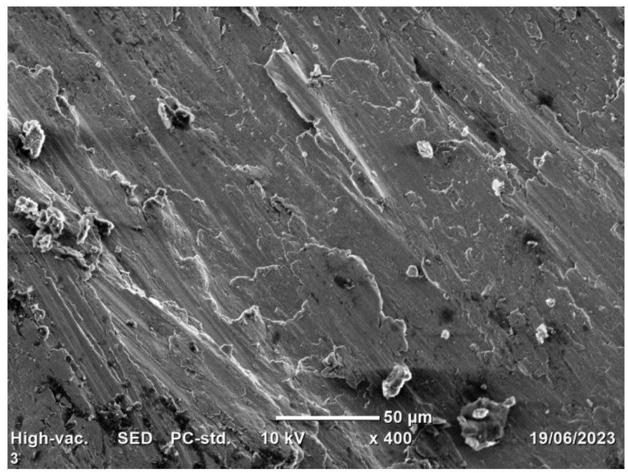
50 µm
High-vac. SED PC-std. 10 kV x 400 19/06/2023
3

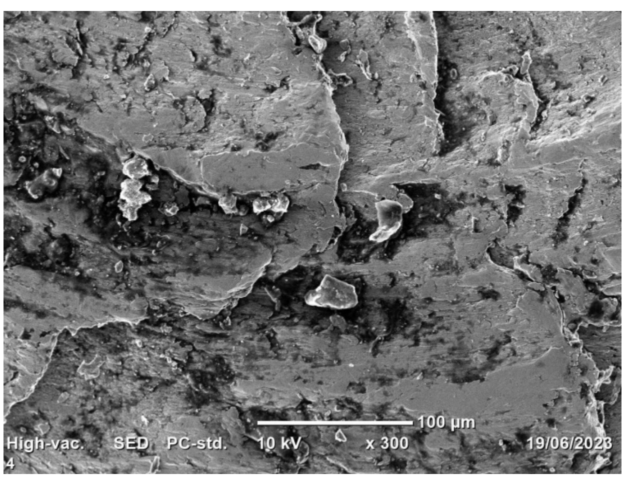
100 µm
High-vac. SED PC-std. 10 kV x 300 19/06/2023
4

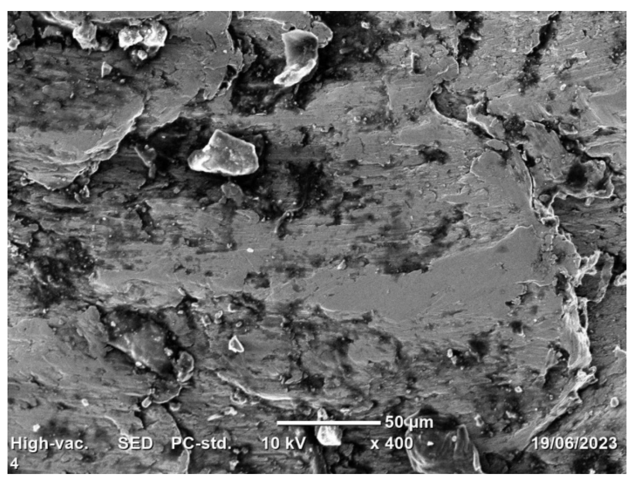
50 µm
High-vac. SED PC-std. 10 kV x 400 19/06/2023
4

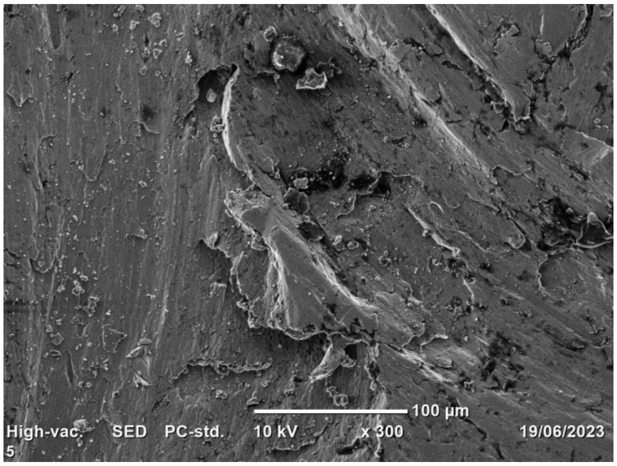
100 µm
High-vac. SED PC-std. 10 kV x 300 19/06/2023
5

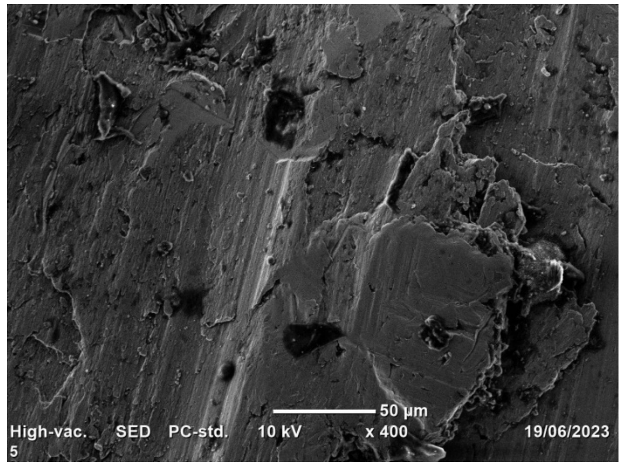
50 µm
High-vac. SED PC-std. 10 kV x 400 19/06/2023
5

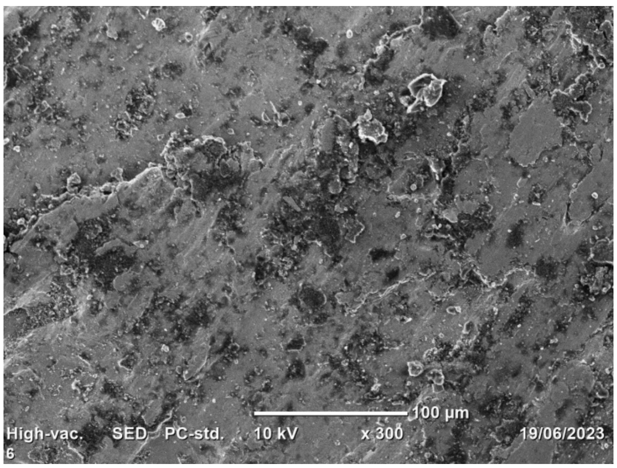
100 µm
High-vac. SED PC-std. 10 kV x 300 19/06/2023
6

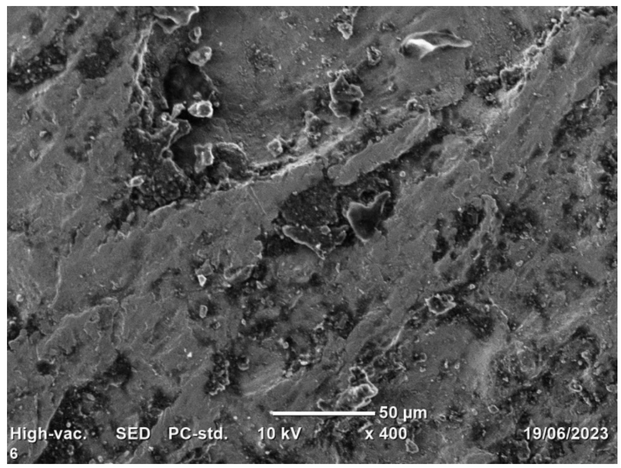
50 µm
High-vac. SED PC-std. 10 kV x 400 19/06/2023
6

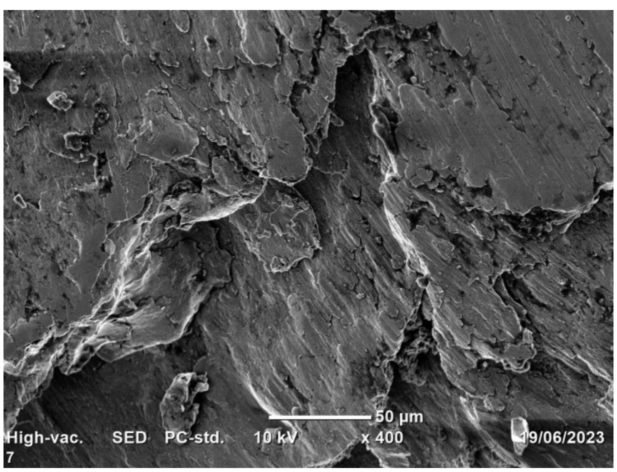
50 µm
High-vac. SED PC-std. 10 kV x 400 19/06/2023
7

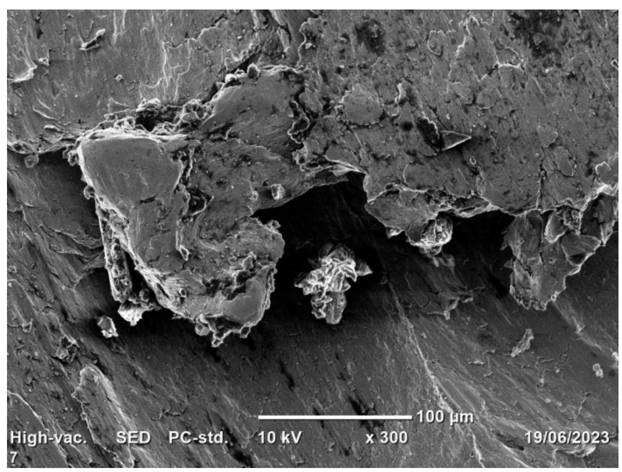
100 µm
High-vac. SED PC-std. 10 kV x 300 19/06/2023
7

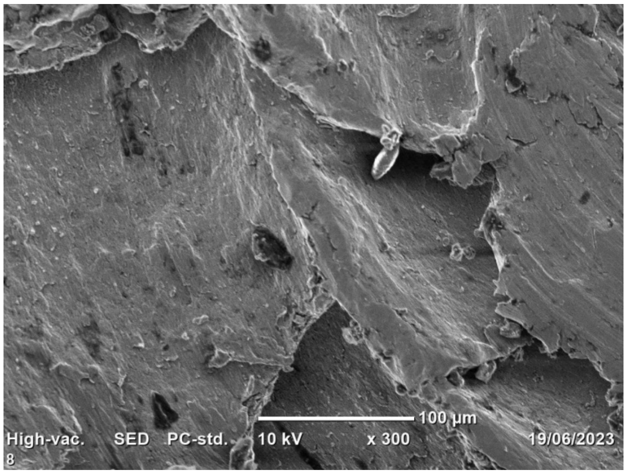

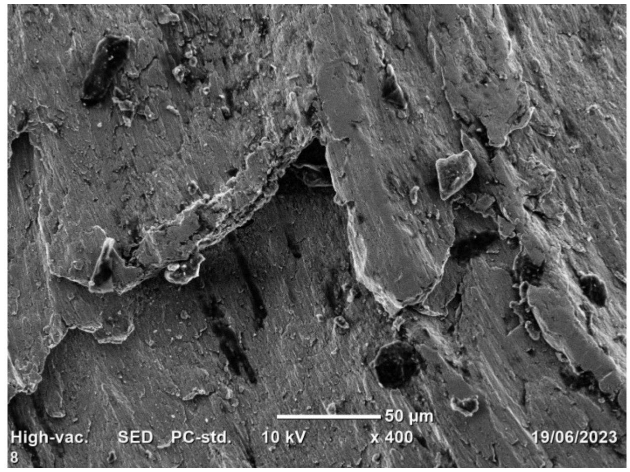

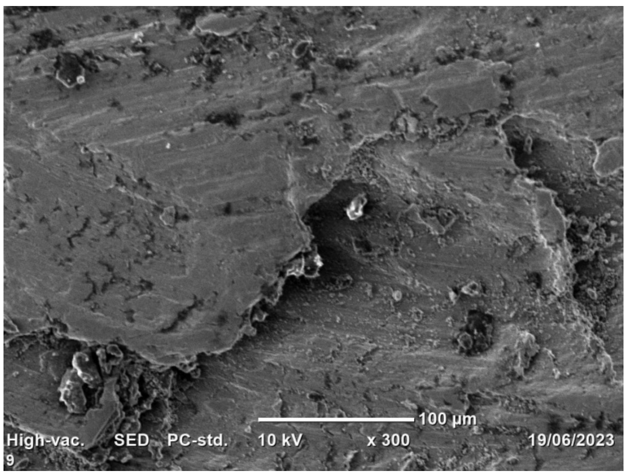

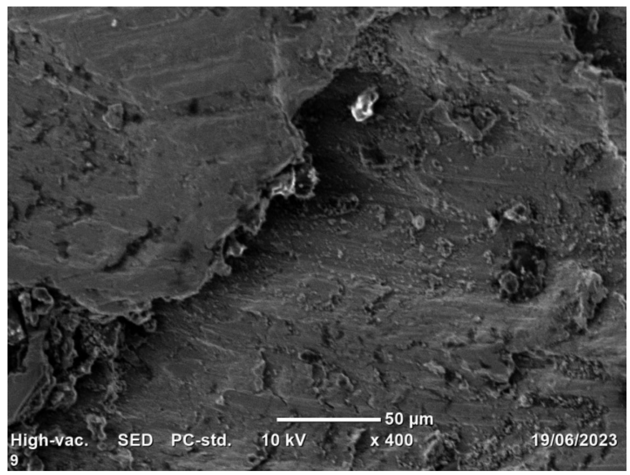

Figures and graphs obtained by LS-DYNA software

Equivalent Stress For load 15N

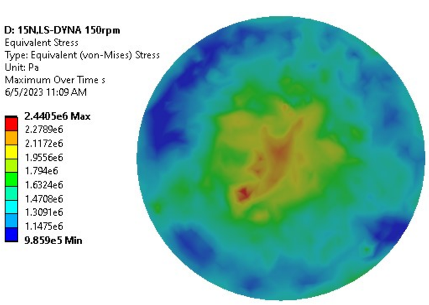

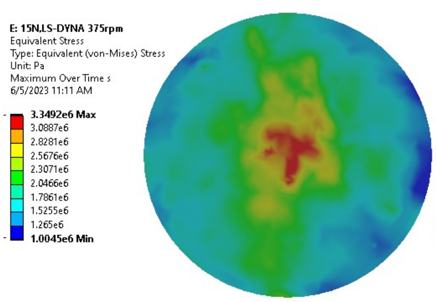

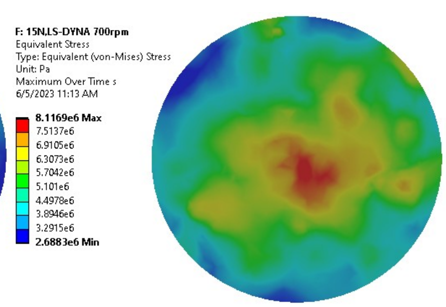

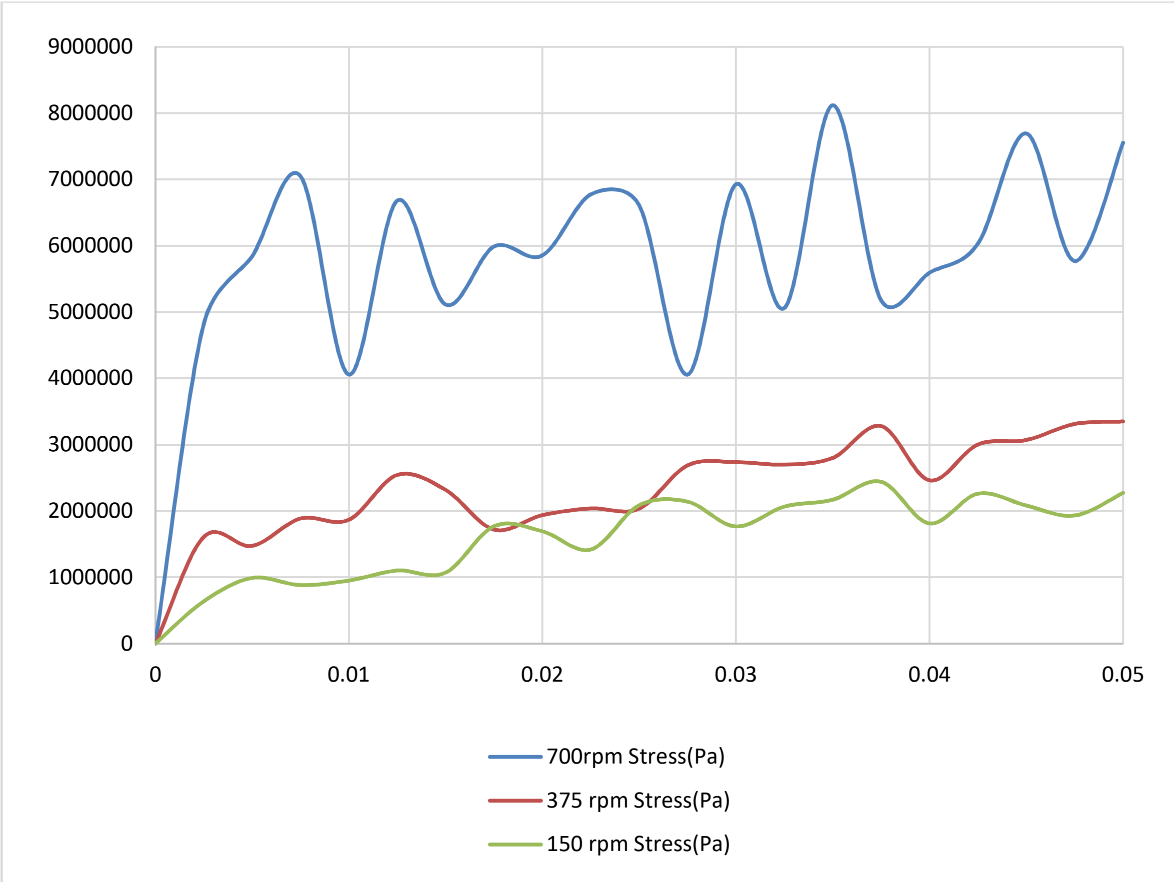

15N						
Time	700rpm Stress(P	375 rpm Stress(Pa)	150 rpm Stress(Pa)	700 rpm Defformation (m)	375 rpm Defformation (m)	150 rpm Defformation (m)
0	0	0	0	0	0	0
2.50E-03	4.81E+06	1.61E+06	6.37E+05	5.50E-04	2.95E-04	1.18E-04
5.00E-03	5.84E+06	1.47E+06	9.90E+05	1.10E-03	5.89E-04	2.36E-04
7.50E-03	7.05E+06	1.89E+06	8.82E+05	1.64E-03	8.83E-04	3.54E-04
1.00E-02	4.06E+06	1.87E+06	9.50E+05	2.17E-03	1.18E-03	4.72E-04
1.25E-02	6.68E+06	2.54E+06	1.10E+06	2.68E-03	1.47E-03	5.89E-04
1.50E-02	5.11E+06	2.32E+06	1.07E+06	3.18E-03	1.75E-03	7.06E-04
1.75E-02	5.99E+06	1.72E+06	1.77E+06	3.65E-03	2.03E-03	8.23E-04
2.00E-02	5.85E+06	1.94E+06	1.69E+06	4.09E-03	2.31E-03	9.39E-04
2.25E-02	6.77E+06	2.04E+06	1.42E+06	4.50E-03	2.59E-03	1.05E-03
2.50E-02	6.61E+06	2.04E+06	2.09E+06	4.87E-03	2.85E-03	1.17E-03
2.75E-02	4.06E+06	2.69E+06	2.14E+06	5.21E-03	3.11E-03	1.28E-03
3.00E-02	6.93E+06	2.74E+06	1.77E+06	5.50E-03	3.37E-03	1.39E-03
3.25E-02	5.06E+06	2.70E+06	2.07E+06	5.75E-03	3.61E-03	1.50E-03
3.50E-02	8.12E+06	2.80E+06	2.17E+06	5.95E-03	3.85E-03	1.61E-03
3.75E-02	5.18E+06	3.28E+06	2.44E+06	6.11E-03	4.08E-03	1.72E-03
4.00E-02	5.59E+06	2.46E+06	1.81E+06	6.22E-03	4.30E-03	1.83E-03
4.25E-02	6.03E+06	3.00E+06	2.26E+06	6.27E-03	4.50E-03	1.93E-03
4.50E-02	7.69E+06	3.07E+06	2.08E+06	6.28E-03	4.70E-03	2.04E-03
4.75E-02	5.77E+06	3.31E+06	1.93E+06	6.24E-03	4.89E-03	2.14E-03
5.00E-02	7.55E+06	3.35E+06	2.27E+06	6.14E-03	5.07E-03	2.24E-03
5.00E-02	7.55E+06	3.35E+06	2.27E+06	6.14E-03	5.07E-03	2.24E-03

For deformation

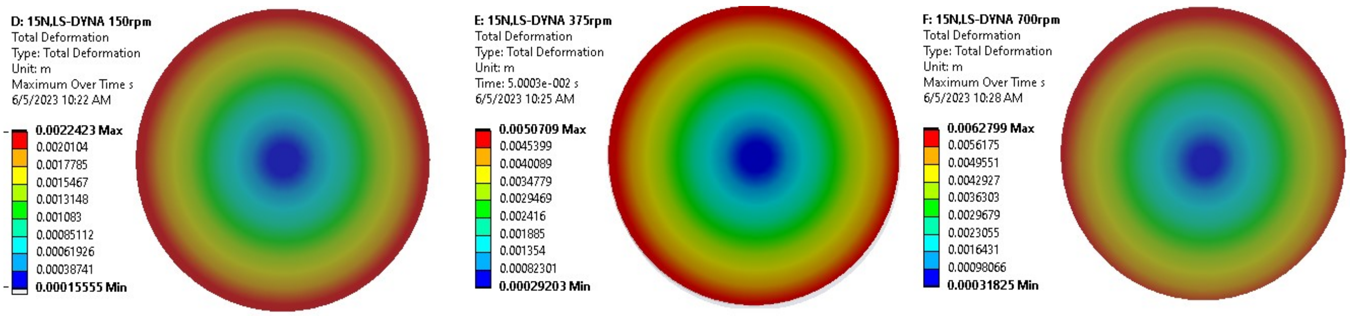

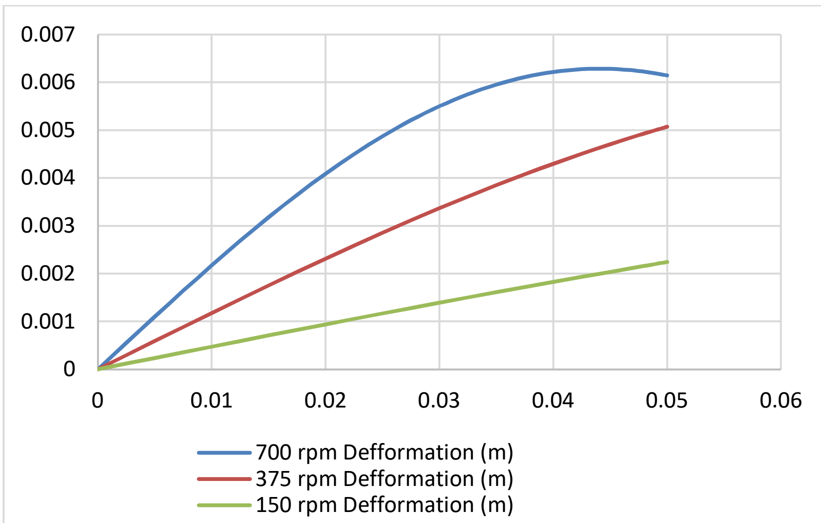

10N						
Time	700rpm Stress(P	375 rpm Stress(Pa)	150 rpm Stress(Pa)	700 rpm Defformation (m)	375 rpm Defformation (m)	150 rpm Defformation (m)
0	0	0	0	0	0	0
2.50E-03	2.49E+06	3.11E+06	1.19E+06	5.49E-04	2.95E-04	1.18E-04
5.00E-03	5.10E+06	2.88E+06	2.76E+06	1.10E-03	5.89E-04	2.36E-04
7.50E-03	2.97E+06	2.69E+06	2.90E+06	1.63E-03	8.83E-04	3.54E-04
1.00E-02	7.70E+06	2.95E+06	1.75E+06	2.16E-03	1.18E-03	4.73E-04
1.25E-02	4.07E+06	2.92E+06	2.29E+06	2.67E-03	1.47E-03	5.91E-04
1.50E-02	5.62E+06	3.43E+06	1.68E+06	3.15E-03	1.75E-03	7.08E-04
1.75E-02	4.76E+06	4.38E+06	2.12E+06	3.61E-03	2.04E-03	8.26E-04
2.00E-02	5.95E+06	4.28E+06	2.04E+06	4.05E-03	2.32E-03	9.42E-04
2.25E-02	5.05E+06	2.67E+06	2.15E+06	4.45E-03	2.59E-03	1.06E-03
2.50E-02	7.70E+06	3.49E+06	1.85E+06	4.81E-03	2.86E-03	1.17E-03
2.75E-02	5.29E+06	3.14E+06	3.10E+06	5.13E-03	3.12E-03	1.29E-03
3.00E-02	6.65E+06	3.00E+06	1.98E+06	5.41E-03	3.37E-03	1.40E-03
3.25E-02	5.63E+06	2.79E+06	2.37E+06	5.65E-03	3.62E-03	1.51E-03
3.50E-02	4.63E+06	2.43E+06	1.92E+06	5.84E-03	3.86E-03	1.62E-03
3.75E-02	6.16E+06	2.82E+06	2.19E+06	5.98E-03	4.09E-03	1.73E-03
4.00E-02	5.44E+06	3.33E+06	2.44E+06	6.08E-03	4.31E-03	1.84E-03
4.25E-02	4.32E+06	2.98E+06	2.06E+06	6.12E-03	4.52E-03	1.95E-03
4.50E-02	6.15E+06	3.37E+06	2.24E+06	6.11E-03	4.72E-03	2.06E-03
4.75E-02	3.68E+06	2.62E+06	2.78E+06	6.06E-03	4.91E-03	2.16E-03
5.00E-02	4.61E+06	2.88E+06	2.27E+06	5.95E-03	5.09E-03	2.27E-03
5.00E-02	4.61E+06	2.88E+06	2.27E+06	5.95E-03	5.09E-03	2.27E-03

20N						
Time	700rpm Stress(P	375 rpm Stress(Pa)	150 rpm Stress(Pa)	700 rpm Defformation (m)	375 rpm Defformation (m)	150 rpm Defformation (m)
0	0	0	0	0	0	0
2.50E-03	3.52E+06	1.28E+06	3.04E+06	5.49E-04	2.94E-04	1.18E-04
5.00E-03	7.50E+06	1.69E+06	2.50E+06	1.10E-03	5.89E-04	2.36E-04
7.50E-03	4.18E+06	1.57E+06	1.54E+06	1.63E-03	8.82E-04	3.54E-04
1.00E-02	3.70E+06	2.68E+06	1.56E+06	2.16E-03	1.17E-03	4.73E-04
1.25E-02	3.07E+06	1.71E+06	2.79E+06	2.67E-03	1.46E-03	5.91E-04
1.50E-02	5.77E+06	1.99E+06	1.89E+06	3.16E-03	1.75E-03	7.09E-04
1.75E-02	5.84E+06	2.36E+06	1.98E+06	3.63E-03	2.03E-03	8.26E-04
2.00E-02	5.58E+06	1.49E+06	2.06E+06	4.06E-03	2.31E-03	9.43E-04
2.25E-02	4.46E+06	2.90E+06	2.48E+06	4.46E-03	2.58E-03	1.06E-03
2.50E-02	4.73E+06	1.92E+06	2.40E+06	4.83E-03	2.85E-03	1.17E-03
2.75E-02	4.16E+06	3.45E+06	2.79E+06	5.16E-03	3.10E-03	1.29E-03
3.00E-02	7.40E+06	3.60E+06	2.54E+06	5.44E-03	3.36E-03	1.40E-03
3.25E-02	6.26E+06	2.93E+06	2.09E+06	5.68E-03	3.60E-03	1.51E-03
3.50E-02	5.46E+06	3.82E+06	2.30E+06	5.88E-03	3.84E-03	1.62E-03
3.75E-02	3.89E+06	2.83E+06	4.29E+06	6.03E-03	4.06E-03	1.73E-03
4.00E-02	7.93E+06	2.59E+06	2.41E+06	6.13E-03	4.28E-03	1.84E-03
4.25E-02	7.56E+06	3.32E+06	2.46E+06	6.18E-03	4.49E-03	1.94E-03
4.50E-02	5.62E+06	3.55E+06	2.58E+06	6.18E-03	4.68E-03	2.05E-03
4.75E-02	4.67E+06	3.58E+06	3.60E+06	6.13E-03	4.87E-03	2.15E-03
5.00E-02	6.91E+06	5.18E+06	2.77E+06	6.03E-03	5.05E-03	2.25E-03
5.00E-02	6.91E+06	5.18E+06	2.77E+06	6.03E-03	5.05E-03	2.25E-03

Mesh and Geometrical Modeling

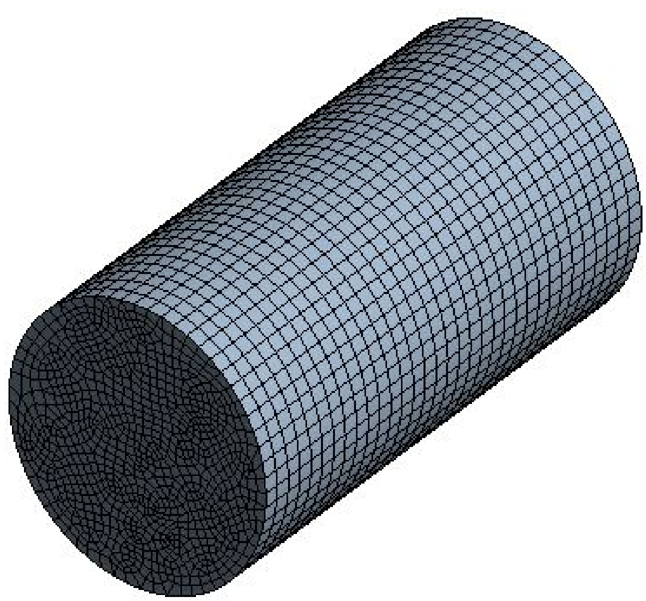

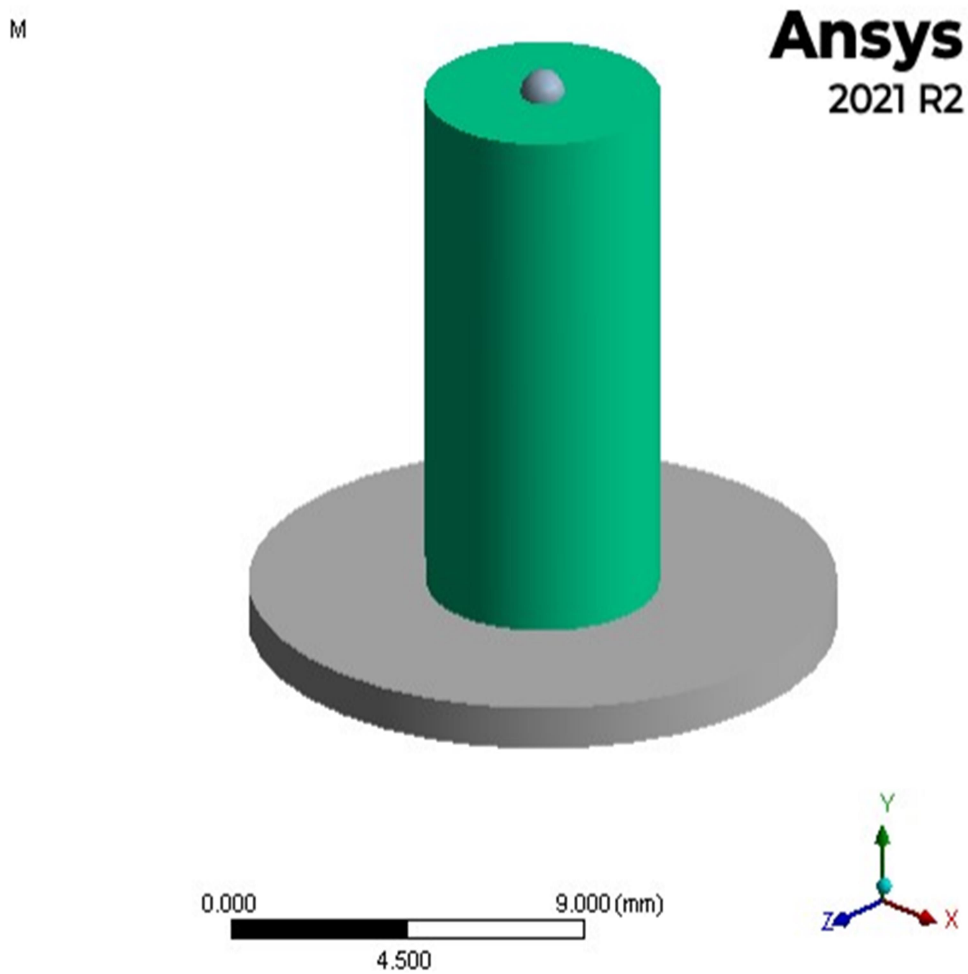
M
Ansys
2021 R2
0.000
9.000 (mm)
4.500
Y
Z
X